2017

Polymer Grafted Nanoparticles for Designed Interfaces in Polymer Nanocomposites

Mohammad Mohammadkhani
University of South Carolina

POLYMER GRAFTED NANOPARTICLES FOR DESIGNED INTERFACES IN POLYMER NANOCOMPOSITES

by

Mohammad Mohammadkhani

Bachelor of Science
Malek Ashtar University, 2007

Master of Science
Tarbiat Modares University, 2010

Submitted in Partial Fulfillment of the Requirements

For the Degree of Doctor of Philosophy in

Chemistry

College of Arts and Sciences

University of South Carolina

2017

Accepted by:

Brian Benicewicz, Major Professor

Chuanbing Tang, Committee Member

Thomas Vogt, Committee Member

Harry Ploehn, Committee Member

Cheryl L. Addy, Vice Provost and Dean of the Graduate School

ACKNOWLEDGMENT

I would like to express my deepest gratitude to my Ph.D. advisor Prof. Brian Benicewicz for his patient guidance, incredible encouragement and support, and inspirational advice on my Ph.D. research. None of this would be possible without his expertise and guidance. I am extremely thankful to the entire Benicewicz group members for their help and support and I am very proud of being a member of this group.

I would also like to thank my doctoral committee members - Prof. Chuanbing Tang, Prof. Thomas Vogt, and Prof. Harry Ploehn for their encouragement and assistance during graduate school.

I would like to thank my collaborators Prof. Linda Schadler (Rensselaer Polytechnic Institute) and her graduate student Tim Krentz, as well as Prof. Sanat Kumar of Columbia University and his graduate student Dan Zhao for their invaluable contributions towards this work.

Finally, I would like to thank my entire family. This achievement could not have been possible without their love, encouragement, and support.

ABSTRACT

This dissertation presents the design, synthesis, and characterization of polymer nanocomposite interfaces and the property enhancement from this interface design. Through the use of reversible addition fragmentation chain transfer (RAFT) polymerization for the grafting of polymer chains to silica nanoparticles, the surface of silica nanoparticles can be manipulated to tune the properties of nanocomposites by controlling the interface between the particles and the polymer matrix.

In the first part of this work, compatibility of 15 nm silica nanoparticles grafted with different alkyl methacrylates with linear low density polyethylene was investigated. SI-RAFT polymerization of hexyl, lauryl, and stearyl methacrylate on silica NPs was studied in detail and revealed living character for all these polymerizations. Composites of linear low density polyethylene filled with PHMA, PLMA, and PSMA-g-SiO_2 NPs were prepared and analyzed to find the effects of side chain length on the dispersibility of particles throughout the matrix. PSMA brushes were the most "olefin-like" of the series and thus showed the highest compatibility with polyethylene. The effects of PSMA brush molecular weight and chain density on the dispersion of silica particles were investigated. Multiple characterizations such as DSC, WAXS, and SAXS were applied to study the interaction between PSMA-g-SiO_2 NPs and the polyethylene matrix.

In the next part, the compatibility of PSMA-g-SiO_2 NPs with different molecular variables with isotactic polypropylene was investigated. Anthracene was used as a conjugated ligand to introduce to the surface of PSMA-g-SiO_2 NPs to develop bimodal architecture on

nanoparticles and use them in polypropylene dielectric nanocomposites. The dispersion of particles was investigated and showed that for both monomodal and bimodal particles where PSMA chains are medium density and relatively high molecular weight, they maintain an acceptable level of dispersion throughout of the matrix. Furthermore, the effects of anthracene surface modification and also level of dispersion towards improving the dielectric breakdown strength under AC and DC conditions were studied.

Finally, the RAFT polymerizations of isoprene in solution and, for the first time, on the surface of silica particles using a high temperature stable trithiocarbonate RAFT agent were studied. The effects of different temperatures, initiators, and monomer feed ratios on the kinetics of the SI-RAFT polymerization were also investigated. Kinetic studies revealed that the rate of SI-RAFT polymerization increased with an increase in the density of grafted RAFT agent. Well-defined polyisoprene-grafted silica NPs (PIP-*g*-SiO_2 NPs) were synthesized and mixed with a polyisoprene matrix to determine the compatibility and dispersion of these particles with the matrix. Hydrogenation of PIP-*g*-SiO_2 NPs were performed using *p*-toluenesulfonyl hydrazide at high temperature to obtain hydrogenated (HPIP)-*g*-SiO_2 NPs. A bimodal octadecylsilane (C18)-HPIP-*g*-SiO_2 NPs sample was synthesized and mixed with isotactic PP matrix analyzed for the compatibility with polypropylene.

TABLE OF CONTENTS

LIST OF TABLES

LIST OF FIGURES

List of Abbreviations

AIBN ..... Azobisisobutyronitrile

ATRP ..... Atom transfer radical polymerization

CPDB ..... 4-cyanopentanoic acid dithiobenzoate

CRP ..... Controlled radical polymerization

CTA ..... Chain transfer agent

DBS ..... Dielectric breakdown strength

DCC ..... N,N'-Dicyclohexylcarbodiimide

DCM ..... Dichloromethane

DoPAT ..... 2-(((dodecylthio)carbonothioyl)thio)propanoic acid

DCP ..... Dicumyl peroxide

dTBP ..... Di-tert-butyl peroxide

DMAP 4-Dimethylaminopyridine

DMF ..... N,N-dimethylformamide

FT-IR ..... Fourier transform infrared spectroscopy

GPC ..... Gel permeation chromatography

HF ..... Hydrofluoric acid

NMP ..... Nitroxide mediated polymerization

NMR ..... Nuclear Magnetic Resonance

NP ..... Nanoparticle

MMA ..... Methylmethacrylate

PMMA .....Poly(methyl methacrylate)

RAFT .....Reversible addition-fragmentation chain transfer

RPM .....Rotations per minute

TEM ..... Transmission electron microscopy

TEMPO .....(2,2,6,6-tetramethylpiperidin-1-yl)oxidanyl

THF ..... Tetrahydrofuran

TGA ..... Thermogravimetric Analysis

SI ..... Surface initiated

UV-vis .....Ultraviolet visible spectroscopy

CHAPTER 1

INTRODUCTION

1.1 Controlled Radical Polymerization

Controlled radical polymerization (CRP) techniques have been developed to precisely control polymers by giving living characteristics to free radial polymerizations. Living polymerizations first emerged as cationic, anionic and ring opening polymerization. However these methods were expensive and not compatible with many functional groups and were challenging in the presence of contaminants.[1,2] Therefore, control over the radical process was desired as it could be performed under relatively mild conditions, was more tolerant of functional groups, and was widely used by industry for many polymers. New CRP methods enabled highly precise control over several molecular variables in the polymerization system including molecular weight, molecular weight distribution, architecture, and the integrity of functional end groups in the polymer. The first CRP technique developed was nitroxide mediated polymerization (NMP)[3] followed by atom transfer radical polymerization (ATRP) in early 1990s.[4] Reversible addition-fragmentation chain transfer polymerization (RAFT) was then invented by Moad and co-workers, in 1998.[5]

NMP

Nitroxide mediated polymerization (NMP) brings control via a reversible activation mechanism of the polymer chain. It utilizes alkoxyamine species to control the kinetics of polymerization.[6] A nitroxide radical end-caps the polymer chain to form a persistent radical effect without the need for a separate initiator or catalyst (The propagating species are formed via dissociation of a nitroxide radical). In the propagation step polymer chains are formed, while reversible termination events mediate the availability of the reactive radical species and therefore, provide control over the polymerization. The equilibrium between

dormant and active species shifts towards the dormant species and therefore, limiting the number of active radical species present during the reaction, which restrict the possibility of termination reactions at the propagating chain end.[7–10]

The most ubiquitous alkoxyamine employed in mediating NMP is 2,2,6,6-tetramthylpiperidnyloxy (TEMPO).[11] NMP has achieved the most success polymerizing styrenic monomers however, other monomers have been successfully polymerized by NMP by developing new alkoxyamines.[12–15] Husseman et al. were the first group to perform NMP on the surface.[16] Polystyrene brushes were generated on the surface using TEMPO functionalized silicon wafers. Chevigny and coworkers have used surface initiated NMP to grow polystyrene on silica nanoparticles.[17] First, an aminosilane coupling agent was attached onto the surface and then a modified alkoxyamines reacted with amine-functionalized particles. While NMP can control the polymerization without added reagents such as initiator, chain transfer agent (CTA), or catalyst, it suffers from some disadvantages. There is no universal alkoxyamine for all monomers so it must be carefully chosen to ensure proper control over the polymerizations. Another disadvantage of conducting NMP method on the surface is the need for addition of a sacrificial nitroxide in solution to ensure the proper control of the polymerization. This, however, allows for the formation of polymer chains in solution which can be difficult to remove and separate from modified substrates. Also, the reaction temperatures to achieve activation of the nitroxide radical is high, limiting the use of monomers with thermally sensitive functional groups.

ATRP

Atom transfer radical polymerization or ATRP is the most popular of CRP methods and was first reported by Matyjaszewski et al. in 1995.[4] The mechanism of control is

through an equilibrium of active and dormant species. First, hemolytic transfer of the halide to a transition metal/ligand complex allows for the propagation of the radically active polymer species. Then the equilibrium quickly goes backwards to return the polymer chain to its dormant state, once again end-capped with the halide. ATRP is a much more versatile method than NMP due to its ability to polymerize a wider range of monomers under a wider range of reaction conditions.[18] The reversible deactivation mechanism of ATRP is found in Scheme 1.1. Living polymerization is achieved with fast initiation and rapid reversible deactivation.

The first surface initiated ATRP was performed by Huang and Wirth.[19] Using silica particles that were functionalized with benzyl chloride, brushes of poly(acrylamide) were grown from the surface. Since then, ATRP has become increasingly popular for the synthesis of polymer brushes on inorganic substrates.[20–28] The contamination of the final polymeric product with metal catalyst can be problematic limiting its application in some functional materials.

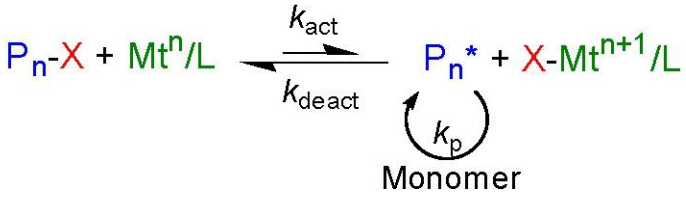

Scheme 1.1. Reversible deactivation with transfer to a metal complex (ATRP mechanism)

RAFT

Reversible addition fragmentation chain-transfer or RAFT polymerization dictates the control through a different mechanism than ATRP and NMP. RAFT uses a degenerative chain transfer method to control polymerization, rather than employing a persistent radical in the system. Control over polymerization is derived from the RAFT

chain transfer agent or CTA. RAFT polymerization has many advantages over the other controlled radical polymerization methods, such as being adaptable to almost all free radical polymerizable monomers, without participation of inorganic catalysts and under mild operational conditions, similar to the ones of conventional free radical polymerization. Also in 1998, macromolecular design by interchange of xanthates (MADIX)[29] was reported by Rhodia Chimie in France. MADIX and RAFT methods function on the same mechanism, and the only difference is on the Z group of the CTA structure. RAFT terminology indicates structures of Z-C(=S)-S-R generally, while MADIX specifies xanthates only with Z = OZ.

The mechanism of polymerization is shown in Scheme 1.2. In the initiation stage, the initiators decompose into free radicals, which add to monomers and grow into oligomeric propagating radicals Pn^*. The addition of Pn^* to the chain transfer agent (A) generates the intermediate radicals (I), which is in an equilibrium and can transfer back to the original state (A) or convert to a macro RAFT agent (B) by fragmentation. After initiation, polymer chains grow by monomer addition, and they rapidly exchange between dormant radicals (II) and the macro RAFT agent (C). The rapid exchange assures that the polymeric species spend most of their times at the stabilized intermediate radicals (II) stage. Therefore, the growing radicals are at lower concentrations than the stabilized intermediate radicals (II), thus minimizing termination.

The Z and R groups of the RAFT agent are responsible for controlling the rate of addition of the propagating radical species to the CTA and thus, the rate of polymerization. The Z group controls reactivity by stabilizing an adjacent radical center. The R group should be a good hemolytic leaving group compared to Pn* and be able to reinitiate

polymerization. In order to achieve a good control over the polymerization, the ratio of initiator to RAFT agent is kept low to limit the number of active radical species in the system and decrease the probability of termination between active radical species. There is a rapid rate of exchange between radical active and dormant chains. Several RAFT CTAs have been synthesized for suitable compatibility with several classes of monomer. Once the appropriate RAFT agent is chosen, the rest of the process is similar to a conventional free radical polymerization.[30]

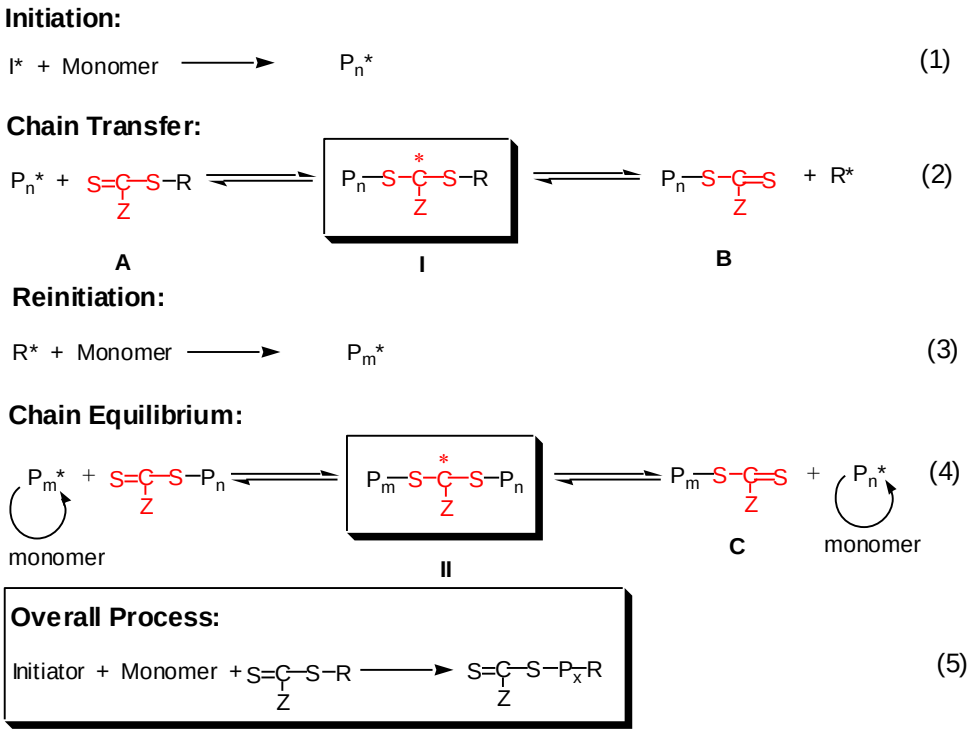

Scheme 1.2. Mechanism of RAFT polymerization.

RAFT technique has been used widely to polymerize a variety of monomers including styrenics, acrylates, methacrylates, and dienes. RAFT polymerization can be performed in various reaction conditions including bulk, solution, suspension and emulsion.[31–33] The reaction temperature in RAFT polymerization is the same as

conventional free radical polymerization processes however the RAFT process is tolerant to higher temperatures as well.

1.2 Nanocomposites

It has been well accepted that the incorporation of a small volume fraction of nanoparticles (NPs) into a polymer matrix can significantly improve the optical, electrical, and thermomechanical properties of the resulting polymer nanocomposites, (PNCs).[34–39] This property enhancement is not seen with the addition of micron-sized particles mostly due to the large interfacial region present in nanocomposites filled with NPs.[35,40] However, these enhancements depend strongly on the NPs dispersion and the nature of the nanoparticle-polymer interface which could become a challenge due to the unfavorable enthalpic interaction of a hydrophobic organic polymer matrix with a hydrophilic inorganic filler.[34,41,42] One strategy to control the interface is to covalently attach a polymer with the same chemistry as that of the matrix onto the surface of NPs so long as the polymer chains of the matrix have a lower molecular weight than those of the brush.[43] Other variables influencing the interface are the grafting density and the chain length of the grafted polymer. Control over such variables can be used to create an attractive interface due to the better entanglement and wetting of the grafted chains and the matrix.[44–47] Tuning these variables, one can obtain a variety of self-assembled anisotropic structures or uniformly dispersed particles. Figure 1.1 shows the experimentally obtained filler morphologies obtained by Kumar et al. Evenly dispersed particles were obtained with sufficient polymer coverage. Numerous polymer chemistries have been achieved on filler surfaces though the majority of polymeric species tend to be derived from chain growth monomers.[48]

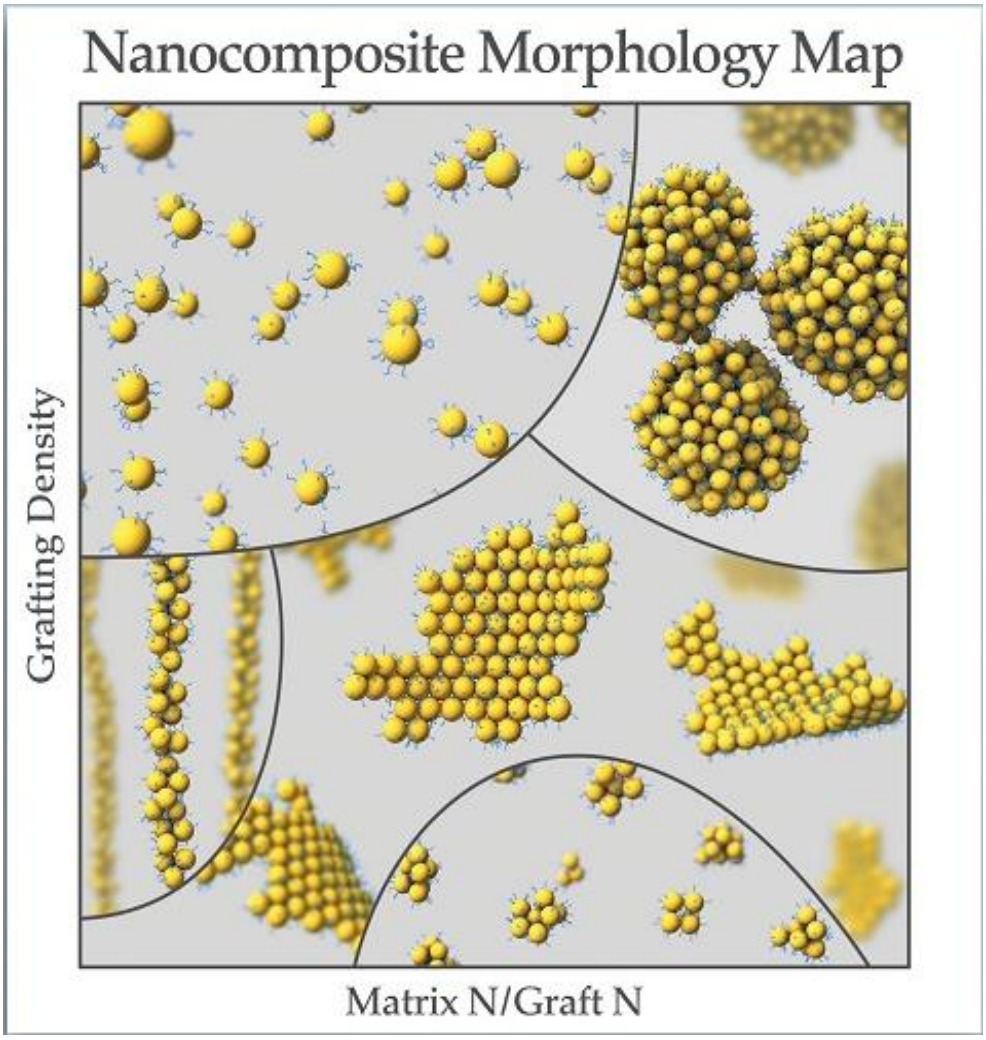

Figure 1.1 Nanocomposite morphology map showing the different nanoparticle dispersion states possible with a variation in graft density (y-axis) and ratio of matrix chain length to grafted chain length (x-axis). N is defined as the number of repeat units in the polymer chain.[48]

1.3 Surface Functionalization of Nanoparticles

Overall, there are two principal synthetic strategies for grafting polymers on nanoparticles: the "grafting to" and "grafting from" strategies (Figure 1.2).[20] As the term implies, in the "grafting to" approach molecules/polymers are attached to the surface of nanoparticles with a reactive chain end. Since polymer synthesis and grafting are performed in separate steps, this approach is universal and many types of polymerization

methods can be applied on various surface chemistries and thus is advantageous for industrial applications.

Coupling via phosphate and silane moieties, and "click chemistry" can all be used for "grafting to" a variety of nanoparticles, such as TiO_2[49] ITO,[50,51] and SiO_2.[52–55] "Grafting to " using silane coupling has been extensively investigated.[56,57] Phosphate coupling has been preferably used to graft molecules to the surface of titania[49,58] and barium titanate.[59] In addition, the use of "click chemistry" via copper-catalyzed azide-alkyne cycloaddition has become a common tool to attach molecules and polymers on the surface and has been studied widely for a variety of polymers[49,50,52–55] due to the facile synthesis of alkyne and azido end-capped moieties, high efficiency and specificity of the reaction. The drawback of this method is that it leaves a copper catalyst residue in the mixture.

RAFT polymerization which is adaptable to almost all radical polymerizable monomers can be used to tailor the brushes before attachment. For example, it can be used through the use of alkyne and azido end-capped polymers for "click" reaction or to prepare a trimethoxysilane containing RAFT agent[57] to generate a polymer that can react with the hydroxyl groups common on silica nanoparticles. ATRP[59] has also been used to graft different polymers to the surfaces.

Using "grafting to" strategies, it is not possible to attain high graft densities because it is difficult for the end-functionalized polymer chains to diffuse near the nanoparticle surface after some grafting sites have been occupied by the earlier grafted polymers due to steric hindrance, especially when the molecular weight of the polymer is high. Moreover, the existence of many free polymers after the grafting can create difficulties in purification. Physisorption is a type of "grafting-to" method and refers to polymers attached to

substrates through non-covalent interactions, mostly via hydrogen bonding or electrostatic interactions. Physisorption is a popular methodology for surface functionalization, however this work will focus on the more robust covalent attachment methods.

In the "grafting from" strategies, initiators or chain transfer agents are anchored on the surface, which can usually have a relatively high graft density ascribed to their smaller size and ease of diffusion. Then, monomers are added to the initiators during the polymerization, they diffuse near the surface of nanoparticles and polymers grow *in-situ* from the surface. Living radical polymerization methods are the most popular methods for grafting polymer from the surface of nanoparticles because very few polymerization methods can tolerate the extremely high local concentration growing chains on the nanoparticle surface and deliver control over the polymerization.

A variety of controlled radical polymerizations, such as ATRP, NMP and RAFT, have been employed to graft a wide range of polymers (block copolymers, branch copolymers, and star-shape polymers) from a variety of surfaces with controlling different variables such as graft densities, chain lengths, polydispersity and morphology.[60–62] Surface initiated controlled radical polymerization started with the work of Wirth and co-workers in 1997 using ATRP to polymerize acrylamide on benzyl chloride attached silica surfaces.[19] Matyjaszewski and co-workers[56,63,64] significantly expanded polymer-modified surfaces through ATRP. Then, the first report of surface initiated NMP was in 1999 by Hawker and co-workers on silicon wafers.[61]

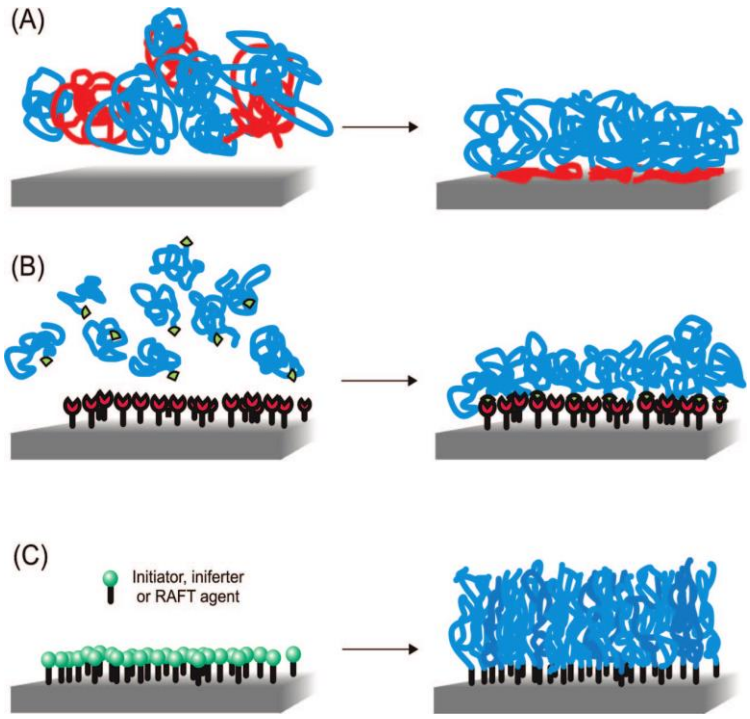

Figure 1.2 Different grafting methods: A) physisorbtion, B) grafting-to and C) grafting-from.[20]

Nanoparticles containing two populations of brushes on the surface known as bimodal nanoparticles, one long matrix compatible population and one short property enhancing brush or ligand, are developing as powerful tools for tailoring nanocomposite properties. Along with long matrix compatible polymer brushes, additional ligands can be attached on the surface with aim of adding functionality to the composite beyond what the intrinsic properties of the filler can offer. Multifunctional nanoparticles have been designed for enhancements in optical, biological, and dielectric properties. Schadler et al. have prepared high refractive index multifunctional grafted ZrO_2 nanoparticles for color converting LED encapsulants. Bimodal polydimethylsiloxane (PDMS) brushes were attached by "grafting-to" method on ZrO_2 nanoparticles with compatibility with a silicone matrix while an organic phosphor was also attached to the particle surface allowing for simultaneous particle dispersion and light color conversion.[65] Benicewicz et al.

investigated dye labeled polymethylacrylic acid (PMAA) grafted nanoparticles where PMAA polymers can bind to biomolecules and a fluorescent dye can be used to track particle movements in biological enviroments.[66] Possible property enhancements through multifunctional ligand engineering is dependent upon synthetic methodology capable of creating the highly decorated particles. Figure 1.3 highlights some of the advances in surface modification of nanoparticles from simple to complex. This thesis will discuss the application of multifunctional nanoparticles in the advancements made in dielectric nanocomposites.

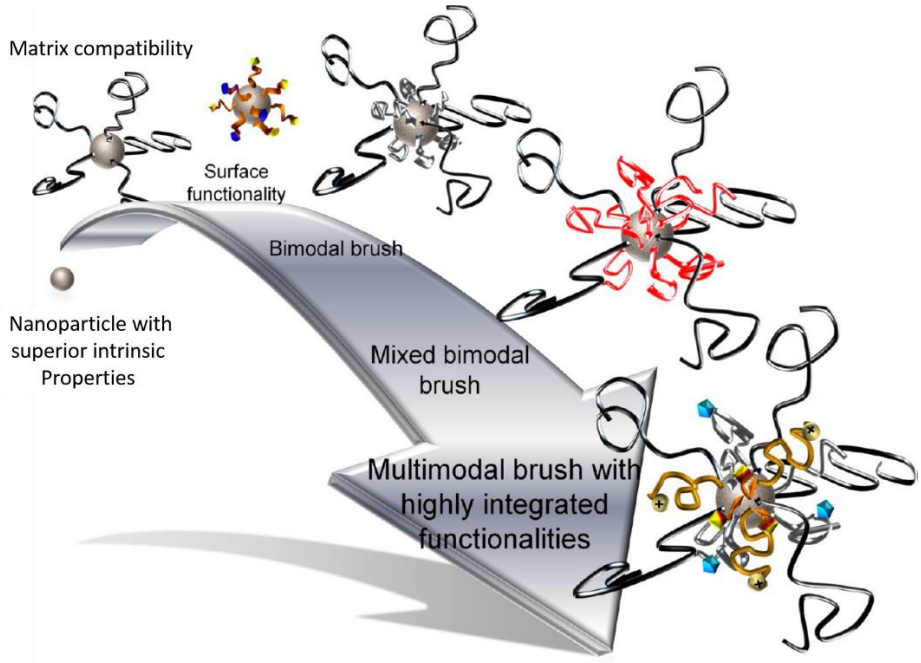

Figure 1.3. Evolution of surface modification on grafted nanoparticles: from simple to complex.[39]

1.4 Surface Functionalization via the RAFT Process

Nanoparticle modification via the RAFT polymerization has been extensively investigated due to its versatility and simplicity.[67] The attachment of the CTA is usually achieved by anchoring either the "Z" group or the "R" group on the nanoparticle surface, when modified accordingly. In the "Z" approach, the growing polymer chains must detach,

propagate, and then reattach to the surface. Therefore, the propagation actually occurs in the solution, so it is more like a "graft to" strategy.[68,69] In this approach, the propagating polymer radicals must get close to the surface to maintain the chain-transfer reaction with the CTA and this is restricted due to the steric hindrance of the neighboring grafted polymer chains. The propagating polymer radicals may drift away from the nanoparticle surface during the polymerization, leading to decreased graft density and free polymers in the solution. On the other hand, the "R" approach does not suffer from these disadvantages and is more popular due to its role as reinitiating species. Since the "R" groups are attached to the surface, thus the propagating polymer radicals are always on the surface during the polymerization. In a previous work from our group, Li and Benicewicz have anchored a CTA – 4-cyanopentanoic acid dithiobenzoate (CPDB) on silica nanoparticles (SiO_2) with precisely controllable graft density measured by UV-vis spectroscopy (Scheme 1.3), and conducted well-controlled RAFT polymerization of different monomers on the nanoparticles.[70] The process proved to be a versatile method for surface modification of silica nanoparticles with effective graft densities of 0.01 – 0.7 ch/nm^2 being achieved. The attachment method is facilitated by using RAFT agents containing carboxylic acids which are activated by 2-Mecatothiazoline and N-hydroxysuccinimide esters. In addition to dithioester-type RAFT agents, trithiocarbonates have also been used extensively both for free and surface initiated polymerization, which are claimed to be more robust and universal.[71–74] This thesis will discuss the application of trithiocarbonate for the polymerization of isoprene at high temperatures and will show that trithiocarbonate RAFT agents are more robust than dithioesters. SI-RAFT has allowed for synthesis of well-defined polymer-grafted particles to be used in nanocomposites for several applications

including hybrid materials, thermo-responsive, optical, electrical, self-healing, bio, and drug delivery.[75]

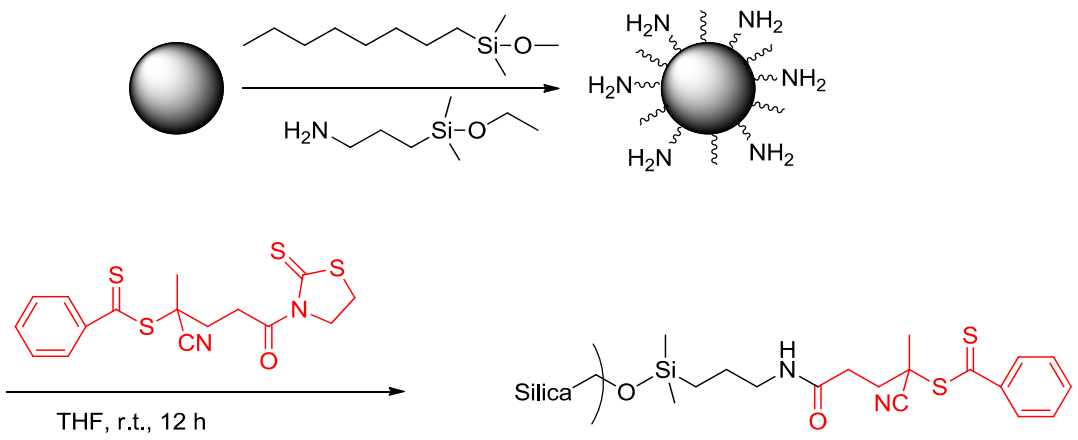

Scheme 1.3 Synthesis of CPDB functionalized silica nanoparticles.

1.6 Polyolefin Nanocomposites

Polyolefin materials account for almost half of the ~300 million tons of the global plastics production. This outstanding economic success reflects the significant progress made in reaction engineering and polyolefin processing by greatly improving manufacturing, performance, and economy of polyolefin products. Today, polyolefins are everywhere in our daily life. They meet the need of the rapidly growing world population for cost-, resource-, and energy-efficient, environmentally benign materials with low greenhouse gas emissions ("carbon footprint"), light weight, and versatility in terms of tailoring properties, applications, and recycling.[76–78] The highly diversified applications of polyolefins such as polyethylene and polypropylene are general packaging, lightweight engineering plastics for automotive and architectural applications, textiles, rubbers, food and medicine packaging, electrical and thermal insulation, as well as earthquake-proof pipes for safe transport of water and gas.[77–79]

Polyethylene is one of the most important and widely used plastics due to its inertness, low cost, good processability, light weight, and good mechanical properties.[80,81] PE nanocomposites are conventionally prepared by extreme extrusion mixing of inorganic particles with the polymer in the melt using small molecules or polymers as compatibilizers to improve the dispersion.[82,83] Jeziorska et al.[82] prepared Low-density polyethylene/spherical silica nanocomposites by melt-mixing method using glycidyl methacrylate grafted ethylene/n-octene copolymer (EOR-g-GMA) as a compatibilizer to improve the interfacial interaction in these nanocomposites to improve the dispersion of NPs and other mechanical properties. However, this method in most cases leads to large aggregates, significantly decreasing reinforcement. In recent years, a variety of new methods have been proposed for improving the dispersion of particles in PE. In situ particle synthesis within the polymer matrix as well as attachment of Ziegler-Natta catalysts on nanoparticle surfaces followed by ethylene polymerization have been reported.[84–87] However, these methods have the disadvantages of complexity, possible aggregation of particles and inhomogeneous dispersion throughout the matrix. Another method which has attracted more attention is grafting a type of alkyl molecule or an end-functionalized PE onto the particle surface through chemical bonding (grafting-to method).[88] This method has shown improvements in the dispersion of particles as well as in the interactions between the modified particles and the matrix. However, this method is restricted to low graft densities and low molecular weights because of the steric hindrance imposed by the already grafted chains, while it has been well established that high graft density brushes are necessary to screen attractive van der Waals interactions between particle cores.[89,90]

Polypropylene is another important and widely used polyolefin due to its good processability, mechanical and dielectric properties. Polypropylene nanocomposites have been extensively prepared by melt compounding with various types of fillers over the past 15 years.[91–95] In these cases, fillers are normally functionalized with a compatibilizer to become miscible and processable with polypropylene. For example, Yuan et al. prepared functionalized graphene oxide by reacting graphene oxide with maleic anhydride grafted polypropylene and then melt-blending with polypropylene to obtain the functionalized graphene oxide/polypropylene nanocomposites.[96]

Another method for dispersion of nanoparticles in polypropylene matrices has been in situ metallocene-catalyzed polymerization of propene in presence of nanoparticles. Zakrzewska et al.[97] used organo-modified aluminophosphate with kanemite-like structure for the in situ metallocene-catalyzed synthesis of polypropylene. However, this method is complicated and not very common or versatile.[94]

Polyolefins have become important dielectric materials because of their low cost, processability, and inherent high dielectric breakdown strength. It has been proven that incorporation of nano sized fillers can increase the dielectric breakdown strength of polymeric materials due to the large interface around the nano filler that introduces a charge trapping layer which can trap migrating charge preventing percolation across the matrix.[83,98–106] However, dispersion of the nano fillers throughout the matrix is believed to be critical for dielectric breakdown strength of the nanocomposites by disrupting the continuity of migrating charge through a torturous pathway.[107–110]

Modifications to dielectric filler surfaces with organic ligands have been made with the intention to improve the enthalpic interaction between nanoparticles and the polymeric

matrix. Shepherd et al.[111] reported the preparation of carbon black polypropylene dielectric nanocomposites through the modification of carbon black with tailored hexyl and dodecyl terminated diarylcarbene derivatives to reduce the incompatibility of the filler and matrix and therefore improve the dielectric properties of the nanocomposite.

1.7 Dissertation Motives and Outline

This dissertation focuses on the design, synthesis, and characterization of polymer nanocomposite interfaces through the functionalization of nanoparticles with new surface chemistries. Reversible addition fragmentation chain transfer (RAFT) polymerization was used for the grafting of polymer chains to the surface of silica nanoparticles to control the interface between the particles and the polymer matrix. Surface functionalization was studied with the aim of understanding the structure-property relationships of polymer grafted nanoparticles in nanocomposites.

Chapter 2 focuses on the SI-RAFT polymerization of long side-chain alkyl methacrylates such as hexyl, lauryl, and stearyl methacrylate on silica NPs. The kinetics of the free RAFT and SI-RAFT polymerizations were studied. Composites of linear low density polyethylene filled with PHMA, PLMA, and PSMA-g-SiO_2 NPs were prepared and analyzed to examine the effects of side chain length on the dispersibility of particles throughout the matrix. PSMA-g-SiO_2 showed the highest state of dispersion among the three modified particles. It was suggested that the 18 carbon long alkyl side chains make the PSMA more "olefin-like" and are responsible for the compatibility of PSMA-g-SiO_2 with polyethylene due to the molecular similarity. The effects of PSMA brush molecular weight and chain density on the dispersion of silica particles were investigated. The

interaction of grafted particles with crystalline polyethylene were also studied using DSC, WAXS, and SAXS.

Chapter 3 expands the findings of Chapter 2 on the compatibility of PSMA brush with polyolefins and takes the further step of introducing a bimodal architecture on the surface of particles containing PSMA brushes and conjugated anthracene ligands and studying its efficacy in polypropylene dielectric nanocomposites. The dispersion of monomodal and bimodal morphology in isotactic polypropylene was investigated. Furthermore, the effects of anthracene surface modification towards improving the dielectric breakdown strength under AC and DC conditions were studied.

Finally, Chapter 4 focuses on the SI-RAFT polymerization of isoprene on silica particles. A high temperature stable trithiocarbonate RAFT agent with controllable graft densities was used to afford the polyisoprene-grafted silica NPs (PIP-*g*-SiO_2 NPs). The polymerization of isoprene mediated by silica anchored RAFT agents with different densities were investigated and compared to the polymerization mediated by free RAFT agents. The effects of different temperatures, initiators, and monomer feed ratios on the kinetics of the SI-RAFT polymerization were also investigated. The well-defined PIP-*g*-SiO_2 NPs were mixed with a polyisoprene matrix to examine the dispersion of these NPs. Hydrogenated polyisoprene (HPIP)-grafted NPs were also synthesized by diimide-based hydrogenation of PIP-*g*-SiO_2 NPs. HPIP-*g*-SiO_2 NPs were then mixed in isotactic PP matrices to investigate their compatibility with polypropylene.

1.8 References

(1) Vazaios, A.; Lohse, D. J.; Hadjichristidis, N. *Macromolecules* **2005**, *38* (13), 5468–5474.

(2) Ishizone, T.; Han, S.; Okuyama, S.; Nakahama, S. *Macromolecules* **2003**, *36* (1), 42–49.

(3) Solomon, D. H.; Rizzardo, E.; Cacioli, P. Polymerization process and polymers produced thereby. U.S.P. 4,581,429, April 1986.

(4) Wang, J. S.; Matyjaszewski, K. *J. Am. Chem. Soc.* **1995**, *117* (6), 5614–5615.

(5) Chiefari, J.; Chong, Y. K. B.; Ercole, F.; Krstina, J.; Jeffery, J.; Le, T. P. T.; Mayadunne, R. T. a; Meijs, G. F.; Moad, C. L.; Moad, G.; Rizzardo, E.; Thang, S. H. *Macromolecules* **1998**, *31* (98), 5559–5562.

(6) Greszta, D.; Mardare, D.; Matyjaszewski, K. *Macromolecules* **1994**, *27*, 638–644.

(7) Catala, J. M.; Bubel, F.; Ouland Hammouch, S. *Macromolecules* **1995**, *28*, 8441–8443.

(8) Georges, M. K.; Veregin, R. P. N.; Kazmaier, P. M.; Hamer, G. K. *Macromolecules* **1993**, *26* (11), 2987–2988.

(9) Moad, G.; Rizzardo, E. *Macromolecules* **1995**, *28*, 8722–8728.

(10) Rizzardo, E.; Serelis, A.; Solomon, D. *Aust. J. Chem.* **1982**, *35* (10), 2013.

(11) Hawker, C. J.; Bosman, A. W.; Harth, E. *Chem. Rev.* **2001**, *101* (12), 3661–3688.

(12) Guillaneuf, Y.; Gigmes, D.; Marque, S. R. A.; Astolfi, P.; Greci, L.; Tordo, P.; Bertin, D. *Macromolecules* **2007**, *40* (9), 3108–3114.

(13) Couvreur, L.; Lefay, C.; Belleney, J.; Charleux, B.; Guerret, O.; Magnet, S. *Macromolecules* **2003**, *36* (22), 8260–8267.

(14) Nicolas, J.; Charleux, B.; Guerret, O.; Magnet, S. *Angew. Chemie* **2004**, *116* (45), 6312–6315.

(15) Chong, Y. K.; Ercole, F.; Moad, G.; Rizzardo, E.; Thang, S. H.; Anderson, A. G.

Macromolecules **1999**, *32* (21), 6895–6903.

(16) Husseman, M.; Malmstrom, E. E.; McNamara, M.; Mate, M.; Mecerreyes, D.; Benoit, D. G.; Hedrick, J. L.; Mansky, P.; Huang, E.; Russell, T. P.; Hawker, C. J. *Macromolecules* **1999**, *32* (5), 1424–1431.

(17) Chevigny, C.; Gigmes, D.; Bertin, D.; Jestin, J.; Boué, F. *Soft Matter* **2009**, *5* (19), 3741.

(18) Colombani, D. *Prog. Polym. Sci.* **1997**, *22* (8), 1649–1720.

(19) Huang, X.; Wirth, M. J. *Anal. Chem.* **1997**, *69*, 4577–4580.

(20) Barbey, R.; Lavanant, L.; Paripovic, D.; Schuwer, N.; Sugnaux, C.; Tugulu, S.; Klok, H.-A. *Chem. Rev.* **2009**, *109*, 5437–5527.

(21) Fristrup, C. J.; Jankova, K.; Hvilsted, S. *Soft Matter* **2009**, *5* (23), 4623.

(22) Singh, N.; Wang, J.; Ulbricht, M.; Wickramasinghe, S. R.; Husson, S. M. *J. Memb. Sci.* **2008**, *309* (1–2), 64–72.

(23) Marutani, E.; Yamamoto, S.; Ninjbadgar, T.; Tsujii, Y.; Fukuda, T.; Takano, M. *Polymer (Guildf).* **2004**, *45* (7), 2231–2235.

(24) Chen, R.; Feng, W.; Zhu, S.; Botton, G.; Ong, B.; Wu, Y. *J. Polym. Sci. Part A Polym. Chem.* **2006**, *44* (3), 1252–1262.

(25) Yang, W. J.; Neoh, K.-G.; Kang, E.-T.; Lee, S. S. C.; Teo, S. L.-M.; Rittschof, D. *Biofouling* **2012**, *28* (9), 895–912.

(26) Lee, S. H.; Dreyer, D. R.; An, J.; Velamakanni, A.; Piner, R. D.; Park, S.; Zhu, Y.; Kim, S. O.; Bielawski, C. W.; Ruoff, R. S. *Macromol. Rapid Commun.* **2010**, *31* (3), 281–288.

(27) Morandi, G.; Heath, L.; Thielemans, W. *Langmuir* **2009**, *25* (14), 8280–8286.

(28) Sun, Y.; Ding, X.; Zheng, Z.; Cheng, X.; Hu, X.; Peng, Y. *Eur. Polym. J.* **2007**, *43* (3), 762–772.

(29) Charmot, D.; Corpart, P.; Adam, H.; Zard, S. Z.; Biadatti, T.; Bouhadir, G. *Macromol. Symp.* **2000**, *150* (Polymers in Dispersed Media), 23–32.

(30) Keddie, D. J.; Moad, G.; Rizzardo, E.; Thang, S. H. *Macromolecules* **2012**, *45* (13), 5321–5342.

(31) Moad, G.; Rizzardo, E.; Thang, S. H. *Aust. J. Chem.* **2005**, *58* (6), 379–410.

(32) Moad, G.; Rizzardo, E.; Thang, S. H. *Aust. J. Chem.* **2009**, *62* (11), 1402–1472.

(33) Moad, G.; Rizzardo, E.; Thang, S. H. *Aust. J. Chem.* **2006**, *59* (10), 669–692.

(34) Schadler, L. S.; Kumar, S. K.; Benicewicz, B. C.; Lewis, S. L.; Harton, S. E. *MRS Bull.* **2007**, *32* (4), 335–340.

(35) Winey, K. I.; Vaia, R. A. *MRS Bull.* **2007**, *32* (4), 314–322.

(36) Hule, R. A.; Pochan, D. J. *MRS Bull.* **2007**, *32* (4), 354–358.

(37) Krishnamoorti, R. *MRS Bull.* **2007**, *32* (4), 341–347.

(38) Baur, J.; Silverman, E. *MRS Bull.* **2007**, *32* (4), 328–334.

(39) Li, Y.; Krentz, T. M.; Wang, L.; Benicewicz, B. C.; Schadler, L. S. *ACS Appl. Mater. Interfaces* **2014**, *6* (9), 6005–6021.

(40) Nelson, J. K.; Hu, Y. *J. Phys. D. Appl. Phys.* **2005**, *38* (2), 213–222.

(41) Mackay, M. E.; Tuteja, A.; Duxbury, P. M.; Hawker, C. J.; Van Horn, B.; Guan, Z.; Chen, G.; Krishnan, R. S. *Science* **2006**, *311* (5768), 1740–1743.

(42) Kumar, S. K.; Krishnamoorti, R. *Annu. Rev. Chem. Biomol. Eng.* **2010**, *1* (1), 37–58.

(43) Hasegawa, R.; Aoki, Y.; Doi, M. *Macromolecules* **1996**, *29* (20), 6656–6662.

(44) Green, P. F. *Soft Matter* **2011**, *7* (18), 7914.

(45) Ojha, S.; Dang, A.; Hui, C. M.; Mahoney, C.; Matyjaszewski, K.; Bockstaller, M. R. *Langmuir* **2013**, *29* (28), 8989–8996.

(46) Bansal, A.; Yang, H.; Li, C.; Benicewicz, B. C.; Kumar, S. K.; Schadler, L. S. *J. Polym. Sci. Part B Polym. Phys.* **2006**, *44* (20), 2944–2950.

(47) Meli, L.; Arceo, A.; Green, P. F. *Soft Matter* **2009**, *5* (3), 533–537.

(48) Kumar, S. K.; Jouault, N.; Benicewicz, B.; Neely, T. *Macromolecules* **2013**, *46* (9), 3199–3214.

(49) García-González, C. A.; Fraile, J.; López-Periago, A.; Domingo, C. *J. Colloid Interface Sci.* **2009**, *338* (2), 491–499.

(50) Tomovska, R.; Daniloska, V.; Asua, J. M. *Appl. Surf. Sci.* **2013**, *264*, 670–673.

(51) Tao, P.; Viswanath, A.; Schadler, L. S.; Benicewicz, B. C.; Siegel, R. W. *ACS Appl. Mater. Interfaces* **2011**, *3* (9), 3638–3645.

(52) Li, J.; Wang, L.; Benicewicz, B. C. *Langmuir* **2013**, *29* (37), 11547–11553.

(53) Ranjan, R.; Ranjan, R.; Brittain, W. J.; Brittain, W. J. *Macromolecules* **2007**, *40* (17), 6217–6223.

(54) Ranjan, R.; Brittain, W. J. *Macromol. Rapid Commun.* **2007**, *28* (21), 2084–2089.

(55) Ranjan, R.; Brittain, W. J. *Macromol. Rapid Commun.* **2008**, *29* (12–13), 1104–1110.

(56) Pyun, J.; Jia, S.; Kowalewski, T.; Patterson, G. D.; Matyjaszewski, K. *Macromolecules* **2003**, *36* (14), 5094–5104.

(57) Huang, Y.; Liu, Q.; Zhou, X.; Perrier, S.; Zhao, Y. *Macromolecules* **2009**, *42* (15), 5509–5517.

(58) Natarajan, B.; Neely, T.; Rungta, A.; Benicewicz, B. C.; Schadler, L. S. *Macromolecules* **2013**, *46* (12), 4909–4918.

(59) Hsiue, G. H.; Chu, L. W.; Lin, I. N. *Colloids Surfaces A Physicochem. Eng. Asp.* **2007**, *294* (1–3), 212–220.

(60) Gao, J.; Li, J.; Benicewicz, B. C.; Zhao, S.; Hillborg, H.; Schadler, L. S. *Polymers (Basel).* **2012**, *4* (1), 187–210.

(61) Husseman, M.; Malmstrom, E. E.; McNamara, M.; Mate, M.; Mecerreyes, D.; Benoit, D. G.; Hedrick, J. L.; Mansky, P.; Huang, E.; Russell, T. P.; Hawker, C. J. *Macromolecules* **1999**, *32* (5), 1424–1431.

(62) Gao, J.; Li, J.; Zhao, S.; Benicewicz, B. C.; Hillborg, H.; Schadler, L. S. *Polym. (United Kingdom)* **2013**, *54* (15), 3961–3973.

(63) Pyun, J.; Matyjaszewski, K.; Kowalewski, T.; Savin, D.; Patterson, G.; Kickelbick, G.; Huesing, N. *Journal of the American Chemical Society* **2001**, *119*, 9445–9446.

(64) Matyjaszewski, K.; Miller, P. J.; Shukla, N.; Immaraporn, B.; Gelman, A.; Luokala, B. B.; Siclovan, T. M.; Kickelbick, G.; Vallant, T.; Hoffmann, H.; Pakula, T. *Macromolecules* **1999**, *32* (26), 8716–8724.

(65) Li, Y.; Tao, P.; Siegel, R. W.; Schadler, L. S. *MRS Proc.* **2013**, *1547*, 161–166.

(66) Wang, L.; Benicewicz, B. C. *ACS Macro Lett.* **2013**, *2* (2), 173–176.

(67) Raula, J.; Shan, J.; Nuopponen, M.; Niskanen, A.; Jiang, H.; Kauppinen, E. I.; Tenhu, H. *Langmuir* **2003**, *19* (8), 3499–3504.

(68) Zhao, Y.; Perrier, S. *Macromolecules* **2006**, *39* (25), 8603–8608.

(69) Stenzel, M. H.; Zhang, L.; Huck, W. T. S. *Macromol. Rapid Commun.* **2006**, *27* (14), 1121–1126.

(70) Li, C.; Han, J.; Ryu, C. Y.; Benicewicz, B. C. *Macromolecules* **2006**, *39* (9), 3175–3183.

(71) Ohno, K.; Ma, Y.; Huang, Y.; Mori, C.; Yahata, Y.; Tsujii, Y.; Maschmeyer, T.; Moraes, J.; Perrier, S. *Macromolecules* **2011**, *44* (22), 8944–8953.

(72) Jitchum, V.; Perrier, S. *Macromolecules* **2007**, *40* (5), 1408–1412.

(73) Germack, D. S.; Wooley, K. L. *J. Polym. Sci. Part A Polym. Chem.* **2007**, *45* (17), 4100–4108.

(74) Khani, M. M.; Abbas, Z. M.; Benicewicz, B. C. *J. Polym. Sci. Part A Polym. Chem.* **2017**.

(75) Boyer, C.; Stenzel, M. H.; Davis, T. P. *J. Polym. Sci. Part A Polym. Chem.* **2011**, *49* (3), 551–595.

(76) Sturzel, M.; Mihan, S.; Mulhaupt, R. *Chemical Reviews*. **2016**, 117 (3), 1398–1433.

(77) Chum, P. S.; Swogger, K. W. *Progress in Polymer Science (Oxford)*. **2008**, 797–819.

(78) Galli, P.; Vecellio, G. *Prog. Polym. Sci.* **2001**, *26* (8), 1287–1336.

(79) Piringer, O. G.; Baner, A. L. *Plastic Packaging: Interactions with Food and Pharmaceuticals, Second Edition*; Piringer, O. G., Baner, A. L., Eds.; Wiley-VCH Verlag GmbH & Co. KGaA: Weinheim, Germany, 2008.

(80) Dorigato, A.; Pegoretti, A. *J Polym Res* **2013**, *20*, 92.

(81) Malpass, B. D. *Introduction to Industrial Polyethylene*; John Wiley & Sons and Scrivener Publishing LCC: Salem, 2010.

(82) Jeziórska, R.; Świerz-Motysia, B.; Zielecka, M.; Szadkowska, A.; Studziński, M.

Journal of Applied Polymer Science **2012,** *125*, 4326–4337.

(83) Ma, D.; Hugener, T. a; Siegel, R. W.; Christerson, A.; Mårtensson, E.; Önneby, C.; Schadler, L. S. *Nanotechnology* **2005**, *16* (6), 724–731.

(84) McNally, T.; Pötschke, P.; Halley, P.; Murphy, M.; Martin, D.; Bell, S. E. J.; Brennan, G. P.; Bein, D.; Lemoine, P.; Quinn, J. P. *Polymer (Guildf).* **2005**, *46* (19), 8222–8232.

(85) Wang, T.-L.; Ou, C.-C.; Yang, C.-H. *J. Appl. Polym. Sci.* **2008**, *109* (5), 3421–3430.

(86) Monteil, V.; Stumbaum, J.; Thomann, R.; Mecking, S. *Macromolecules* **2006**, *39* (6), 2056–2062.

(87) Zhu, J.; Wei, S.; Li, Y.; Sun, L.; Haldolaarachchige, N.; Young, D. P.; Southworth, C.; Khasanov, A.; Luo, Z.; Guo, Z. *Macromolecules* **2011**, *44* (11), 4382–4391.

(88) Bieligmeyer, M.; Taheri, S. M.; German, I.; Boisson, C.; Probst, C.; Milius, W.; Altstädt, V.; Breu, J.; Schmidt, H.-W.; D'Agosto, F.; Förster, S. *J. Am. Chem. Soc.* **2012**, *134* (44), 18157–18160.

(89) Rungta, A.; Natarajan, B.; Neely, T.; Dukes, D.; Schadler, L. S.; Benicewicz, B. C. *Macromolecules* **2012**, *45* (23), 9303–9311.

(90) Ferreira, P. G.; Ajdari, A.; Leibler, L. *Macromolecules* **1998**, *31* (12), 3994–4003.

(91) Motha, K.; Hippi, U.; Hakala, K.; Peltonen, M.; Ojanperä, V.; Löfgren, B.; Seppälä, J. *J. Appl. Polym. Sci.* **2004**, *94* (3), 1094–1100.

(92) Jiang, C.; Markutsya, S.; Pikus, Y.; Tsukruk, V. V. *Nat. Mater.* **2004**, *3* (10), 721–728.

(93) Kaempfer, D.; Thomann, R.; Mülhaupt, R. *Polymer (Guildf).* **2002**, *43* (10), 2909–

2916.

(94) Leone, G.; Bertini, F.; Canetti, M.; Boggioni, L.; Stagnaro, P.; Tritto, I. *J. Polym. Sci. Part A Polym. Chem.* **2008**, *46* (16), 5390–5403.

(95) Xu, L.; Nakajima, H.; Manias, E.; Krishnamoorti, R. *Macromolecules* **2009**, *42* (11), 3795–3803.

(96) Yuan, B.; Bao, C.; Song, L.; Hong, N.; Liew, K. M.; Hu, Y. *Chem. Eng. J.* **2014**, *237*, 411–420.

(97) Zakrzewska, S.; Dos Ouros, A. C.; Schramm, N.; Jehnichen, D.; Häussler, L.; Pospiech, D.; Voit, B.; Schulze, U.; Pastore, H. O. *Eur. Polym. J.* **2015**, *65*, 238–251.

(98) Brandstetter, S. S.; Drummy, L. F.; Horwath, J. C.; Schweickart, D. L.; Vaia, R. A. In *2008 IEEE International Power Modulators and High-Voltage Conference*; IEEE, 2008; pp 287–290.

(99) Tomer, V.; Manias, E.; Randall, C. A. *J. Appl. Phys.* **2011**, *110* (4), 0–10.

(100) Tomer, V.; Polizos, G.; Manias, E.; Randall, C. A. *J. Appl. Phys.* **2010**, *108* (7).

(101) Tomer, V.; Polizos, G.; Randall, C. A.; Manias, E. *J. Appl. Phys.* **2011**, *109* (7).

(102) Imai, T.; Sawa, F.; Nakano, T.; Ozaki, T.; Shimizu, T.; Kozako, M.; Tanaka, T. *IEEE Trans. Dielectr. Electr. Insul.* **2006**, *13* (2), 319–325.

(103) Tanaka, T.; Kozako, M.; Fuse, N.; Ohki, Y. *IEEE Trans. Dielectr. Electr. Insul.* **2005**, *12* (4), 669–681.

(104) Smith, R.; Liang, C.; Landry, M.; Nelson, J.; Schadler, L. *IEEE Trans. Dielectr. Electr. Insul.* **2008**, *15* (1), 187–196.

(105) Roy, M.; Nelson, J. K.; MacCrone, R. K.; Schadler, L. S.; Reed, C. W.; Keefe, R.;

Zenger, W. *IEEE Trans. Dielectr. Electr. Insul.* **2005**, *12* (4), 629–643.

(106) Roy, M.; Nelson, J. K.; MacCrone, R. K.; Schadler, L. S. *J. Mater. Sci.* **2007**, *42* (11), 3789–3799.

(107) Gao, M.; Zhang, P.; Wang, F.; Li, L.; Li, Z. In *2013 Annual Report Conference on Electrical Insulation and Dielectric Phenomena*; IEEE, 2013; pp 234–237.

(108) Tkalya, E.; Ghislandi, M.; Otten, R.; Lotya, M.; Alekseev, A.; Van Der Schoot, P.; Coleman, J.; De With, G.; Koning, C. *ACS Appl. Mater. Interfaces* **2014**, *6* (17), 15113–15121.

(109) Grabowski, C. a.; Fillery, S. P.; Westing, N. M.; Chi, C.; Meth, J. S.; Durstock, M. F.; Vaia, R. a. *ACS Appl. Mater. Interfaces* **2013**, *5* (12), 5486–5492.

(110) Tan, D.; Cao, Y.; Tuncer, E.; Irwin, P. *Mater. Sci. Appl.* **2013**, *4* (April), 6–15.

(111) Shepherd, C.; Hadzifejzovic, E.; Shkal, F.; Jurkschat, K.; Moghal, J.; Parker, E. M.; Sawangphruk, M.; Slocombe, D. R.; Foord, J. S.; Moloney, M. G. *Langmuir* **2016**, *32* (31), 7917–7928.

CHAPTER 2

POLY(ALKYL METHACRYLATE)-GRAFTED SILICA NANOPARTICLES IN LINEAR LOW DENSITY POLYETHYLENE NANOCOMPOSITE*

*This chapter was adapted from Khani et al., *Polymer* **2017**, *109*, 339-348.[1]

2.1 Abstract

Surface-initiated reversible addition-fragmentation chain transfer (SI-RAFT) polymerization has been widely used to synthesize various polymers grafted from nanoparticles (NPs) for incorporation into polymer nanocomposites. It is believed that these grafted polymer brushes, with a similar chemistry as the matrix polymer, can be employed to improve NP dispersion by reducing unfavorable interactions between the inorganic NPs and organic matrices. While controlled radical polymerization methods do not allow the polymerization of polyolefins, a substitute strategy is controllably attaching polyolefin-like polymers onto the NP surface. In the present work, the SI-RAFT polymerization was used to anchor poly(hexyl, lauryl, and stearyl methacrylate) on silica NPs, showing good control of the polymerizations. The long alkyl side chains can create an "olefin-like" interface and improve the compatibility of modified particles with polyolefins. Subsequently, we investigated the dispersion of these poly(alkyl methacrylate)-modified silica NPs in linear low density polyethylene (LLDPE). Poly(stearyl methacrylate)-grafted silica NPs (PSMA-g-SiO_2) demonstrated improved dispersion of particles when compared to shorter alkyl side chain methacrylates. TEM images showed that the dispersion of these particles was highly dependent upon the molecular weight and density of the grafted PSMA chains. Differential scanning calorimetry (DSC), wide-angle X-ray scattering (WAXS), small-angle X-ray scattering (SAXS), and dynamic mechanical analysis (DMA) were used to characterize these nanocomposites. SAXS showed that the inter-particle distance (distribution of particle spacings) in the semicrystalline state was broader than in the melt, suggesting that particles spacing was affected by the polyethylene crystallization particularly at lower loadings.

Nanocomposites at low loadings, 0.5 wt% core content, showed significant improvement in storage modulus due to the compatible particle-matrix interface. Further increases in particle loadings, however reversed this trend likely due to the increase in soft PSMA content.

2.2 Introduction

It has been well accepted that the incorporation of a small volume fraction of nanoparticles into a polymer matrix can lead to a large property enhancement.[2,3] However, these enhancements depend strongly on the NPs dispersion and the nature of the nanoparticle−polymer interface.[4–6] One strategy to control the interface is to covalently attach a polymer with the same chemistry as that of the matrix onto the surface of NPs. Other variables influencing the interface are the grafting density and the chain length of the grafted polymer. Control over such variables can be used to create an attractive interface due to the better entanglement and wetting of the grafted chains and the matrix.[7–10] For example, we have shown that grafting of polystyrene chains onto the silica nanoparticles in a suitable range of chain densities and chain lengths and mixing it with polystyrene matrix can result in superior dispersion and offer improved mechanical properties.[11–13]

In contrast to the case of non-crystalline polystyrene nanocomposites, dispersion of NPs in polyolefins is a greater challenge. Polyolefins are semi-crystalline polymers with phase separated amorphous and crystalline domains. As the size of the particles decreases to the nano-level and especially smaller than higher-order structures in semi-crystalline polymers, particles can interact with these crystalline structures which may lead to even more aggregation of NPs or changes in the matrix crystalline structure.[14,15]

Polyethylene (PE) is one of the most important and widely used plastics due to its inertness, low cost, good processability, light weight, and good mechanical properties.[16,17] PE nanocomposites are conventionally prepared by extreme extrusion mixing of inorganic particles with the polymer in the melt which in most cases leads to large aggregates, significantly decreasing reinforcement.[18] In recent years, a variety of new methods have been proposed for improving the dispersion of particles in PE. In situ particle synthesis within the polymer matrix as well as attachment of Ziegler-Natta catalysts on nanoparticle surfaces followed by ethylene polymerization have been reported.[19–22] However, these methods have the disadvantages of complexity, possible aggregation of particles and inhomogeneous dispersion throughout the matrix. Another method which has attracted more attention is grafting a type of alkyl molecule or an end-functionalized PE onto the particle surface through chemical bonding (grafting-to method).[15,18] This method has shown some improvements in the dispersion of particles as well as in the interactions between the modified particles and the matrix. However, this method is restricted to low graft densities and low molecular weights because of the steric hindrance imposed by the already grafted chains, while it has been well established that high graft density brushes are necessary to screen attractive van der Waals interactions between particle cores.[23,24] An alternative is the grafting-from approach in which the initiating sites are attached to the substrate surface. Polymerization is then conducted from the particle surface to prepare polymer-grafted NPs.[25,26] We have previously shown that the grafting-from strategy has advantages over the grafting-to since we can achieve a wide range of chain densities and molecular weights by performing the radical polymerization of the desired monomer on the surface of the substrate.[27] While controlled radical polymerization methods do not

allow the polymerization of PE, a substitute strategy could be controllably attaching polyolefin-like polymers onto the NP surface. In this work, we studied the RAFT polymerization of long side-chain methacrylates on silica NPs. These polymers were chosen because of the chemical similarity of their "olefin-like" side-chains to PE. We then investigated the dispersion and properties of the poly(alkyl methacrylate)-modified silica NPs with different side-chain lengths, chain densities, and overall chain lengths in a linear low density polyethylene (LLDPE) matrix.

2.3 Experimental

Materials

LLDPE (Dowlex 2045, Mn = 34676 g/mol, PDI = 3.55) was supplied by Sealed Air Co. HPLC grade anhydrous THF was purchased from Fisher Scientific and used without further purification. Colloidal silica nanoparticles (15 nm, 30 wt % in methyl isobutyl ketone (MIBK)) were supplied by Nissan Chemicals Inc. Lauryl methacrylate (97%, Acros), stearyl methacrylate (95%, TCI America), and hexyl methacrylate (98%, TCI America) were passed through a basic alumina column to remove the inhibitor before use. Other materials utilized in the RAFT polymerization synthesis of grafted nanoparticles have been reported earlier.[23]

Synthesis of CPDB-g-SiO_2 nanoparticles

In a typical experiment, a solution (20 mL) of colloidal silica particles (30 wt % in methyl isobutyl ketone) was added to a two-necked round bottom flask and diluted with 40 mL of THF. 3-Aminopropyldimethylethoxysilane (0.32 mL, 2 mmol) was added and the mixture was refluxed in a 75 °C oil bath for 5 hours under nitrogen protection. The reaction was then cooled to room temperature and precipitated in a large amount of hexanes (300

mL). The particles were then recovered by centrifugation and dispersed in THF using sonication and precipitated in hexanes again. The amine-functionalized particles were then dispersed in 40 mL of THF for further reaction. Then 0.2 g, (0.4 mmol) of activated 4-cyano-4-(phenylcarbonylthioylthio)pentanoate (CPDB) was prepared as described previously [27] and added dropwise to a THF solution of the amine functionalized silica nanoparticles (40 mL, 6 g) at room temperature. After complete addition, the solution was stirred overnight. The reaction mixture was then precipitated into a large amount of hexanes (300 mL). The particles were recovered by centrifugation at 3000 rpm for 8 min. The particles were redispersed in 30 mL THF using sonication and precipitated in hexanes. This dissolution−precipitation procedure was repeated two more times until the supernatant layer after centrifugation was colorless, indicating the complete removal of ungrafted CPDB from the particles. The pink CPDB-anchored silica nanoparticles were dried under vacuum at room temperature and analyzed using UV analysis to determine the chain density using a calibration curve constructed from standard solutions of free CPDB.

Surface-initiated RAFT polymerization of alkyl methacrylate

CPDB-g-SiO_2 NPs with surface density of 41.9 μmol/g (6 g, 0.251 mmol), monomer (125.7 mmol), THF (1 L), and AIBN initiator (0.025 mmol) with a ratio between species of [monomer]:[CTA]:[initiator] = 500:1:0.1 were added to a round bottom flask. The particles were dispersed into the solution via sonication for 2 min and subsequently the mixture was purged by nitrogen for 30 min and then was placed in an oil bath set at 60 °C. The polymerization was stopped after various times (hr) by quenching in ice water. The resultant polymer grafted particles were then precipitated into a large amount of isopropanol and centrifuged at 5,000 rpm for 5 min and the particles were dispersed back

into THF. A small number of particles were set aside and the chains were cleaved using hydrofluoric acid and analyzed for molecular weight and PDI measurements.

Composite preparation

Various poly(alkyl methacrylate)-modified NPs solutions in THF were mixed with a 5% solution of LLDPE in toluene in appropriate quantities at 100 °C. The solution was stirred for 10 minutes and was cast on glass and dried in vacuum for 24 hrs and then annealed at 150 °C for several hours. The final film was peeled off to be used for further characterizations.

Instrumentation

The composites were embedded in epoxy and cryo-microtomed at -160 °C into 100-150 nm slices using a diamond knife. Sections were collected on a copper grid for transmission electron microscopy (TEM). The microstructures were imaged on a Hitachi H8000 TEM operating at an accelerating voltage of 200 kV. TGA characterization was operated using a TA Instruments Q5000 with a heating rate of 10 °C/min from 25 °C to 1000 °C under nitrogen flow. NMR spectra for kinetic studies were recorded on a Varian 300 spectrometer using $CDCl_3$ as a solvent. Molecular weights and dispersity ($Đ$) were measured using a Polymer Labs PL-GPC-120 gel permeation chromatograph (GPC) associated with a 515 HPLC pump, a 2410 refractive index detector, and three Styragel columns. The columns consisted of HR1, HR3 and HR4 which have corresponding effective molecular weight ranges of 100-5000, 500-30000, and 5000-500000, respectively. The GPC used tetrahydrofuran (THF) as eluent at 30 °C and a flow rate of 1.0 mL/min with the calibration of poly(methyl methacrylate) standards obtained from Polymer Laboratories. Differential scanning calorimetry (DSC) was performed using a TA

Instruments DSC Q-2000 with steady heating and cooling rates of 10 °C/min and nitrogen flow rate of 20 mL/min. Dynamic mechanical analysis tests were performed using a TA Instruments RSAIII dynamic mechanical analyzer (DMA). The tests were run on 0.2 mm thick films from -140 to 100 °C, using a heating rate of 3 °C min^{-1}. They were performed in tensile mode with strain rate of 0.1% and at frequency of 1Hz. Small-angle X-ray scattering (SAXS) experiments were conducted using a SAXS LAB Ganesha at the South Carolina SAXS Collaborative of the University of South Carolina. A Xenocs GeniX3D microfocus source was used with a copper target to generate a monochromic beam with a 0.154 nm wavelength. The instrument was calibrated using a silver behenate reference with the first order scattering vector $q^* = 1.076\ nm^{-1}$, where $q = 4\pi\lambda^{-1}\sin\theta$ with a total scattering angle of 2θ. Each data were acquired for about 30 min with an incident X-ray flux of ~1.5 M photons/s. Samples were first analyzed at room temperature and then heated to 150 °C for 1 hour and analyzed in the melt in order to compare the dispersion of particles.

2.4 Results and Discussion

Surface initiated RAFT polymerization of alkyl methacrylate

Scheme 2.1 shows three different polymers studied in this work: Poly(hexyl methacrylate) (PHMA), poly(lauryl methacrylate) (PLMA), and poly(stearyl methacrylate) (PSMA). PLMA and PSMA are semicrystaline polymers since their alkyl side chains crystallize in spite of an amorphous backbone.[28]

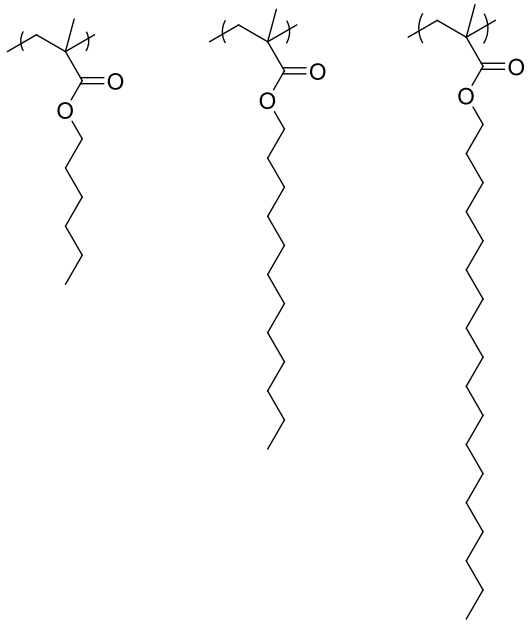

Scheme 2.1. Chemical structures of poly(hexyl, lauryl, and stearyl methacrylates).

Using the grafting-from approach, we have previously demonstrated the synthesis of polymer-grafted particles using the RAFT polymerization technique from surface-anchored chain transfer agents, which in this work were used to prepare poly(alkyl methacrylate)-g-silica NPs (Scheme 2.2).[27] In this process, a mercaptothiazoline activated-CPDB (4-cyano-4-(phenylcarbonylthioylthio)pentanoate) chain transfer agent was anchored onto the surface of silica nanoparticles functionalized with amine groups. This approach has been used to prepare CPDB-grafted silica nanoparticles (CPDB-g-SiO_2) with graft densities varying from 0.01−0.68 RAFT agents/nm^2 by controlling the ratio of silica nanoparticles to 3-aminopropyldimethylethoxysilane.[27,29]

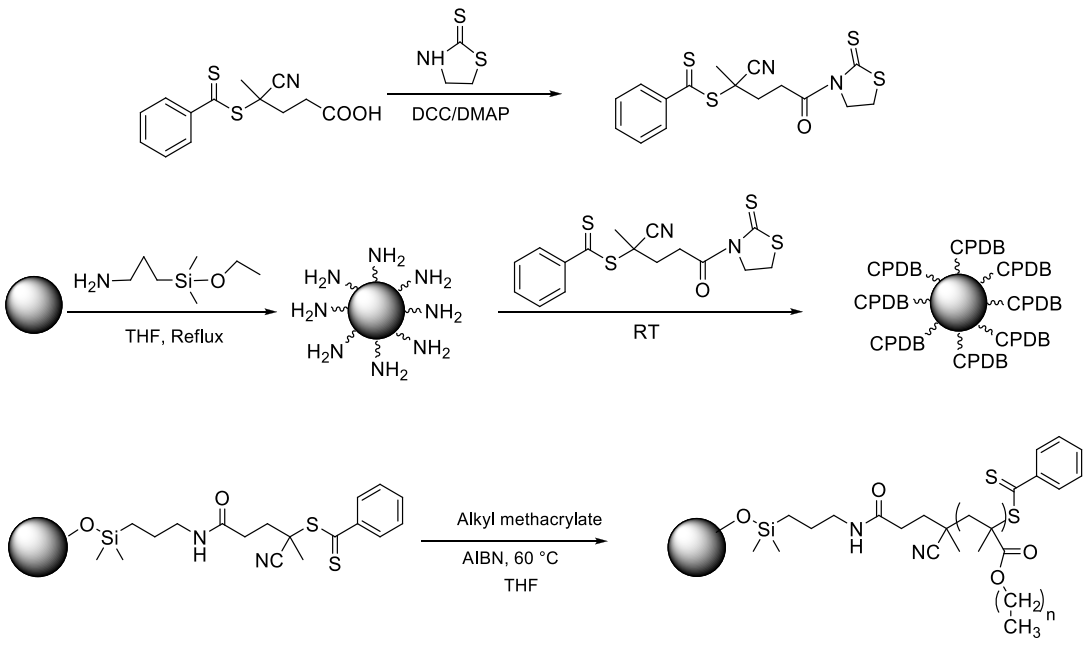

Scheme 2.2. Modification of silica nanoparticles by poly(alkyl methacrylates) using the RAFT technique.

We have previously reported the synthesis and kinetic studies of the surface-initiated RAFT polymerization of HMA.[30] Here we studied the RAFT polymerization of SMA and LMA in solution and on the surface of nanoparticles. SI-RAFT polymerization of stearyl methacrylate was carried out from the surface of CPDB-g-SiO_2 to give poly(stearyl methacrylate) brush-anchored silica nanoparticles (PSMA-g-SiO_2). Azobisisobutyronitrile was used as the initiator and a 10:1 [CPDB]/[AIBN] ratio utilized for all polymerizations. Low AIBN concentrations minimized the amount of free polymer and still maintained a moderate polymerization rate.[25] The weight ratio of THF/SMA was kept high (~ 6) for all SMA polymerizations since high concentrations of hydrophobic SMA caused silica particles to aggregate. Therefore, particles were diluted down in THF prior to addition of monomer. The polymerization reaction was carried out at 60 °C for a desired time and then precipitated in methanol. PSMA chains were etched from the silica

nanoparticles by hydrofluoric acid and were analyzed by GPC analysis. The GPC traces of the cleaved PSMA and PLMA are shown in Figures 2.1 and 2.2 respectively.

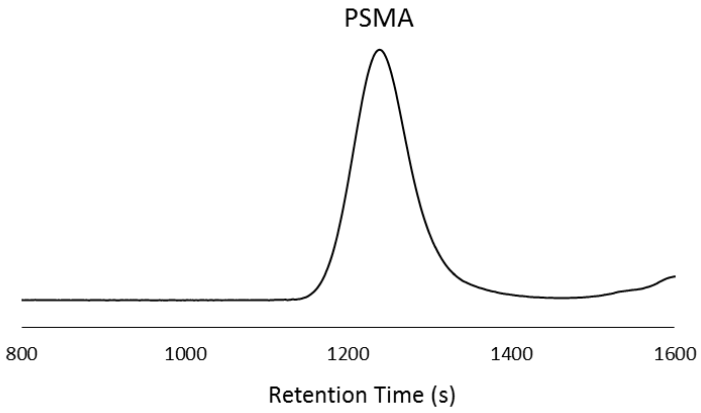

Figure 2.1. GPC trace of PSMA chains (Mn = 110 kg/mol, relative to PMMA standards, *Đ* = 1.25) cleaved from PSMA-g-SiO_2 NPs.

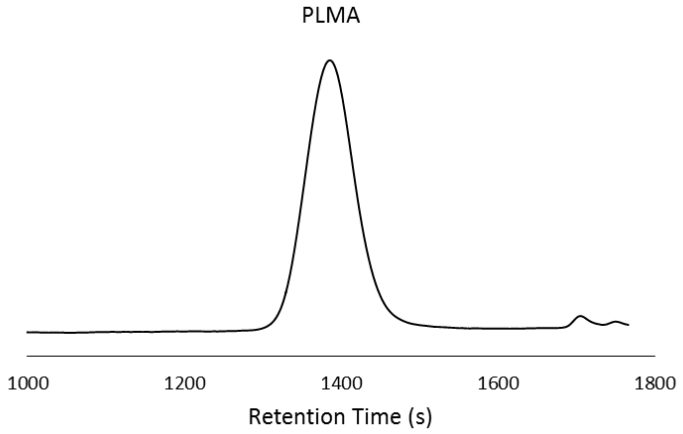

Figure 2.2. GPC trace of PLMA chains (Mn = 55 kg/mol, relative to PMMA standards, *Đ* = 1.12) cleaved from PLMA-g-SiO_2 NPs.

The kinetic study of SI-RAFT polymerization of SMA on nanoparticles (coated CPDB density: 0.16 agents/nm^2) was followed over 19 h to demonstrate the living character of the RAFT process. Figure 2.3a shows the pseudo-first-order rate plot for this polymerization. The ratio between the species of [SMA]/[CPDB]/[AIBN] was 1000:1:0.1 in THF with a monomer concentration of 25% wt/vol. Conversion of monomer was

determined by ^{1}H NMR by comparing the vinyl hydrogens of the monomer with those of trioxane. A linear relationship between $\ln([M_0]/[M_t])$ (where M_0 is the initial monomer concentration and M_t is the monomer concentration at time t) and polymerization time was observed after an induction time of 3 hours, which implies a constant radical concentration. The Mn determined by GPC (calibrated with PMMA standards) increased nearly linearly with monomer conversion for molecular weights up to approximately 100 kg/mol. (Figure 2.3b). The higher experimental molecular weights (compared to the theoretical) are likely due to the use of PMMA standards in GPC analysis. The same trend was observed for the kinetic studies of the solution RAFT polymerization of SMA and LMA (Figures 2.4 and 2.5). Demetriou et al.[31] have reported similar observations for the RAFT polymerization of LMA in benzene and related this difference to the partial CTA deactivation. However, we believe this difference arises from the relative molecular weights obtained from a GPC calibrated with PMMA standards.

The dispersity for the SI-RAFT polymerization of SMA ($Đ$ ~ 1.4) was larger at higher molecular weights compared to solution polymerization of SMA ($Đ$ ~ 1.2) (Figure 2.4). This could be attributed to either the dilute polymerization media (solvent to monomer ratio was ~6) which would increase the dispersity by limiting the access of monomer to the growing chain, or that the bulky immobilized PSMA chains on the particle hinder access of the growing radicals to the monomers.

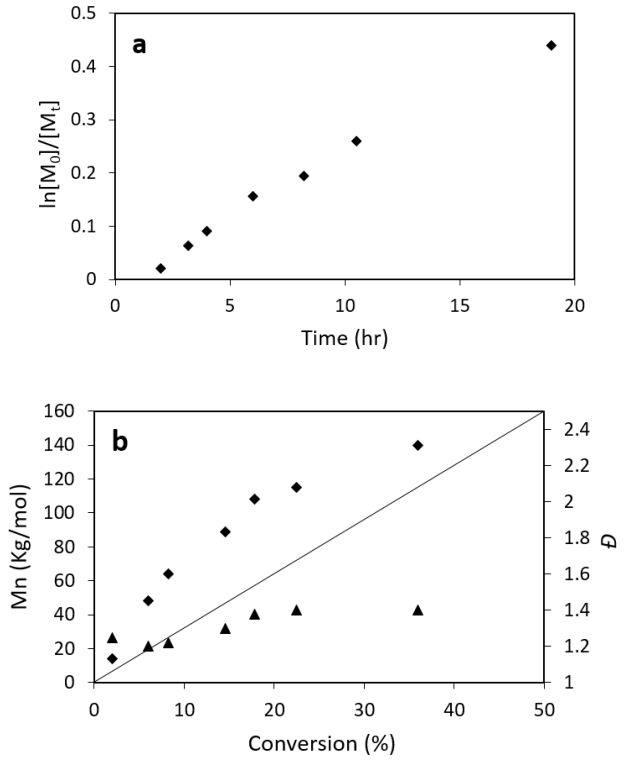

Figure 2.3. (a) Kinetic plot and (b) dependence of the GPC molecular weight (diamond), theoretical molecular weight (solid line), and dispersity (triangle) on the conversion for the surface-initiated RAFT polymerization of stearyl methacrylate on modified nanoparticles with CPDB density: 0.16 agents/nm^2 ([SMA]/[CPDB]/[AIBN] = 1000:1:0.1).

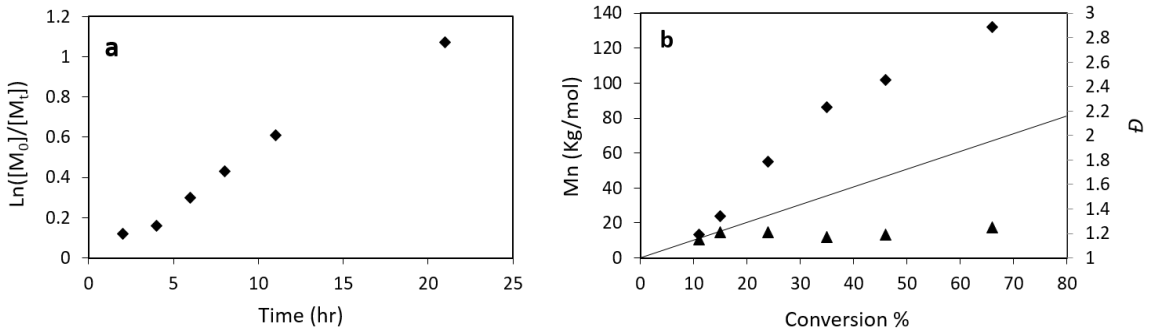

Figure 2.4. (a) Kinetic plot and (b) dependence of the GPC molecular weight (diamond), theoretical molecular weight (solid line), and polydispersity (triangle) on the conversion for the RAFT polymerization of stearyl methacrylate ([SMA]/[CPDB]/[AIBN] = 300:1:0.1)

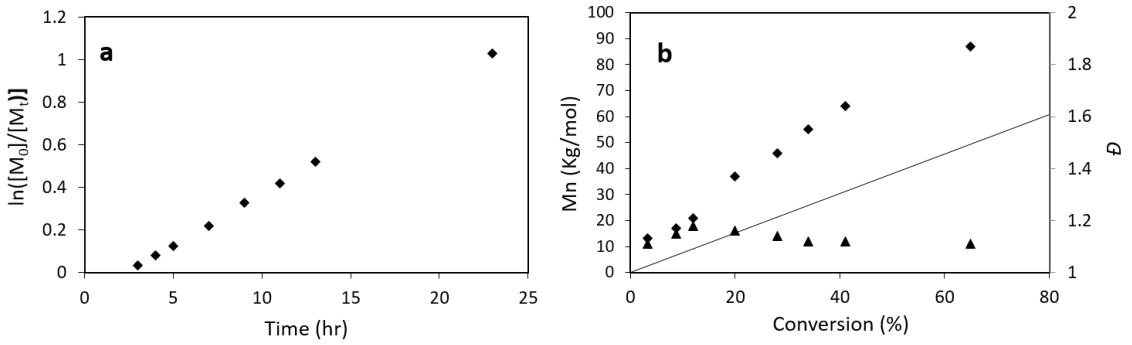

Figure 2.5. (a) Kinetic plot and (b) dependence of the GPC molecular weight (diamond), theoretical molecular weight (solid line), and polydispersity (triangle) on the conversion for the RAFT polymerization of lauryl methacrylate ([LMA]/[CPDB]/[AIBN] = 300:1:0.1)

The kinetic study of the SI-RAFT polymerization of LMA is shown in Figure 2.6. It was performed by the same method and conditions as for SMA. However, the polymerization of LMA proceeded to higher monomer conversions and higher molecular weights. This result may be attributed to the smaller size of LMA monomer compared to SMA, which then allows for easier access of monomers to the growing radicals.

The surface initiated RAFT polymerization method described above was then used to prepare several different polymer-grafted particles, some of which are summarized in Table 2.1. PHMA, PLMA, and PSMA grafted NPs were synthesized at a constant chain density of 0.16 ch/nm^2 with molecular weights of 70, 165, and 115 kg/mol, respectively. Then, PSMA-g-SiO_2 with various chain densities and molecular weights were also synthesized.

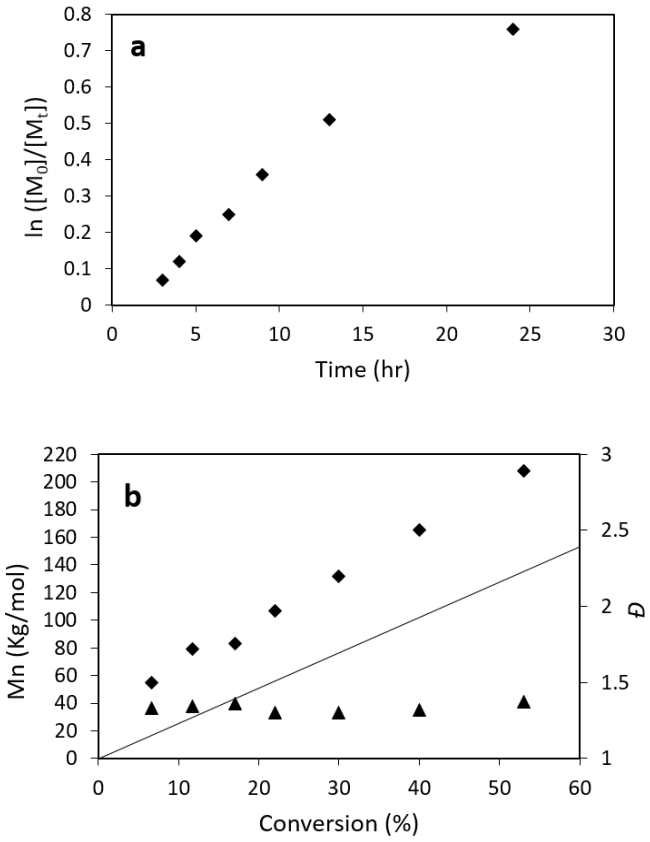

Figure 2.6. (a) Kinetic plot and (b) dependence of the GPC molecular weight (diamond), theoretical molecular weight (solid line), and dispersity (triangle) on the conversion for the surface-initiated RAFT polymerization of lauryl methacrylate on modified nanoparticles with CPDB density: 0.16 agents/nm^2 ([LMA]/[CPDB]/[AIBN] = 1000:1:0.1).

Table 2.1. Various poly(alkyl methacrylate)-g-SiO_2 NPs synthesized using RAFT polymerization.

Number	Polymer	Graft density, chains/nm^2	MW, Kg/mol
NP-1	PHMA	0.16	70
NP-2	PLMA	0.16	165
NP-3	PSMA	0.16	115
NP-4	PSMA	0.06	132
NP-5	PSMA	0.03	121
NP-6	PSMA	0.16	10
NP-7	PSMA	0.16	40
NP-8	PSMA	0.33	86

LLDPE nanocomposites filled with various poly(alkyl methacrylate)-grafted nanoparticles

The main goal of this study was to investigate the compatibility of various poly(alkyl methacrylate) grafted silica NPs with a polyolefin such as LLDPE. During the preparation of this paper, Sanchez et al.[32] reported on the preparation of low density polyethylene nanocomposites filled with poly(lauryl methacrylate) grafted Al_2O_3 nanoparticles. However, they did not fully investigate the role of the molecular graft variables on the dispersion of nanoparticles in the matrix. Moreover, this work reports significant differences between lauryl methacrylate and the longer stearyl methacrylate and their compatibility with polyethylene matrices.

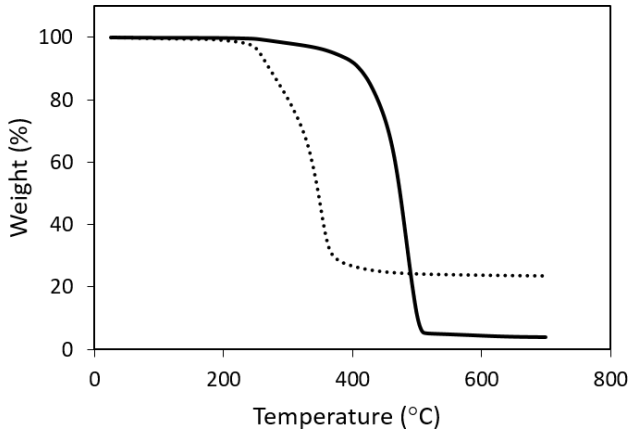

Figure 2.7. TGA curves for the NP-3 nanoparticles (dashed line) and 4 wt% NP-3/LLDPE composite (solid line).

To study the effect of different chemistries on the dispersion and the properties of LLDPE nanocomposites, PHMA, PLMA, and PSMA-grafted NPs (NP-1, NP-2, and NP-3 from Table 2.1) were prepared and studied. Samples were prepared at 4 wt% silica core loading which were determined by Thermogravimetric Analysis (TGA). Figure 2.7 shows the TGA measurements for PSMA-g-SiO_2 (NP-3) and NP-3 mixed with LLDPE at 4 wt% silica core loading.

The dispersion of the grafted silica NPs was examined using Transmission Electron Microscopy (TEM). Figure 2.8 shows a representative comparison of dispersion states for nanocomposites filled with bare silica, PHMA, PLMA, and PSMA-grafted nanoparticles. Nanocomposites filled with bare silica (Figure 2.8a) showed a compact aggregation of particles due to the incompatibility and poor interface between silica and PE. PHMA-g-SiO_2 also showed particle aggregates (Figure 2.8b). Although the particles were grafted with PHMA, micrometer size agglomerates still formed due to the incompatibility between the PHMA brush and PE matrix. We suggest that the hexyl side chain in PHMA does not make the PHMA sufficiently "olefin-like" and the mixing is thus enthalpically unfavorable. PLMA-g-SiO_2, with a dodecyl pendent group, is more olefin-like compared to PHMA and showed some level of compatibility with PE (Figure 2.8c). The TEM images of PLMA-g-SiO_2 showed less firmly packed agglomerates than the bare silica and PHMA-g-SiO_2 filled nanocomposites. The compact agglomerated structures observed previously were not observed, instead replaced by swollen self-associated structures (intermediate morphology). Figure 2.8d shows the TEM image for nanocomposites filled with PSMA-g-SiO_2 nanoparticles with randomly distributed particles. PSMA, with 18 carbon side chains, is believed to be sufficiently olefin-like to show a good level of compatibility with PE. Since PSMA-g-SiO_2 particles showed better compatibility with the PE matrix, these particles were the focus for further studies.

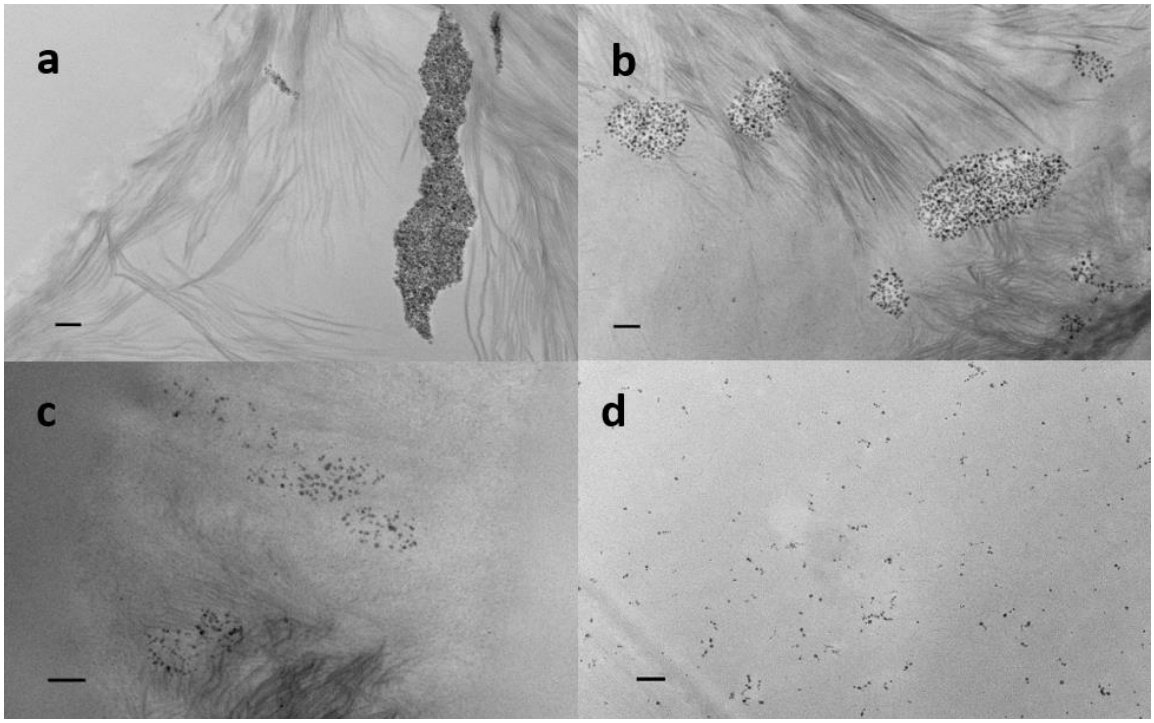

Figure 2.8. TEM micrographs of LLDPE nanocomposites filled with 4% loading of a) bare silica, b) PHMA-g-silica (NP-1), c) PLMA-g-silica (NP-2), and d) PSMA-g-silica (NP-3) at a fixed chain density of 0.16 ch/nm^2. (scale bars are 200 nm).

Effect of grafting chain densities

In order to investigate the role of polymer chain grafting density on the dispersion of PSMA-g-SiO_2 NPs in a PE matrix, PSMA-g-SiO_2 NPs with chain densities of 0.03, 0.06, 0.16 and 0.33 ch/nm^2 with molecular weights of 121, 132, 115, and 86 kg/mol, respectively, were synthesized. Figure 2.9 shows the TEM micrographs of the nanocomposites attributed to these samples. It is evident that as the chain density increased, the dispersion of the particles improved. A chain density of 0.03 ch/nm^2 corresponds to about 20 chains per particle which appears to be insufficient to screen the core-core interactions between silica particles leading to large aggregated structures. The 0.06 ch/nm^2 particles also appeared insufficient to alleviate the core-core interactions between silica particles. However, the sizes of the agglomerates were smaller than nanocomposites prepared with 0.03 ch/nm^2

particles. Particles with densities of 0.16 and 0.33 ch/nm^2 showed much improved dispersions of particles. The density of 0.16 ch/nm^2 corresponds to about 100 polymer chains per particle and is believed to be enough to moderate the core-core interactions. It is worth mentioning that the molecular weights of the PSMA brushes were chosen to ensure that the chain segments at the outer portions of the nanoparticles would be in the semi-dilute brush conformations.

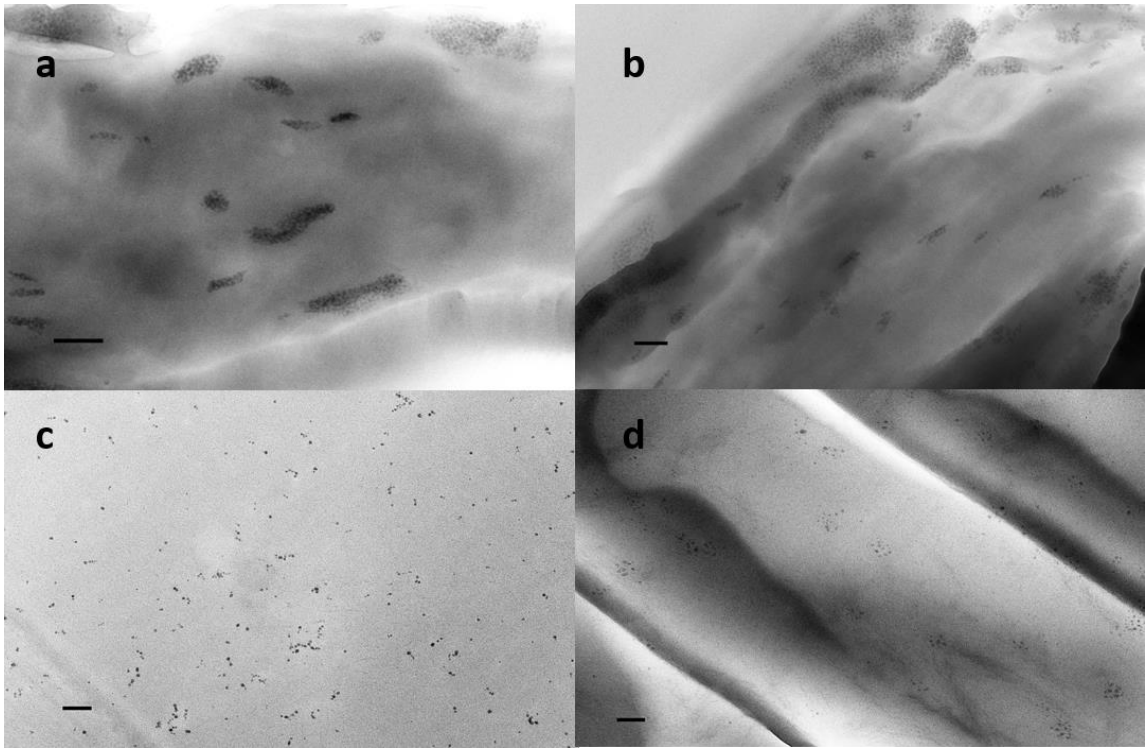

Figure 2.9. TEM micrographs of LLDPE nanocomposites filled with approximately 4% silica loading of PSMA-g-silica NPs with chain densities of a) 0.03 (NP-5), b) 0.06 (NP-4), c) 0.16 (NP-3), and 0.33 ch/nm^2 (NP-8). (Scale bars are 200 nm)

Effect of grafted polymer chain length

In order to investigate the role of grafted PSMA chain length on the nanoparticles dispersion, PSMA-g-SiO_2 NPs at the same chain density of 0.16 ch/nm^2 with different molecular weights of 10, 40, and 115 kg/mol were prepared and used to fabricate LLDPE nanocomposites (Table 2.1). Figure 2.10 shows a comparison of TEM micrographs of these

nanocomposites. The dispersion of nanoparticles is evidently improved with the increase in the molecular weight of the grafted PSMA. Particles with 10 kg/mol grafted PSMA formed large agglomerates, despite the compatibility of the grafted chains and matrix chains discussed earlier. Although the particles were grafted with PSMA chains to screen the core-core attractions, particles still aggregated because of the poor entanglement between the short grafted PSMA and long LLDPE chains (matrix cannot wet the polymer-grafted particles).[7–10,23] Increasing the molecular weight of the PSMA brush to 40 kg/mol improved the entanglement but not sufficient to fully disperse the nanoparticles. When the grafted chain length finally increased to 115 kg/mol, favorable interaction and entanglement with the matrix chains led to spatially dispersed particles.

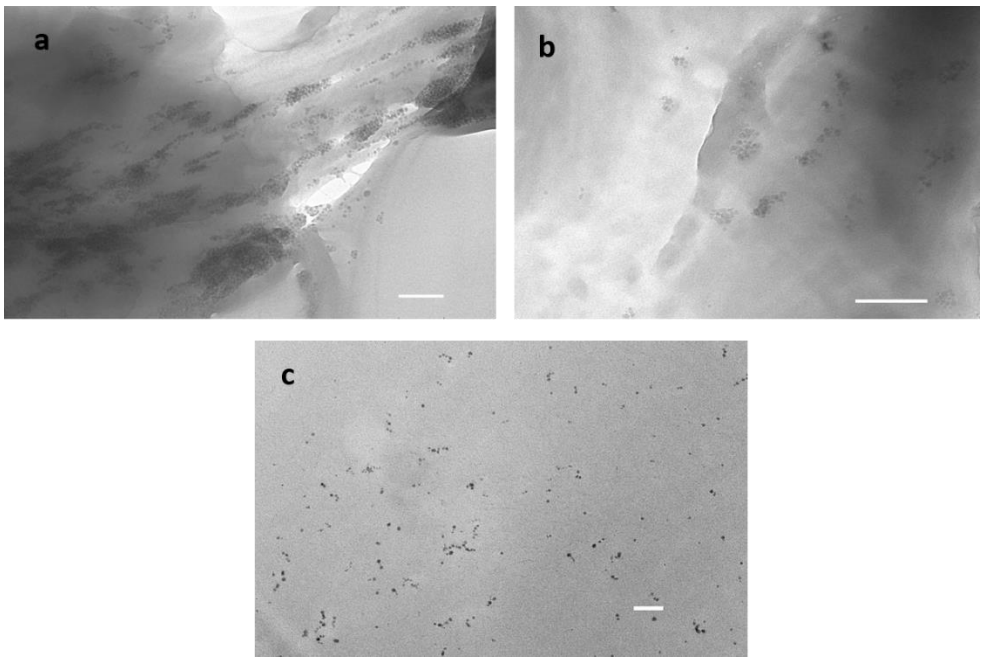

Figure 2.10. TEM micrographs of LLDPE nanocomposites filled with approximately 4% silica loading of PSMA-g-silica NPs with different grafted molecular weights of a) 10 (NP-6), b) 50 (NP-7), and c) 115 kg/mol (NP-3), at a set chain density of 0.16 ch/nm^2. (Scale bars are 200 nm)

Characterization of PSMA-g-SiO_2 filled LLDPE nanocomposites

The composite with NP-3 (highly dispersed sample) was used for initial screening studies to probe the interactions between the PSMA-g-SiO_2 particles and LLDPE. Composites with 10, 20, 30, 40, and 60 wt% PSMA-g-SiO_2 nanoparticles were prepared which contained 2, 4, 6, 8, and 12 wt% core silica, respectively. Samples were solution cast on glass and after solvent evaporation, annealed for 24 hours. DSC was used to study the thermal properties of the composites (Figure 2.12). The temperature was increased at a rate of 10 °C/min from -50 to 150 °C and then cooled at 10 °C/min to -50 °C. This was repeated two times per specimen. Data from the first cycle was not considered in order to eliminate thermal history effects. The cyclic heating-cooling DSC curves for LLDPE filled with 20% PSMA-g-SiO_2 (NP-3) are illustrated in Figure 2.11.

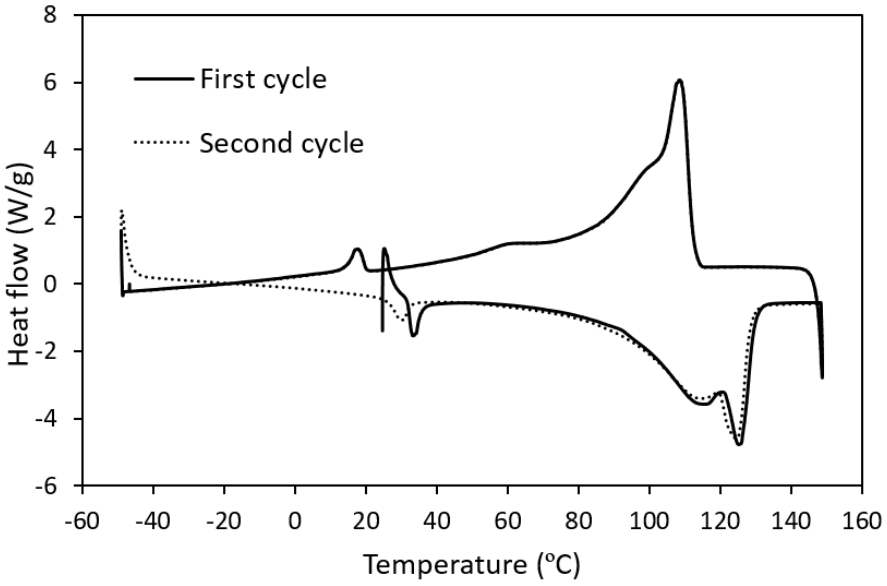

Figure 2.11. Cyclic heating-cooling DSC curves for LLDPE filled with 20 wt% PSMA-g-SiO_2 (NP-3)

The unfilled LLDPE showed a peak at 124 °C for the melting transition with a shoulder at ~113 °C which was attributed to the composition distribution of the side chains

in the LLDPE. This peak did not move with addition of up to 60 wt% particles. The crystallization peak for the unfilled LLDPE was at 110.1 °C. This peak also did not seem to be greatly affected by the incorporation of particles. Composites containing PSMA-g-SiO_2 showed a melting transition at 30 °C attributed to the side-chain crystallization of PSMA which increased with increasing particles loading. It is worth mentioning that the melting transition for the pure PSMA-g-SiO_2 was 33 °C which is higher than that of the related composite. The decrease for the melting point could be due to the perturbation of the molecular ordering of PSMA in the composite.[33] DSC results for these nanocomposites are summarized in Table 2.2.

Wide angle x-ray scattering (WAXS) patterns of neat LLDPE and 20% filled composite shown in Figure 2.13 show two main peaks at 21.5 and 23.6 degrees (2θ) which correspond to the (110) and (200) planes of PE.[34] The WAXS pattern of the nanocomposite shows no measurable changes in the crystalline lattice structure of the PE matrix, which suggests that the crystallinity of the LLDPE matrix is not affected by the particles.[35]

Table 2.2. Thermal and crystalline properties of LLDPE composites

LLDPE/Fillers	Filler loading (wt%)[a]	T_m (°C)	T_c (°C)
LLDPE	0	123.9	110.1
LLDPE/NP-3	10	123.9	109.5
LLDPE/NP-3	20	124.5	109.2
LLDPE/NP-3	30	123.9	108.6
LLDPE/NP-3	40	124.8	108.0
LLDPE/NP-3	60	123.5	107.1

[a] The weight percent is based on the total PSMA-g-SiO_2 (nanocomposite with 20% filler contains 4% silica and 16% grafted PSMA)

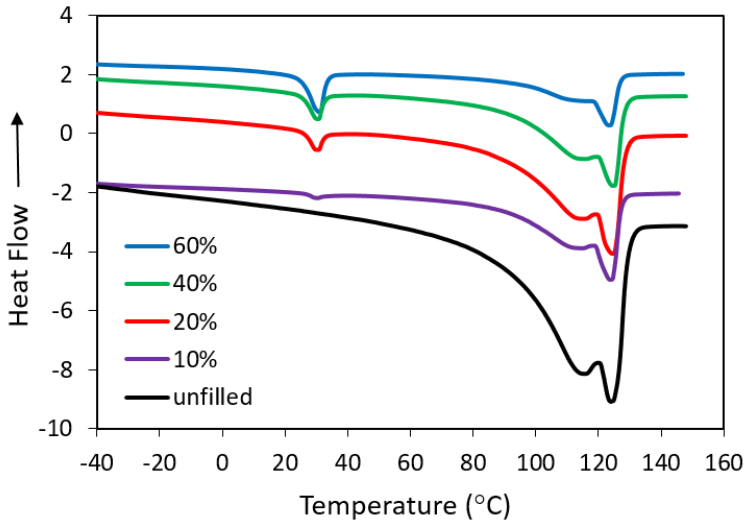

Figure 2.12. DSC curves of different LLDPE systems filled with PSMA-g-SiO_2 with 0.16 ch/nm^2 density and 115 kg/mol molecular weight. Percent loading is based on total weight of filler.

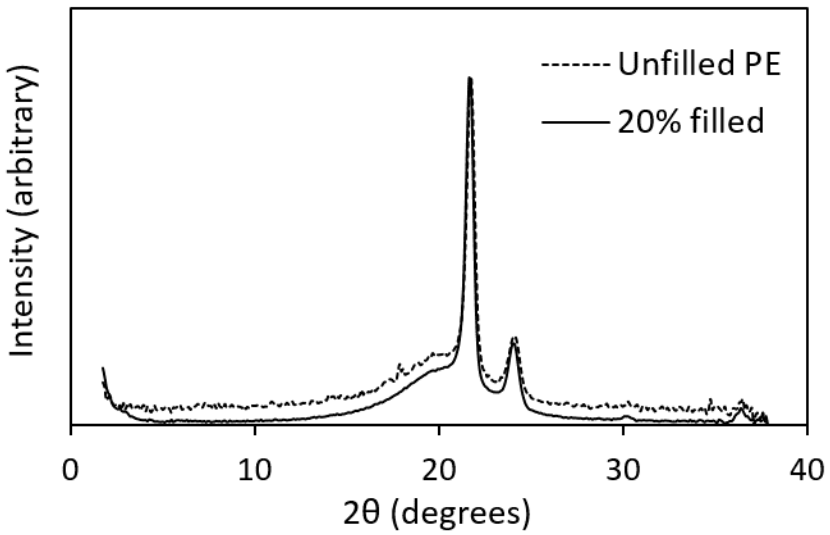

Figure 2.13. WAXS results showing negligible changes in the patern for the pure LLDPE and LLDPE filled with 20% NP-3.

The results from the SAXS of the 20, 40, and 60% PSMA-g-SiO_2 (NP-3) filled nanocomposites at solid state (room temperature) and melt state (140 °C) are shown in Figures 2.14a and b, respectively. The scattering peak originates from the contrast between the silica particle and the polymeric matrix (~ 80% increase in electron density for silica over crystalline PE) which is completely different from the primary scattering contrast between the crystalline and amorphous phase (Figure 2.15). The effective surface-to-surface distance between the particles, h_{eff} was determined using

$$h_{\text{eff}} = \frac{2\pi}{q_m} - d_{\text{eff}}$$

where q_m is the first-order scattering maximum and d_{eff} is the effective particle diameter which is approximately 14 nm. Using this formula h_{eff} was calculated to be 24, 19, and 17 nm for 20, 40, and 60% filler loadings, respectively, in both the melt and solid state. Therefore, mean particle spacing remained unchanged when the sample was cooled from the melt to below the crystallization temperature (T_c). However, the x-ray peaks broadened in the crystalline state (Figure 2.14a). This has been quantified from the half-width-at half-maximum (Δq) on the high-q side of the peaks (Δq = 0.05, 0.04, and 0.04 nm^{-1} for 20, 40, and 60% loadings above T_m, respectively, and Δq = 0.09, 0.06, and 0.06 nm^{-1} for 20, 40, and 60% loadings below T_c, respectively). This means that the distribution of particle separation is broadened in the semicrystalline polymer. It is clear that the broadening is much more significant for the 20% filled sample compared to samples with higher particle loadings. This phenomenon has been observed in our previous work on polyethylene oxide composites filled with PMMA-g-SiO_2 NPs that showed samples with particle loadings below 20% did not contribute to the crystalline structure of the matrix and the particles are forced away from the crystalline sites.[35] This was further investigated by SAXS analysis

of two 20% loading nanocomposites at room temperature. Both samples were cooled after a 24 hr thermal annealing period, one quenched in liquid nitrogen and the other cooled at a rate of 0.5 °C/min (Figure 2.16). The slow cooled sample showed a broader peak compared to the fast cooled sample, which indicates a broader distribution of particle separation for the slow cooled sample. This result suggests that when the composite was cooled fast, particles did not have time to move away from the crystallizing fronts and were trapped, resulting in a narrower particle separation. Therefore, we conclude from these differences especially at lower particle loadings, the growing polyethylene crystallites push some of the particles out of the way, resulting in a broader distribution of particle spacing in the solid state. TEM imaging over a range of particle loadings did not present obvious differences in dispersion, but showed that particles were generally well-dispersed within the PE matrix. Figure 2.17 illustrates the TEM results for the 60% filled composite which shows a good state of dispersion even at such high loading.

Film samples (0.2 mm) of neat LLDPE, nanocomposites containing 2.5% and 12% PSMA-g-SiO_2 (NP-3), and a control sample containing 0.5% silica and 2% of free PSMA were prepared and analyzed by dynamic mechanical analysis (DMA) in the temperature range of -140-100 °C. Note that a 2.5% PSMA-g-SiO_2 composite contains 0.5% of core silica and approximately 2% of grafted PSMA. Both storage (Figure 2.18) and loss moduli (Figure 2.19) of all composites were increased compared to the neat LLDPE films and the increase was more significant at lower temperatures. The increases of the storage modulus at -100 °C for 2.5% control, 2.5%-NP-3, and 12%- NP-3 were found to be 15%, 87%, and

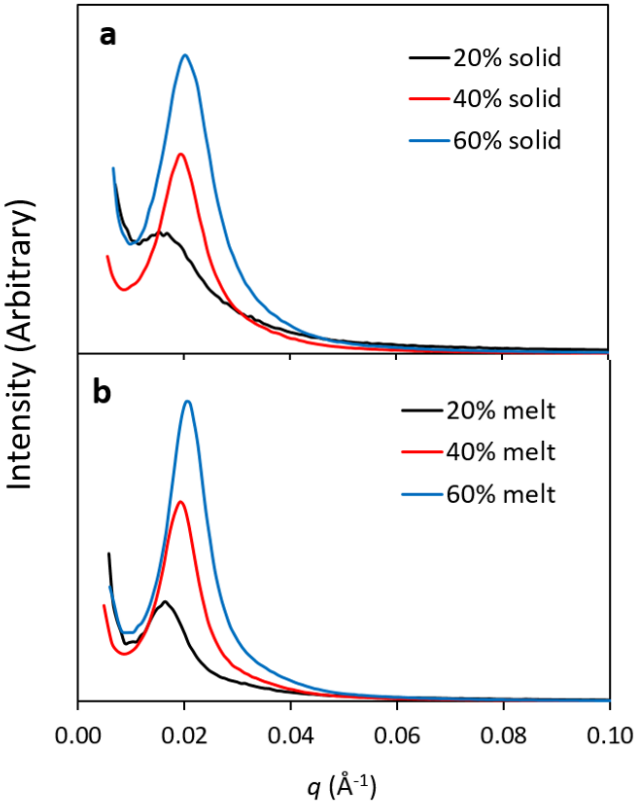

Figure 2.14. SAXS results of the 20, 40, and 60% (NP-3) loading nanocomposite as a function of scattering vector, *q*, at solid state (room temperature) and melt state (140 °C). Note that the scattering peak originated from the contrast between the silica particle and the polymeric matrix (not the scattering between the crystal and amorphous phase).

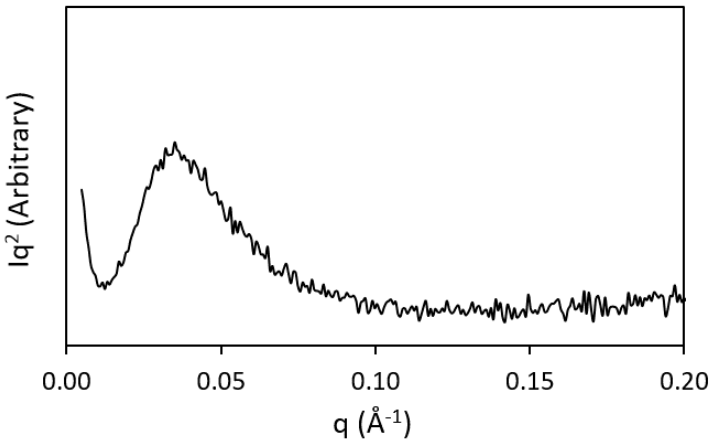

Figure 2.15. Lorentz-corrected SAXS of semicrystalline PE as a function of the scattering vector, *q*.

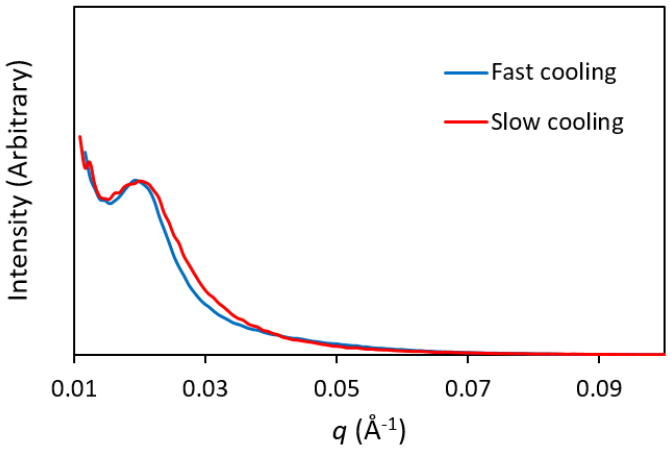

Figure 2.16. SAXS results of the 20% loading nanocomposite as a function of scattering vector, q, at room temperature cooled from two annealed samples, one quenched in liquid nitrogen and the other one slowly cooled down with a rate of 0.5 degree/min.

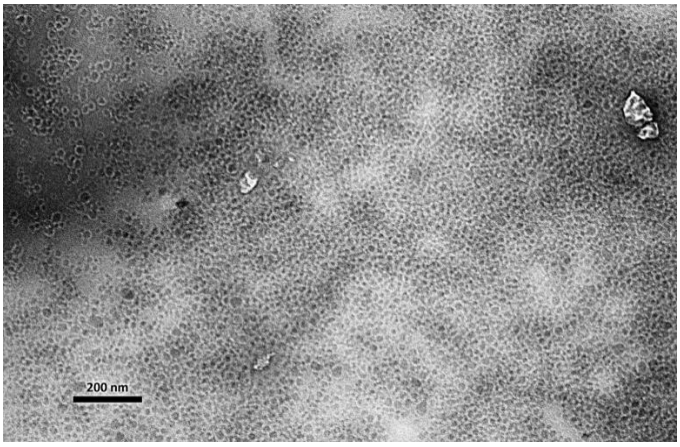

Figure 2.17. TEM results for LLDPE nanocomposite filled with 60% NP-3.

62% respectively while these increases at 25 °C for 2.5% control, 2.5%-NP-3, and 12%-NP-3, were found to be 18%, 52%, and 38%, respectively. Therefore, the composite containing 0.5% bare silica + 2% free PSMA showed the smallest increase in modulus. A similar increase was observed in the case of addition of 0.5% bare silica and is consistent with previous reports for polyethylene composites.[32,36,37] These results support that a composite containing 2.5% of well-dispersed PSMA-g-silica has a greater interfacial adhesion between the particles and the matrix due to the compatibility of PSMA brushes

and the polyethylene matrix which causes a better load transfer at the particle-matrix interface. The further increase of PSMA-g-SiO_2 loading to 12% did not further increase the storage modulus. This trend has been previously seen in other cases of polyethylene composites, i.e., that by increasing the nanoparticles concentration, the mechanical reinforcement becomes smaller.[32,36] This phenomenon was attributed to the possible aggregation of particles at loadings above 1%. However, we know that PSMA-g-SiO_2

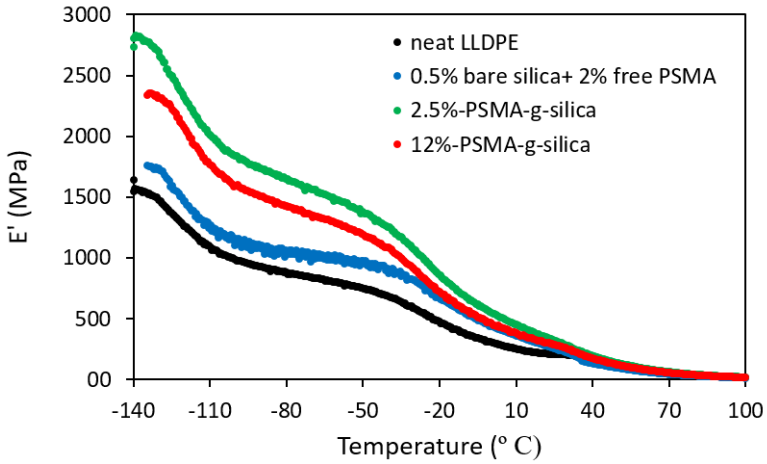

Figure 2.18. Storage modulus of the LLDPE nanocomposites measured by dynamic mechanical analysis.

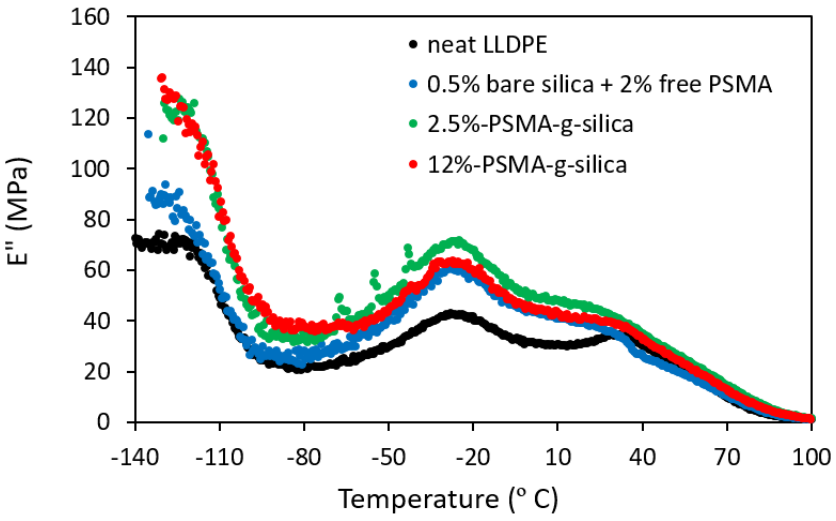

Figure 2.19. Loss modulus of the LLDPE nanocomposites measured by dynamic mechanical analysis.

particles (NP-3) were well-dispersed in LLDPE even at higher loadings, therefore other reasons could be involved in our work. A 12% PSMA-g-SiO_2 composite contains approximately 2.5% core silica and 9.5% of grafted PSMA chains. Since PSMA has much lower modulus compared to polyethylene, we believe that further increases in concentration of PSMA on the grafted particle negates the effect of the dispersed silica particles on the modulus especially at higher temperatures (melting point of PSMA is ~ 33 °C). Therefore, maintaining a low concentration of particles is necessary for achieving higher mechanical reinforcement. While these data confirm the compatibility of PSMA-g-SiO_2 with polyethylene, more detailed studies are needed to investigate the effect of these particles on other properties of polyethylene composites which will be the focus of our research for the future.

2.5 Conclusion

We have demonstrated a method for the preparation of poly(alkyl methacrylate)-grafted silica nanoparticles using surface-initiated RAFT polymerization. Composites of LLDPE filled with PHMA, PLMA, and PSMA-g-SiO_2 NPs were prepared and examined by TEM to test the effects of side chain length on the dispersibility. PSMA-g-SiO_2 showed the highest state of dispersion among the three modified particles. It was suggested that the 18 carbon long alkyl side chains make the PSMA more “olefin-like” and are responsible for the compatibility of PSMA-g-SiO_2 with polyethylene due to the molecular similarity. The graft density of PSMA chains was also shown to be crucial in the dispersion of particles throughout the matrix. Particles with lower grafting densities agglomerated where the higher densities showed improved dispersions. The agglomeration of lower graft density particles was due to the core-core interaction of silica particles. The effect of chain

molecular weight was also studied and showed that low molecular weight PSMA grafted particles agglomerated and as the molecular weight increased the state of dispersion improved which was ascribed to the enhanced entanglement of high molecular weight brushes with the LLDPE matrix. DSC and WAXS revealed that PSMA-g-SiO_2 particles did not greatly affect the thermal and crystalline properties of LLDPE. SAXS studies showed the particle spacing distribution broadened when cooling the samples slowly from the melt to the crystalline state. For the nanocomposites with nanoparticle loadings especially below 20 wt%, it is likely that some of the nanoparticles were pushed out of the way of the growing crystallites, resulting in a broadening of the particle distribution. Storage and loss modulus of the samples were analyzed by DMA and showed improvement by the addition of PSMA-g-SiO_2 NPs. The storage modulus of the polyethylene improved by addition of only 2.5% PSMA-g-SiO_2 (NP-3) and this improvement was found to be more significant at lower temperatures (up to 90%). The detailed investigation of the effect of these compatible particles on the properties of polyethylene is an interesting issue that we shall probe in future work.

2.6 References

(1) Khani, M. M.; Woo, D.; Mumpower, E. L.; Benicewicz, B. C. *Polymer (Guildf).* **2017**, *109*, 339–348.

(2) Vaia, R. A.; Maguire, J. F. *Chem. Mater.* **2007**, *19* (11), 2736–2751.

(3) Zou, H.; Wu, S.; Shen, J. *Chem. Rev.* **2008**, *108* (9), 3893–3957.

(4) Mackay, M. E.; Tuteja, A.; Duxbury, P. M.; Hawker, C. J.; Van Horn, B.; Guan, Z.; Chen, G.; Krishnan, R. S. *Science* **2006**, *311* (5768), 1740–1743.

(5) Schadler, L. S.; Kumar, S. K.; Benicewicz, B. C.; Lewis, S. L.; Harton, S. E. *MRS*

Bull. **2007**, *32* (4), 335–340.

(6) Kumar, S. K.; Krishnamoorti, R. *Annu. Rev. Chem. Biomol. Eng.* **2010**, *1* (1), 37–58.

(7) Green, P. F. *Soft Matter* **2011**, *7* (18), 7914.

(8) Ojha, S.; Dang, A.; Hui, C. M.; Mahoney, C.; Matyjaszewski, K.; Bockstaller, M. R. *Langmuir* **2013**, *29* (28), 8989–8996.

(9) Bansal, A.; Yang, H.; Li, C.; Benicewicz, B. C.; Kumar, S. K.; Schadler, L. S. *J. Polym. Sci. Part B Polym. Phys.* **2006**, *44* (20), 2944–2950.

(10) Meli, L.; Arceo, A.; Green, P. F. *Soft Matter* **2009**, *5* (3), 533–537.

(11) Akcora, P.; Kumar, S. K.; Moll, J.; Lewis, S.; Schadler, L. S.; Li, Y.; Benicewicz, B. C.; Sandy, A.; Narayanan, S.; Ilavsky, J.; Thiyagarajan, P.; Colby, R. H.; Douglas, J. F. *Macromolecules* **2010**, *43* (2), 1003–1010.

(12) Balazs, A. C.; Emrick, T.; Russell, T. P. *Science* **2006**, *314* (5802), 1107–1110.

(13) Akcora, P.; Liu, H.; Kumar, S. K.; Moll, J.; Li, Y.; Benicewicz, B. C.; Schadler, L. S.; Acehan, D.; Panagiotopoulos, A. Z.; Pryamitsyn, V.; Ganesan, V.; Ilavsky, J.; Thiyagarajan, P.; Colby, R. H.; Douglas, J. F. *Nat. Mater.* **2009**, *8* (4), 354–359.

(14) Taniike, T.; Toyonaga, M.; Terano, M. *Polymer (Guildf).* **2014**, *55* (4), 1012–1019.

(15) Bieligmeyer, M.; Taheri, S. M.; German, I.; Boisson, C.; Probst, C.; Milius, W.; Altstädt, V.; Breu, J.; Schmidt, H.-W.; D'Agosto, F.; Förster, S. *J. Am. Chem. Soc.* **2012**, *134* (44), 18157–18160.

(16) Dorigato, A.; Pegoretti, A. *J Polym Res* **2013**, *20*, 92.

(17) Malpass, B. D. *Introduction to Industrial Polyethylene*; John Wiley & Sons and

Scrivener Publishing LCC: Salem, 2010.

(18) Jeziórska, R.; Świerz-Motysia, B.; Zielecka, M.; Szadkowska, A.; Studziński, M. *J. Appl. Polym. Sci.* **2012**, *125* (6), 4326–4337.

(19) McNally, T.; Pötschke, P.; Halley, P.; Murphy, M.; Martin, D.; Bell, S. E. J.; Brennan, G. P.; Bein, D.; Lemoine, P.; Quinn, J. P. *Polymer (Guildf).* **2005**, *46* (19), 8222–8232.

(20) Wang, T.-L.; Ou, C.-C.; Yang, C.-H. *J. Appl. Polym. Sci.* **2008**, *109* (5), 3421–3430.

(21) Monteil, V.; Stumbaum, J.; Thomann, R.; Mecking, S. *Macromolecules* **2006**, *39* (6), 2056–2062.

(22) Zhu, J.; Wei, S.; Li, Y.; Sun, L.; Haldolaarachchige, N.; Young, D. P.; Southworth, C.; Khasanov, A.; Luo, Z.; Guo, Z. *Macromolecules* **2011**, *44* (11), 4382–4391.

(23) Rungta, A.; Natarajan, B.; Neely, T.; Dukes, D.; Schadler, L. S.; Benicewicz, B. C. *Macromolecules* **2012**, *45* (23), 9303–9311.

(24) Ferreira, P. G.; Ajdari, A.; Leibler, L. *Macromolecules* **1998**, *31* (12), 3994–4003.

(25) Li, C.; Benicewicz, B. C. *Macromolecules* **2005**, *38* (14), 5929–5936.

(26) Prucker, O.; Rühe, J. *Macromolecules* **1998**, *31* (3), 592–601.

(27) Li, C.; Han, J.; Ryu, C. Y.; Benicewicz, B. C. *Macromolecules* **2006**, *39* (9), 3175–3183.

(28) Dutertre, F.; Pennarun, P.-Y.; Colombani, O.; Nicol, E. *Eur. Polym. J.* **2011**, *47* (3), 343–351.

(29) Li, Y.; Benicewicz, B. C. *Macromolecules* **2008**, *41* (21), 7986–7992.

(30) Gao, J.; Li, J.; Benicewicz, B. C.; Zhao, S.; Hillborg, H.; Schadler, L. S. *Polymers*

(Basel). **2012**, *4* (1), 187–210.

(31) Demetriou, M.; Krasia-Christoforou, T. *J. Polym. Sci. Part A Polym. Chem.* **2008**, *46* (16), 5442–5451.

(32) Cobo Sánchez, C.; Wåhlander, M.; Taylor, N.; Fogelström, L.; Malmström, E. *ACS Appl. Mater. Interfaces* **2015**, *7* (46), 25669–25678.

(33) Mallik, A. K.; Rahman, M. M.; Czaun, M.; Takafuji, M.; Ihara, H. *J. Chromatogr. A* **2008**, *1187* (1), 119–127.

(34) Irani, M.; Ismail, H.; Ahmad, Z. *Polym. Test.* **2013**, *32* (3), 502–512.

(35) Khan, J.; Harton, S. E.; Akcora, P.; Benicewicz, B. C.; Kumar, S. K. *Macromolecules* **2009**, *42* (15), 5741–5744.

(36) Roumeli, E.; Pavlidou, E.; Avgeropoulos, A.; Vourlias, G.; Bikiaris, D. N.; Chrissafis, K. *J. Phys. Chem. B* **2014**, *118* (38), 11341–11352.

(37) Chee, C. Y.; Song, N. L.; Abdullah, L. C.; Choong, T. S. Y.; Ibrahim, A.; Chantara, T. R. *J. Nanomater.* **2012**, *2012*, 1–6.

CHAPTER 3

POLYPROPYLENE DIELECTRIC NANOCOMPOSITES WITH MATRIX COMPATIBLE FILLERS CONTAINING ANTHRACENE*

*This chapter was partially adapted from Krentz et al. *J. Appl. Polym Sci.* **2017**, 134, 44347-57.[1]

3.1 Abstract

In this work, we investigate the synthesis of a new bimodal surface ligand morphology on silica nanoparticles to achieve compatibility with a polypropylene matrix, demonstrating the efficacy of anthracene surface modification towards improving the dielectric breakdown strength (DBS) under AC and DC conditions.[1] Ligand modified spherical colloidal SiO_2 nanoparticles (NPs) (~ 14 nm diameter) were mixed into polypropylene and the resulting dispersion was improved over unmodified particles as shown with transmission electron microscopy (TEM). The results suggest that the electronic structure of anthracene particle surface modification is critical to the DBS improvements. In addition, the DBS of the composite is shown to depend on the dispersion state of the filler and the mode of stress, indicating that individually dispersed nanoparticles are not necessarily the optimal morphology for all stress conditions. Additionally, the precise nature of the matrix compatible brush is less important than the morphology it produces. Bimodal grafted architecture design provides a promising solution to control dispersion and surface properties, especially for high molecular weight polypropylene matrices.

3.2 Introduction

Dielectric polymer nanocomposites can exhibit significant improvements in permittivity, loss, voltage endurance, and dielectric breakdown strength compared to the unfilled polymer.[2–6] Improvements to high-voltage capacitors are an enabling technology for high voltage power transmission.[7] The dispersion of nanofillers (NFs) is difficult to control, especially when scaling up from laboratory to industrial processing.[8,9] The driving

force for agglomeration is typically the hydrophilic nature of the NF or the use of surface modifiers to stabilize properties[10] that are enthalpically incompatible with the matrix.

In order to improve the NF dispersion, chemical surface modification may be used to decrease the enthalpic penalty for the creation of the NF-matrix interface.[11] However, these modifications, in general, achieve unstable NF dispersion within high molecular weight polymer matrices.[12,13] When densely grafted longer enthalpically matrix-compatible chains are used as surface ligands, entropic penalties arise as long matrix chains give up conformations to associate with the interface, which can also lead to agglomeration.[14]

Dielectric breakdown is a process by which an insulator undergoes an abrupt increase in passed current under an applied external electric field thereby going from an insulator to a conductor. This threshold field is referred as the dielectric breakdown strength of the material. There are three mechanisms of dielectric breakdown to consider when examining polymeric materials; intrinsic, thermal, and avalanche. Intrinsic breakdown describes the inherent properties of a material and is independent of external conditions. Intrinsic breakdown is less important in polymers and composites since these materials contain defects and impurities that can cause alternative breakdown mechanisms before reaching the intrinsic breakdown field. Thermal breakdown occurs due to thermal conduction arising from polarization in the material. Avalanche breakdown occurs when a free electron is accelerated by the field and gains sufficient energy to impact ionization of another atom. The collisions result in the liberation of bound electrons, causing the rapid multiplication of an avalanche, ultimately resulting in a conducting pathway along the mean free path in the material.[15–17] Avalanche breakdown is thought to be one of the most

common mechanisms of dielectric breakdown in polymers. Figure 3.1 shows an image of avalanche breakdown in epoxy resin.

Figure 3.1. Optical microscopy image of tree formed as a result of avalanche breakdown in epoxy resin.

Dielectric breakdown strength (DBS) enhancement is effected through the introduction of extrinsic trap states via small molecule NF modification. Electronic avalanches are assumed to be the dominant mechanism for dielectric breakdown of polypropylene, as has been advanced in other olefins.[18] Anthracene has been shown to improve DBS when grafted to well dispersed silica NFs[19] and while some works indicate it also may improve DBS as a free additive,[18,20] this work indicates free anthracene molecules reduces DBS in polypropylene, which is likely related to increased conductivity.[21] The DBS improvements seen in systems with anthracene have been attributed to trap states for electrons due to the anthracene molecule, and maybe present at a NF surface (in this study) or in phase separated regions. These trap states are hypothesized to allow energetic electrons to fall into lower energy states and reduce impact ionization events, reducing the incidence of avalanches reaching a critical size. This indicates that, in addition to the trapping functionality introduced by additives like anthracene, dispersion

control is critical, as an avalanche may encounter a filler particle before reaching critical size.

Previously, when adding functionality to the surface of nanofillers, researchers had to choose between adding functionality to improve dispersion or functionality to alter the electronic nature of the filler surface. The use of a bimodal architecture allows for the modification of the filler surface with two separate populations so both parameters can be studied independently. In this work, a novel NF surface modification is developed to independently control dispersion and dielectric properties through the use of two populations of surface ligands: one of small molecules chosen to enhance high voltage performance and one of longer matrix compatible chains to control NF dispersion. This enables separate control of dispersion, through matrix compatible long chains, and functionality, though appropriate small molecules like anthracene. Bimodal architectures of surface ligands in bimodal-brush-grafted SiO_2/epoxy NCs have exhibited improved DBS.[22] A grafting-from approach was used in this work to control dispersion of silica nanoparticles in polypropylene. Anthracene surface groups were grafted to the nanoparticle surface, and a methacrylate backbone bottlebrush polymer with stearyl side chains (poly(stearyl methacrylate) or PSMA) was chosen for its compatibility with the polymerization method used and the compatibility that olefinic side chains should create between the brush and the matrix. The dielectric breakdown performance of composites with a range of dispersions was then investigated under AC and DC conditions, and measurements of the permittivity are presented. Samples were prepared for AC voltage endurance testing with neat polypropylene as well as from the best performing NC loaded with PSMA and anthracene surface modified silica nanoparticles.

3.3 Experimental

Materials

All reagents were used as received from Fisher Scientific unless otherwise stated below. Polypropylene (Borclean^{TM} HB311BF) was supplied by Borealis AG. Colloidal silica nanoparticles (15 nm, 30 wt % in methyl isobutyl ketone (MIBK)) were supplied by Nissan Chemicals Inc. Stearyl methacrylate (95%, TCI America) was passed through a basic alumina column to remove the inhibitor before use. AIBN was purchased from Sigma Aldrich and recrystallized 3x from methanol. 4-Cyanopentanoic acid dithiobenzoate (CPDB) was received from Strem Chemical, Inc. 3-Aminopropyldimethylethoxysilane was obtained from Gelest.

Instrumentation

NMR spectra were recorded on a Varian Mercury 400 spectrometer using $CDCl_3$ as the solvent. The molecular weights and molecular weight distributions were determined using a Waters gel-permeation chromatograph equipped with a 515 HPLC pump, a 2410 refractive index detector, three Styragel columns (HR1, HR3, HR4 in the effective molecular weight range of 100–5000, 500–30 000, and 5000–500 000, respectively). Tetrahydrofuran (THF) was used as the eluent at 30 °C and a flow rate of 1.0 mL min^{-1}. The GPC system was calibrated with polymethyl methacrylate standards obtained from Polymer Laboratories. Samples were processed by filtration through microfilters with a pore size of 0.2 μm before analysis. Quantification of surface groups was performed using either UV-vis or TGA. UV-vis absorption spectra were taken on a Perkin-Elmer Lamda 4C UV/vis spectrophotometer. TGA characterization was conducted using a TA Instruments Q5000 with a heating rate of 10°C/min from 25°C to 800°C~1000°C under nitrogen flow.

Activated 9-anthracene acetic acid

2-(Anthracen-9-yl)acetic acid was prepared as described previously.[23] 2-(Anthracen-9-yl)acetic acid (1.00 g, 4.2 mmol) was dissolved into 30 ml dichloromethane along with 2-mercaptothiazoline (0.56 g, 4.7 mmol), and 4-dimethylaminopyridine (50 mg, 0.4 mmol). The solution was cooled to 0°C and flushed with N_2 for 20 minutes. N,N'-dicyclohexylcarbodiimide (0.87 g, 4.2 mmol) was dissolved into a minimal amount of dichloromethane and added dropwise to the anthracene acetic acid solution. The solution was allowed to warm to room temperature and stirred over night. The solids were then removed via vacuum filtration and solvent was removed under reduced pressure. The crude product was purified via column chromatography (SiO_2, 7:3, dichloromethane: hexane) leaving the product as a yellow powder (0.62 g, 43% yield). MP: 200-203°C. ^{1}H NMR (400 MHz, $CDCl_3$): δ (ppm) 8.46 (s, 1H), 8.02 (d, J = 9.6 Hz, 4H), 7.49 (m, 4H), 5.64 (s, 2H), 4.63 (t, J = 7.6 Hz, 2H), 3.39 (t, J = 7.6 Hz, 2H), ^{13}C NMR (400 MHz, $CDCl_3$): δ (ppm) 202.3, 172.4, 131.5, 130.6, 129.3, 127.5, 126.4, 126.3, 124.9, 124, 56.3, 38.1, 28.5. HRMS (EI-DP) m/z: [M^+] Calcd for $C_{19}H_{15}NOS_2$ 330.9788; Found 330.9783

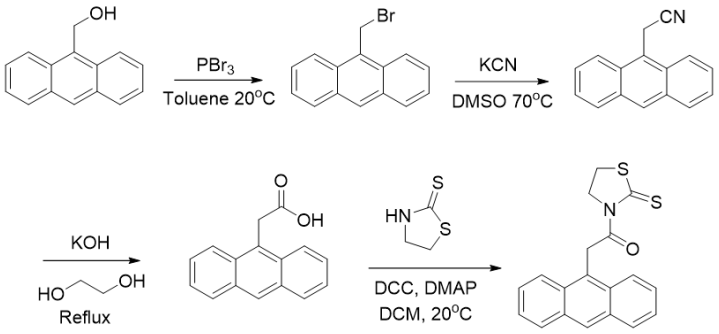

Scheme 3.1: Synthesis of activated anthracene methanol.

Synthesis of PSMA monomodal grafted silica nanoparticles

PSMA grafted silica nanoparticles samples were synthesized as described in the experimental section of Chapter 2.

Synthesis of bimodal anthracene-PSMA grafted nanoparticles

Silica nanoparticles (3 g) were dispersed into THF (50 ml). 3-Aminopropyldimethylethoxysilane (150 mg, 930 μmol) was then added to the solution at room temperature and the solution was stirred at 70 ^{o}C for 3 hrs under N_2. The nanoparticles were precipitated in a large amount of hexanes and isolated via centrifuge at 5,000 rpm. The particles were re-dispersed into THF. The precipitation and dispersion was repeated three times. An excess of activated anthracene ligand was added to the particle suspension and stirred overnight under N_2. The particles were precipitated in a large amount of hexanes, centrifuged, and re-dispersed in THF. Precipitation and isolation was repeated until the supernatant was clear. The particles were redispersed into THF and a second population of 3-aminopropyldimethylethoxysilane was added just as described above. A THF solution of activated CPDB was added dropwise to the amine functionalized particles. The reaction was left to stir overnight at room temperature. Next the particles were precipitated and washed three times as described above. After the particles were dried in vacuum, quantification of surface groups was determined using UV-vis spectroscopy. PSMA was grown from the particle surface as described previously in Chapter 2.

Composite preparation

Particles in THF solution were refluxed with toluene and polypropylene powder for 30 min to allow for dissolution of the polypropylene. Solvent-based pre-mixing has been reported in the literature to improve dispersion in polymer based nanocomposites.[24] Solvent was removed in a vacuum oven at 120°C for 72 hours and the resulting composite was used as a master batch for later processing.

The master batch was diluted to 2wt% loading of silica via melt mixing in a twin screw Thermo-Haake melt compounder. The melt was mixed at 185 °C and 60 RPM for 10 minutes. The as-received nanoparticles were mixed in the above manner as a control. The neat polypropylene control was melt blended to create pellets from the as-received polymer powder in the same way. Ungrafted PSMA chains were also added to polypropylene for a control using the same procedure. Three batches of bimodally modified silica nanoparticles were created as shown in Table 3.1.

The "PSMA2" control containing silica nanoparticles with a PSMA brush was prepared without the solvent pre-mixing step to cause more brush-brush entanglement and create a dispersion state similar to the bimodally modified particle composites with elongated agglomerates as well as to highlight the impact of processing. For this sample, the particles were dried and then combined with neat polypropylene in the melt mixing step.

Films for AC breakdown testing were pressed to approximately 100 μm thickness, and films for DC testing were pressed to approximately 50 μm thickness. These films were tested at a ramp rate of 500 V/s using a ball-plane electrode geometry under silicone oil to avoid flashover. Thicker films of approximately 400 μm were prepared in the same manner for dielectric spectroscopy. Samples for voltage endurance were prepared from the neat polypropylene as well as from the Anth1 and the Anth2 systems using a needle-plane geometry. Needles with a nominal radius of curvature of 6 μm were imbedded with a 2 mm separation tip-to-plane to create a highly divergent field. The field at the tip can be calculated from[25]

$$E_{tip} = \frac{2V}{r \ln \frac{4d}{r}}$$

Where V is the applied voltage, r is the tip radius of curvature, and d is the tip-to-plane spacing.

Table 3.1. Surface modification and composite processing. All samples were prepared by solvent pre-mixing followed by melt compounding, except for PSMA2 which was prepared by dry pre-blending & melt compounding.

Sample	PSMA brush graft density (chains/ nm^2); M_n (kg/mol)	Small ligands (σ = 0.3 molecules/nm^2)
As Received	NA	NA
PSMA1	0.13; 86	NA
PSMA2	0.14; 81	NA
Anth1	0.13; 75	Anthracene
Anth2	0.06; 80	Anthracene
Anth3	0.13; 10	Anthracene

3.4 Results and Discussion

Activated anthracene synthesis

Anthracene ligand was synthesized to contain 2-mercaptothiazoline activated acids for particle attachment. Previously, our group reported using azide-alkyne Huisgen cycloaddition, or the classic "click" reaction to attach surface ligands to silica nanoparticles.[22] While the click approach is advantageous in many instances for its efficiency, in this case the click reaction was unfavorable as it required: 1) additional synthetic steps for azide functionalization of the silica surface, 2) strict anaerobic conditions, and 3) a copper catalyst that could remain bound to the silica surface and interfere with electrical activity. Using activated acids allowed for easy attachment to amine functionalized nanoparticles without a catalyst, metal contamination, or the need for

anaerobic conditions. The only byproduct of amidation, 2-mercaptothiazoline, was washed away in subsequent particle work up. The activated anthracene was synthesized by reacting carboxylic acid containing anthracene molecules with 2-mercaptothiazoline in a Steglich Coupling reaction. Synthesis of activated anthracene was achieved in four steps starting from commercially available 9-anthracenemethanol. Detailed synthetic schemes can be found in the experimental section.

Bimodal anthracene-PSMA grafted nanoparticles

Bimodal ligand grafted nanoparticles were synthesized in multiple steps through sequential addition of surface groups. In general, 3-aminopropyldimethylethoxy silane was first attached to the particle surface. A higher concentration of silane was used in this step compared to the monomodal synthesis, as the target graft density (0.25 ch/nm^2) for the anthracene population was higher than that of the PSMA population. Subsequent covalent bonding of the desired activated anthracene through amidation was performed. Next, a second population of 3-aminopropyldimethylethoxy silane was added to the particle surface before attaching CPDB as described in the monomodal synthesis. Lastly, SMA was polymerized using surface initiated RAFT polymerization. Scheme 3.2 shows the synthetic process to achieve anthracene-PSMA bimodal particles. Polymer graft densities were controlled through the feed ratio of the second 3-aminodimethylethoxy silane population.

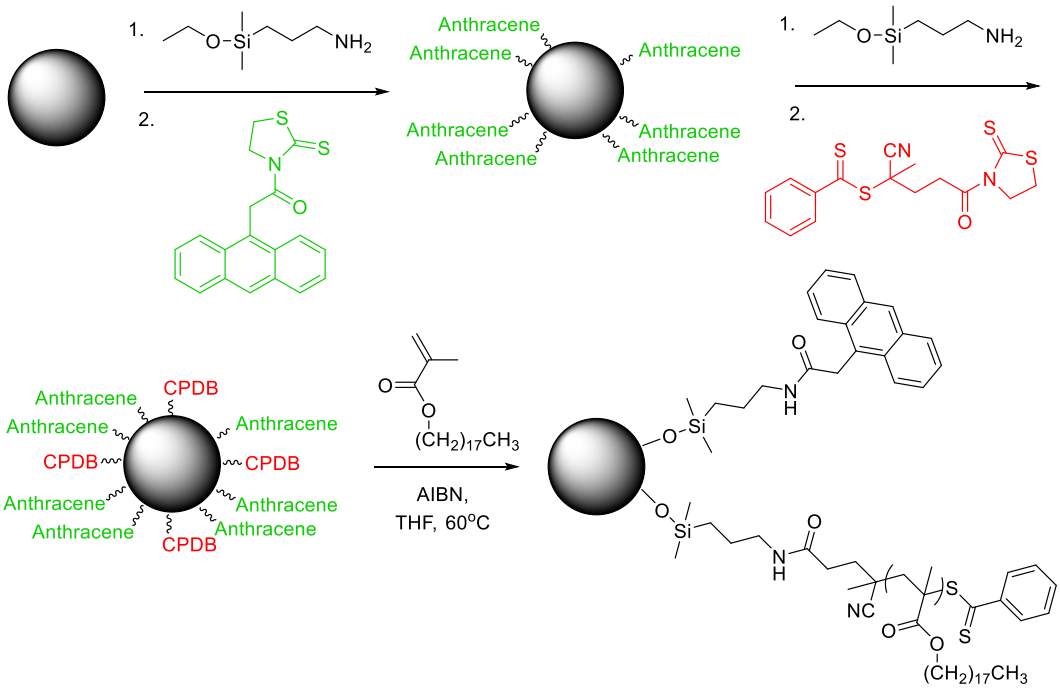

Scheme 3.2. Synthesis of bimodal anthracene-PSMA silica nanoparticles.

Attachment of the activated anthracene was confirmed by UV-vis spectroscopy and quantified using a standard calibration curve. Target graft densities for the anthracene were between 0.2 ch/nm^2 and 0.3 ch/nm^2. The UV-vis spectrum for anthracene functionalized particles is shown in Figure 3.2. The characteristic absorbance maxima for anthracene is represented by the peak at 365 nm. The characteristic CPDB absorbance maxima at 302nm can also be seen along with anthracene, after addition of the RAFT agent. Anthracene (365 nm) has absorbance maximum value distinct from CPDB (302 nm), therefore individual graft densities can be quantified via UV-vis spectroscopy before polymerization.

Dispersion effects on DBS

Figure 3.3 displays TEM micrographs and corresponding AC DBS data from the composites with surface modified NFs as well as the as received silica NFs in the order of qualitative dispersion. Micrographs of PSMA2 (the melt-processed sample) displayed elongated agglomerates of silica oriented approximately parallel to the film surface and to

each other. Orthogonal agglomerates and transverse cross sections were not found. The strings in the micrographs were hypothesized to be projections of flattened plate-like agglomerates with consideration of the biaxial stress state in the hot-pressing procedure. Most likely, the stress applied during molding caused the agglomerates to elongate in directions normal to the applied stress; this yielded a platelike morphology in a parallel stacked arrangement. In the as-received sample, the image displayed clustered agglomerates. Although the sample was still aligned, the aspect ratio was reduced compared to PSMA2. PSMA1 displayed relatively well-dispersed NFs with a greater degree of smaller, isolated agglomerates and some individual nanoparticles. The improved dispersion was due to the high density of long PSMA chains, which provided enhanced enthalpic screening.

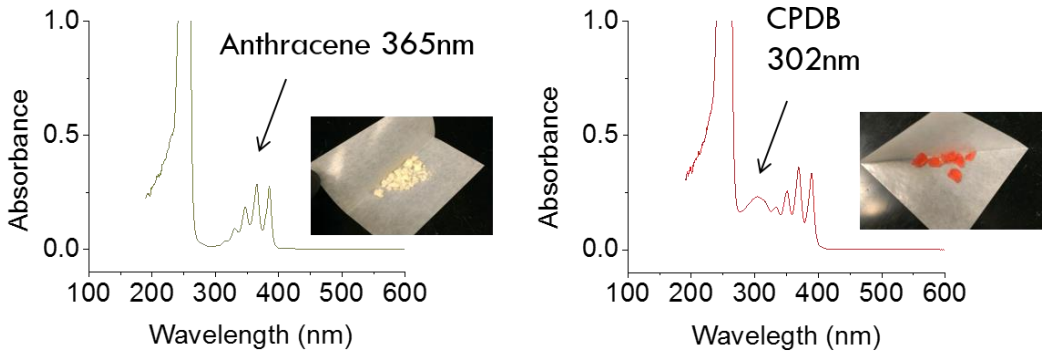

Figure 3.2. UV-vis spectrum of anthracene coated silica nanoparticles (left) and silica particles containing both anthracene and CPDB (right).

All of the composites displayed a generally aligned dispersion state because of the shear from the extrusion and pressing process used to create the test films. The cause of alignment was supported by annealed samples, where the elongated agglomerates relaxed to a spherical shape during annealing. Despite the PSMA2 system having graft density and molecular weight values in the brush similar to the PSMA1 system, the morphologies were

starkly different; this indicated that exclusion of the solvent-processing step permitted the formation of large agglomerates. This may have been the ramification of brush entanglement leading to resilient interparticle bridges.[26] This difference could thus only be due to the use of the solvent premix for the PSMA1 composite; by separating particles with neat polypropylene before drying, this premix should have reduced the formation of strong interparticle entanglements. These results reveal that even systems that are predicted to produce thermodynamically stable dispersed filler states can result in metastable agglomerations when inappropriate processing is used. The bimodal systems with anthracene displayed qualitatively similar dispersion states to those without anthracene. Therefore, the presence of high density anthracene molecules on the surface seems not to have a significant effect on the compatibility of the particles with the polypropylene matrix.

Accompanying the TEM images are AC breakdown strength data for composites with and without anthracene surface modification. In each case, the gross morphology of the nanoparticle dispersion had a major effect on the performance of the composite; this was as significant as a change in the surface chemistry of the filler itself. Well dispersed NFs with anthracene outperformed the neat polymer, and the system with elongated agglomerates performed more poorly than the similarly dispersed composite without anthracene. The effect of the elongated agglomerates seen in PSMA2 and Anth2 was reversed under DC conditions, where they led to a significant increase in DBS, whereas under AC stress, elongated agglomerates led to the highest decrease in DBS. These results and percent changes in the 63% Weibull scale parameter are collected in Table 3.2.

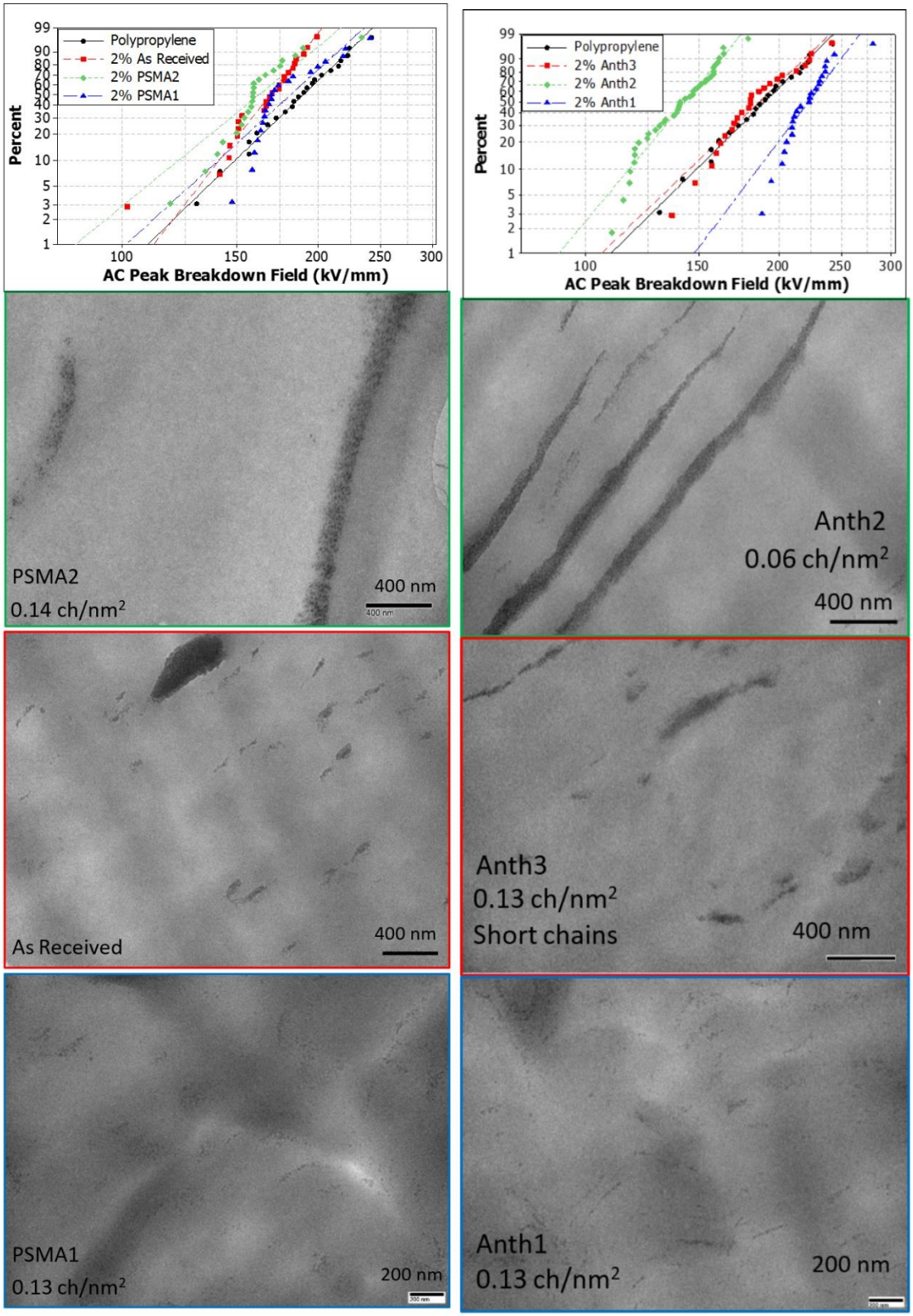

Figure 3.3. AC breakdown results and corresponding TEM images from polypropylene control and composites with and without anthracene surface modification

The disparity between the ac and dc performance in the composite containing high-aspect-ratio agglomerates revealed that the surface treatment was responsible for substantially altering not only the DBS behavior in the nanoparticle-filled polypropylene composites but also the dispersion state, and thus, the arrangement of the particles and the trap states they induced were critical. Anthracene was demonstrated to reduce DBS under DC conditions when it was introduced as a free molecule to polypropylene. This was in agreement with previous work in epoxy under AC conditions, and reinforced the importance of grafting the molecule to nanoparticles if its benefits are to be realized.[19] Weibull scale parameters and their percent change compared to neat polypropylene are tabulated in Table 3.2. Unsurprisingly, the systems with larger cluster type agglomerates performed poorly under both AC and DC test conditions, and the addition of anthracene, while it does moderate this effect, still leads to a composite with reduced performance. As reported in the literature, improving the dispersion can be used to alleviate the DBS penalties that arise from filler agglomeration and the addition of anthracene surface modification to a dispersed nanoparticle containing composite shows significant improvement in DBS under both conditions. The importance of the morphology on the composite's bulk properties is seen in systems with elongated agglomerates and increased in magnitude in the similar system with anthracene surface modification where a disparity is seen between AC and DC DBS performance. A possible explanation for this phenomenon lies in the buildup of space charge. Nanoparticles have been demonstrated to alter the movement of space charge. In the case of an applied DC stress, delaying homocharge near the electrode from which it was injected lowers the local field at the interface, reducing the total injected charge.[27,28]

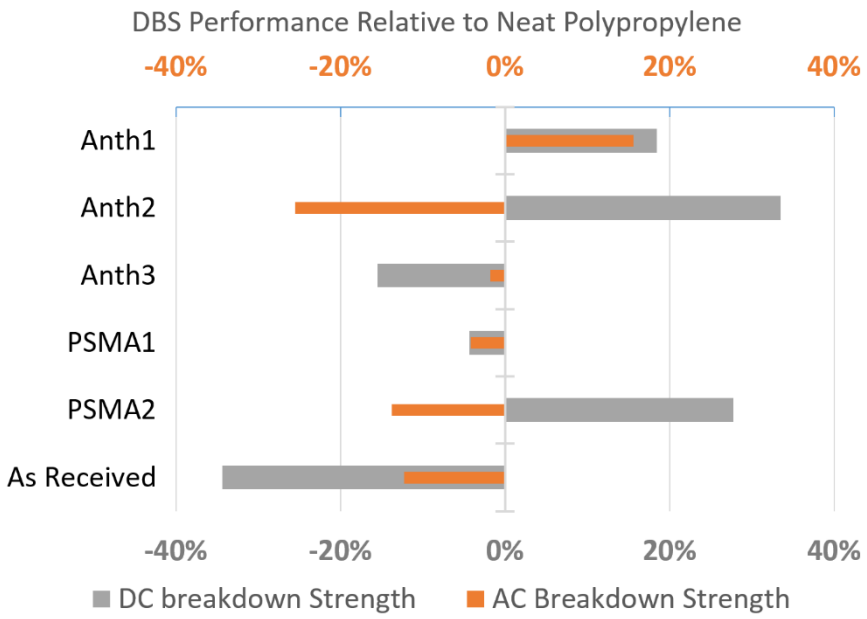

Figure 3.4 Collected 63% characteristic breakdown strength values under AC and DC conditions

Table 3.2. Weibull scale parameters for DBS and respective percent change for each composite under AC and DC test conditions

Sample	AC 63% (kV/mm)	AC %Δ	DC 63% (kV/mm)	DC %Δ
Neat Polypropylene	200	NA	526	NA
As Received	175	-12%	346	-34%
PSMA1	196	-2%	445	-15%
PSMA2	172	-14%	672	28%
Anth2	149	-26%	702	33%
Anth3	191	-4%	503	-15%
Anth1	231	16%	623	18%

The effect of the elongated agglomerates seen in PSMA2 and Anth2 was reversed under DC conditions, where they led to a significant increase in DBS, whereas under AC stress, elongated agglomerates led to the highest decrease in DBS. These results and percent changes in the 63% Weibull scale parameter are collected in Figure 3.4 and Table 3.2. Large elongated agglomerates perpendicular to the field should be effective at trapping

mobile charge before it can advance into the bulk; thus, the composites with such agglomerates should be expected to outperform even the well dispersed systems under DC stress.

Permittivity

The relative permittivity of the composites compared to the neat polymer baseline is displayed in Figure 3.5. The composites with both high aspect ratio agglomerates and dispersed systems comprised of silica nanoparticles grafted with PSMA exhibited a broad peak in the imaginary part of the permittivity (~10^3 Hz). This peak is attributed to the relaxation of PSMA, which exhibits a relaxation in this same frequency range. Additionally, while poorly dispersed silica particles showed increased low frequency losses, the same morphologies with anthracene show a reduction in the imaginary permittivity below 1 Hz compared to the systems without anthracene. This is attributed to the traps introduced by anthracene surface modification reducing mobility of charges otherwise contributing to low frequency losses.

Since the agglomerates were well aligned perpendicular to the field, the larger permittivity enhancement in agglomerated systems was only marginally different than observed in systems with randomly oriented high-aspect-ratio fillers. Improvement of dispersion also reduced losses at low frequency compared to that of the elongated agglomerates. Anthracene containing systems displayed an increase in the real permittivity across the entire tested range when compared to their comparably dispersed control composites with brushes comprised only of PSMA.

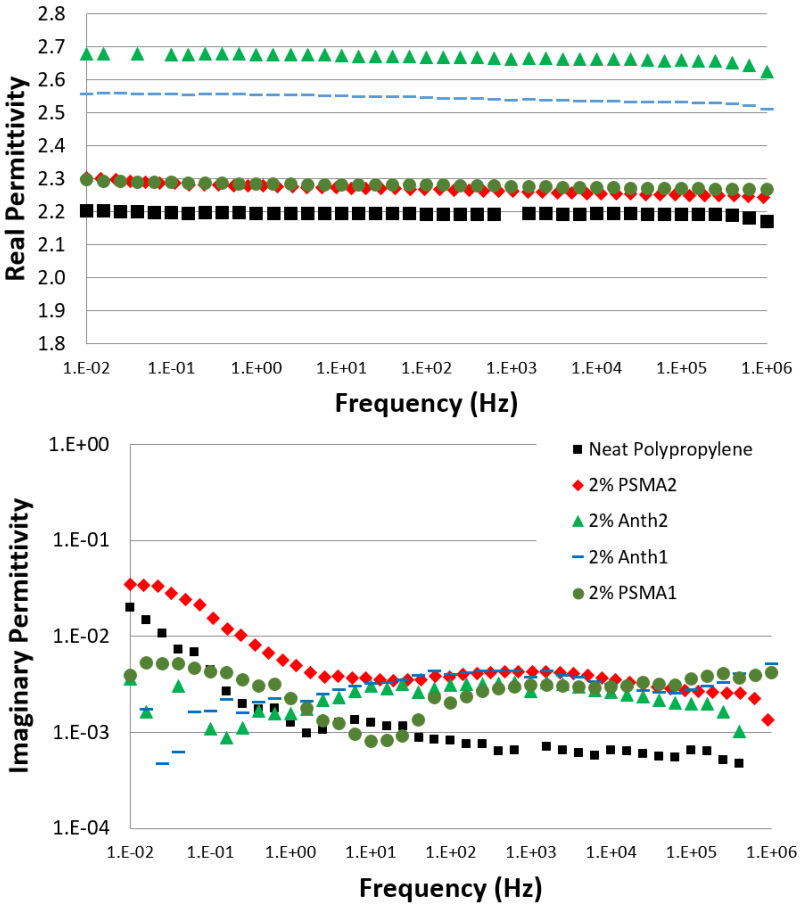

Figure 3.5. Real and imaginary permittivity from example composites compared to neat polypropylene

Voltage Endurance

To investigate the performance of these composites under time-to-failure conditions, AC test conditions were chosen. Thus, the composite system with the best DBS performance under AC conditions was tested, along with the elongated agglomerate system with anthracene. These are compared in Figure 3.6 to a neat polypropylene control where values are in agreement with the literature.[29]

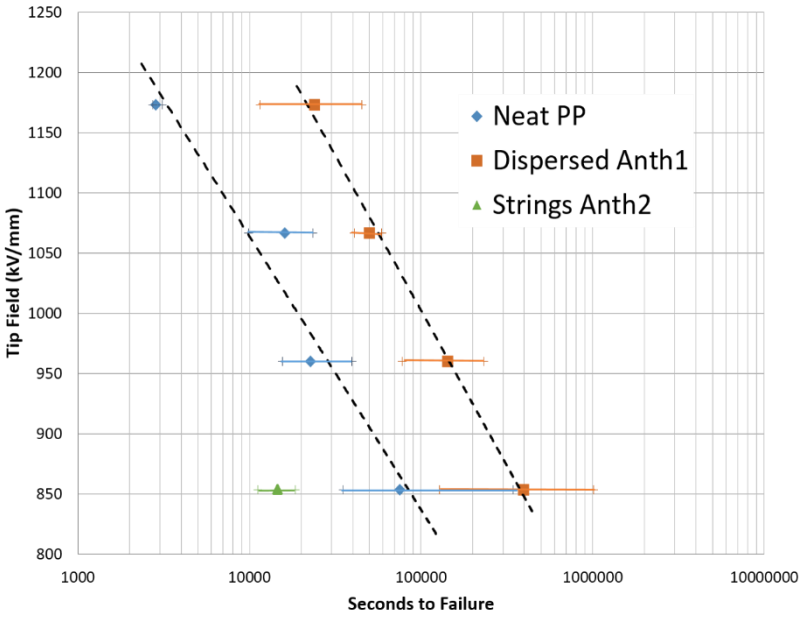

Figure 3.6. Voltage endurance data from polypropylene composites under AC 60 Hz applied voltage. 95% confidence intervals are shown with tick marks

The literature has shown that inorganic nanofillers have the potential to improve voltage endurance of polymer based insulation.[30–32] Improved performance under this test modality may carry more engineering significance than dielectric breakdown strength. Due to the significant time required to gather data, only the best dispersed and elongated agglomerate composites with anthracene modification were chosen as test cases. Figure 3.6 shows that endurance lifetime under AC conditions is greatly improved with well dispersed anthracene modified silica/polypropylene composite, while agglomerates with anthracene significantly reduce time to failure. Only one stress was used for the elongated agglomerates, due to the short times to failure at higher fields. Each point shows the these results indicate that the composite containing dispersed silica particles with anthracene significantly outperform the neat polypropylene. These improvements may be attributed to two combined effects. As anthracene modified silica particles have been shown to increase the breakdown strength under ramped tests and the improvement is indicated to result from

trapping of injected charge carriers, these extrinsic traps may be responsible for slowing homocharge movement near the needle, in the region of highest field concentration. Homocharge buildup lowers the local field and decreases further charge injection, delaying the inception of an electrical tree. Additionally, silica nanofillers have been shown to delay erosion under partial discharge, even at low loadings.[32] Preferential erosion of the polymer results in the residual nanofiller forming a surface coating resistant to discharge. This same phenomenon may also slow tree growth under conditions of internal partial discharges.

3.5 Conclusion

Grafting anthracene to silica nanoparticles as well as successfully polymerizing PSMA from the particle surface allowed for significant improvements to dielectric breakdown strength. Different brushes generated dispersion states dependent on brush graft density, molecular weight, and processing conditions. The dispersions include a high aspect ratio agglomerated system as well as a relatively well dispersed system. These dispersion states were shown to occur independent of the presence or absence of anthracene molecules on the nanoparticle surface and were effected by both processing parameters and the inherent thermodynamics of the brush, indicating a need for more research in systems where the filler may be kinetically trapped in metastable states. Same solvent processing employed to achieve thermodynamically stable dispersions is impractical for industrial applications. Nanoparticles and the addition of anthracene to their surface increased the real permittivity by as much as 20%. The addition of anthracene also decreased the low frequency losses compared to each anthracene-free silica filled control with similar dispersion state, which is attributed to a decrease in the hopping conduction partially responsible for the low frequency behavior. Dispersed silica nanoparticles with anthracene on their surfaces increased the DBS under both AC and DC test conditions by more than

15%, attributed to the trap states introduced by these particles interfering with electron avalanches. This same composite also displayed improved AC voltage endurance over the neat control. Systems with high aspect ratio agglomerates displayed different behavior under AC and DC conditions, improving DC performance more than the dispersed particles but substantially reducing AC breakdown performance. The hypothesis put forth in this work is that this effect may be due to space charge transport being substantially altered in the system where string-like agglomerates oriented perpendicular to the applied field act as barriers to charge motion. By trapping homocharge near the electrode, injection and ultimately breakdown strength under DC test conditions can be improved. Conversely, the same trapped charge could be causing field enhancement every half cycle of applied AC voltage, leading to more charge injection. Calculations from literature values of charge mobility in polypropylene indicate that charge may move on the order of 100 nm each half cycle. This number corresponds to the length scale of the inter-agglomerate separation observed in the high aspect ratio agglomerate composite, and lends some credence to this theory. These results reveal that ideal dispersion may be the best way to guarantee performance under a wide range of conditions in an isotropic material; but anisotropic, partially agglomerated dispersion states are a way to further optimize performance under specific conditions if the proper nanostructuring can be designed for the stress condition.

3.6 Acknowledgements

This work was performed in collaboration with Tim Krentz, and Linda Scadler of the Schadler research group at Rensselaer Polytechnic Institute, as well as, Su Zhao and Henrik Hillborg of ABB corporate research.

3.7 References

(1) Krentz, T.; Khani, M. M.; Bell, M.; Benicewicz, B. C.; Nelson, J. K.; Zhao, S.; Hillborg, H.; Schadler, L. S. *J. Appl. Polym. Sci.* **2017**, *134* (1), 44347–44357.

(2) Lewis, T. J. *IEEE Trans. Dielectr. Electr. Insul.* **1994**, *1* (5), 812–825.

(3) Travelpiece, A. M.; Nelson, J. K.; Schadler, L. S.; Schweickart, D. In *Conference on Electrical Insulation and Dielectric Phenomena*; IEEE, 2009; pp 535–538.

(4) Zhao, S. Mechanical and thermal properties of nanoparticle filled epoxy nanocomposites, 2007.

(5) Nelson, J. K.; Fothergill, J. C. J. *Nanotechnology* **2004**, *586* (5), 586–595.

(6) Roy, M.; Nelson, J. K.; MacCrone, R. K.; Schadler, L. S.; Reed, C. W.; Keefe, R.; Zenger, W. *IEEE Trans. Dielectr. Electr. Insul.* **2005**, *12* (4), 629–643.

(7) Davidson, C.; Trainer, D. In *9th IET International Conference on AC and DC Power Transmission,*; IEEE: London, 2010; pp 1–5.

(8) Calebrese, C.; Hui, L.; Schadler, L. S.; Nelson, J. K. *IEEE Trans. Dielectr. Electr. Insul.* **2011**, *18* (4), 938–945.

(9) Rytöluoto, I.; Lahti, K.; Karttunen, M.; Koponen, M.; Virtanen, S.; Pettersson, M. *IEEE Trans. Dielectr. Electr. Insul.* **2015**, *224*, 2196–2206.

(10) Siddabattuni, S.; Schuman, T. P.; Dogan, F. *ACS Appl. Mater. Interfaces* **2013**, *5* (6), 1917–1927.

(11) Natarajan, B.; Li, Y.; Deng, H.; Brinson, L. C.; Schadler, L. S. *Macromolecules* **2013**, *46* (7), 2833–2841.

(12) Tao, P.; Li, Y.; Siegel, R. W.; Schadler, L. S. *J. Mater. Chem. C* **2013**, 86–94.

(13) Tao, P.; Viswanath, A.; Li, Y.; Siegel, R.; Benicewicz, B. C.; Schadler, L. S. *Polymer (Guildf).* **2013**, *54* (6), 1639–1646.

(14) Meli, L.; Arceo, A.; Green, P. F. *Soft Matter* **2009**, *5* (3), 533–537.

(15) Seitz, F. *Phys. Rev.* **1948**, *73* (6), 549–564.

(16) Seitz, F. *Phys. Rev* **1949**, *76* (9), 1376–1393.

(17) Sparks, M.; Mills, D.; Warren, R.; Holstein, T.; Maradudin, A. A.; Sham, L. J.; Loh, E. J.; King, D. F. *Phys. Rev. B* **1981**, *24* (6).

(18) Yamano, Y. *IEEE Trans. Dielectr. Electr. Insul.* **2006**, *13* (4), 773–781.

(19) Krentz, T. M.; Huang, Y.; Nelson, J. K.; Schadler, L. S.; Bell, M.; Benicewicz, B. In *2014 Annual Report Conference on Electrical Insulation and Dielectric Phenomena*; IEEE: Des Moines, 2014; pp 643–646.

(20) Yamano, Y.; Ilzuka, M. In *Proceedings of 2008 International Symposium on Electrical Insulating Materials*; IEEE, 2008; pp 392–395.

(21) Das-Gupta, D. K.; Barbarez, M. K. *J. Phys. D. Appl. Phys.* **1973**, *6*, 867–871.

(22) Virtanen, S.; Krentz, T.; Nelson, J.; Schadler, L.; Bell, M.; Benicewicz, B.; Hillborg, H.; Zhao, S. *IEEE Trans. Dielectr. Electr. Insul.* **2014**, *21* (2), 563–570.

(23) Shah, J. R.; Mosier, P. D.; Roth, B. L.; Kellogg, G. E.; Westkaemper, R. B. *Bioorganic Med. Chem.* **2009**, *17* (18), 6496–6504.

(24) Song, Y. S.; Youn, J. R. *Carbon N. Y.* **2005**, *43* (7), 1378–1385.

(25) Smith, R.; Liang, C.; Landry, M.; Nelson, J.; Schadler, L. *IEEE Trans. Dielectr. Electr. Insul.* **2008**, *15* (1), 187–196.

(26) Loverso, F.; Egorov, S. a.; Binder, K. *Macromolecules* **2012**, *45* (21), 8892–8902.

(27) Castellon, J.; Agnel, S. In *Annual Report Conference on Electrical Insulation and Dielectric Phenomena*; IEEE, 2006; pp 345–348.

(28) Ma, D.; Hugener, T. a; Siegel, R. W.; Christerson, A.; Mårtensson, E.; Önneby, C.;

Schadler, L. S. *Nanotechnology* **2005**, *16* (6), 724–731.

(29) Holto, J.; Ildstad, E. In *Proceedings of the 2010 IEEE International Conference on Solid Dielectrics*; IEEE, 2010; pp 1–4.

(30) Takala, M.; Ranta, H.; Nevalainen, P.; Pakonen, P.; Pelto, J.; Karttunen, M.; Virtanen, S.; Koivu, V.; Pettersson, M.; Sonerud, B.; Kannus, K. *IEEE Trans. Dielectr. Electr. Insul.* **2010**, *17* (4), 1259–1267.

(31) Roy, M.; Nelson, J. K.; MacCrone, R. K.; Schadler, L. S. *J. Mater. Sci.* **2007**, *42* (11), 3789–3799.

(32) Iizuka, T.; Zhou, Y.; Maekawa, T.; Tanaka, T.; Tatsumi, K. *Conf. Electr. Insul. Dielectr. Phenom.* **2014**, No. 5, 703–706.

CHAPTER 4

POLYISOPRENE-GRAFTED SILICA NANOPARTICLES VIA THE RAFT PROCESS[*]

[*]This chapter was partially adapted from Khani et al., *J. Polym. Sci, Part A: Polym. Chem.* **2017**, DOI: 10.1002/pola.28514[1]

4.1 Abstract

The preparation of well-defined polyisoprene-grafted silica nanoparticles (PIP-*g*-SiO_2 NPs) was investigated. Surface initiated-reversible-addition fragmentation chain transfer (SI-RAFT) polymerization was used to polymerize isoprene from the surface of 15 nm silica NPs. A high temperature stable trithiocarbonate RAFT agent was anchored onto the surface of particles with controllable graft densities. The polymerization of isoprene mediated by silica anchored RAFT with different densities were investigated and compared to the polymerization mediated by free RAFT agents. The effects of different temperatures, initiators, and monomer feed ratios on the kinetics of the SI-RAFT polymerization were also investigated. Using this technique, block copolymers of polyisoprene and polystyrene on the surface of silica particles were also prepared. The well-defined synthesized PIP-*g*-SiO_2 NPs were then mixed with a polyisoprene matrix which showed a good level of dispersion throughout the matrix. Hydrogenated polyisoprene (HPIP)-grafted NPs were also synthesized by diimide-based hydrogenation of PIP-*g*-SiO_2 NPs. HPIP-*g*-SiO_2 NPs were then mixed in isotactic PP matrices to investigate their compatibility with polypropylene. These tunable grafted particles have potential applications in the field of polymer nanocomposites.

4.2 Introduction

Polymer-grafted nanoparticles are of great interest due to their applications in sensors, coatings, optoelectronics, and bioapplications.[2–5] RAFT polymerization has proven to be a powerful controlled radical polymerization technique for preparation of polymer-grafted particles due to the easy attachment and precise control over the grafting densities of RAFT agents. Since the first report on the application of SI-RAFT

polymerization for the modification of silica particles using a surface-anchored RAFT agent by Tsujii et al.,[6] this technique has been widely utilized for the surface modification of various nanoparticles with a wide range of polymers.[7–16]

Polyisoprene and its copolymers have been recognized as an important class of rubber materials and are extensively used in the automotive and medical device industries.[17–20] Polyisoprene contains many double bonds in the polymer backbone which allows for further functionalization or chemical modifications. Isoprene-based polymers have been prepared by coordination, anionic,[21,22] cationic,[23,24] and radical polymerizations,[25,26] among which anionic polymerization has been the major method for the synthesis of such polymers. Anionic polymerization provides excellent control of the polymerization and produces polymers with predictable molecular weights and narrow polydispersities, however, it is expensive and not compatible with electrophilic and acidic functional groups and is challenging in the presence of contaminants.[27,28]

Surface polymerization of isoprene has been reported by living anionic polymerization from the surface of silica particles. Kir et al.[29] applied anionic polymerization on the surface of silica nanoparticles. They modified the surface of particles with a diphenylethylene silane agent that served as the initiating site for the anionic polymerization of isoprene.

There have been significant reports on controlled radical polymerization (CRP) of isoprene by RAFT and nitroxide-mediated polymerization (NMP). Jitchum et al.[30] and Germack et al.[31] have reported RAFT polymerization of isoprene in bulk using high temperature stable trithiocarbonate RAFT agents. However, to the best of our knowledge, surface polymerization of isoprene has not been investigated by any of these CRP

techniques. Herein, the SI-RAFT polymerization of isoprene on silica nanoparticle surfaces was investigated. The kinetics of isoprene surface graft polymerization mediated by RAFT agent anchored onto silica nanoparticles at different conditions was investigated and compared with the RAFT polymerization kinetics mediated by free RAFT agents. Homopolymer, block copolymers, and hydrogenated polyisoprene-grafted silica were also prepared and characterized. Well-defined PIP-*g*-SiO_2 and HPIP-*g*-SiO_2 NPs were then mixed with matrices and the resulting composites were characterized.

4.3 Experimental

Materials

Isoprene was obtained from TCI America and was purified by passage over a neutral alumina prior to use. The RAFT agent 2-(((dodecylthio)carbonothioyl)thio)propanoic acid (DoPAT) (97%) was generously donated by Boron Molecular. Spherical SiO_2 nanoparticles with a diameter of 15 ± 4 nm were purchased from Nissan Chemical Co. Tetrahydrofuran (THF) (HPLC grade, Fisher), xylenes (Fisher), dicumyl peroxide (DCP) (Acros, 99%), di-tert-butyl peroxide (dTBP) (Acros, 99%), azobisisobutyronitrile (AIBN) (Acros, 98%), dicyclohexylcarbodiimide (Acros, 99%), 4-(dimethylamino)pyridine (Acros, 99%), 2-mercaptothiazoline (Acros, 98%), triethylamine (Alfa Aesar, 99%), octadecyldimethylmethoxysilane (Silar, 97%), *p*-toluenesulfonyl hydrazide (Alfa Aesar, 98%), tetrakis(trimethylsilyl)silane (Alfa Aesar, 98%), and 3-aminopropyldimethylethoxysilane (Gelest, 95%) were used as received.

Instrumentation

NMR spectra of products were recorded on a Varian 300 spectrometer using $CDCl_3$ as a solvent and anisole as internal standard. Molecular weights and dispersity (*Đ*) were

measured using a Polymer Labs PL-GPC-120 gel permeation chromatograph (GPC) associated with a 515 HPLC pump, a 2410 refractive index detector, and three Styragel columns. The columns consisted of HR1, HR3 and HR4 which have corresponding effective molecular weight ranges of 100-5000, 500-30000, and 5000-500000, respectively. The GPC used tetrahydrofuran (THF) as eluent at 30 °C and a flow rate of 1.0 mL/min with the calibration of polystyrene standards obtained from Polymer Laboratories. TGA characterization was operated using a TA Instruments Q5000 with a heating rate of 10 °C/min form 25 °C to 1000 °C under nitrogen flow. Transmission electron microscopy (TEM) images were obtain using a Hitachi H8000 TEM operating at an accelerating voltage of 200 kV. The composite sample was cryo-microtomed at -120 °C into 100-150 nm slices using a diamond knife.

Polymerization of isoprene mediated by free DoPAT

In a typical polymerization, isoprene (2g, 30 mmol), DoPAT (35 mg, 0.1 mmol), dicumyl peroxide (2.7 mg, 0.01mol), and THF (2.8 mL) with a ratio between species of [monomer]:[CTA]:[initiator] = 300:1:0.1 were added to a Schlenk tube. The mixture was degassed by three freeze-pump-thaw cycles, filled with nitrogen, and then the Schlenk tube was placed in a 115 °C oil bath. The polymerization was stopped by quenching in ice water. Molecular weights were measured using gel permeation chromatography (GPC) in THF which was calibrated with polystyrene standards.

Preparation of DoPAT-functionalized silica nanoparticles

A solution (20 mL) of colloidal silica particles (30 wt % in methyl isobutyl ketone) was added to a two-necked round bottom flask and diluted with 35 mL of THF. Dimethylmethoxy-n-octylsilane (0.1 mL) was added to improve dispersibility along with

3-aminopropyldimethylethoxysilane (0.7 mL, 5 mmol) and the mixture was refluxed for 5 hours under nitrogen protection. The reaction was then cooled to room temperature and precipitated in a large amount of hexanes (300 mL). The particles were recovered by centrifugation and dispersed in THF using sonication, precipitated in hexanes again. The amine-functionalized particles were dispersed in 40 mL of THF for further reaction. Then 2.5 g, (5.5 mmol) of activated DoPAT was prepared similarly to a procedure described previously[10] and added dropwise to a THF solution of the amine-functionalized silica nanoparticles (40 mL, 6 g) at room temperature. After complete addition, the solution was stirred overnight. The reaction mixture was then precipitated into a large amount of methanol (400 mL). The particles were recovered by centrifugation at 3000 rpm for 5 min. The particles were re-dispersed in 30 mL THF and precipitated in methanol. This dissolution−precipitation procedure was repeated 2 more times until the supernatant layer after centrifugation was colorless. The yellow DoPAT-functionalized silica nanoparticles were dried at room temperature and analyzed using UV-vis spectroscopy to determine the chain density using a calibration curve constructed from standard solutions of free DoPAT. The RAFT agent density of the particles was calculated to be 100 μmol/g of grafted NPs (0.42 chains/nm^2).

RAFT polymerization of isoprene from DoPAT-functionalized silica nanoparticles

In a typical polymerization, isoprene (1.42 g, 21 mmol), DoPAT-g-silica NPs with surface density of 0.10 mmol/g (0.7g, 70 μmol), THF (2.2 ml) and dicumyl peroxide initiator (7.0 μmol) with a ratio between species of [monomer]:[CTA]:[initiator] = 300:1:0.1 were added to a Schlenk tube. The particles were dispersed into the solution via sonication for 1 min and subsequently the mixture was degassed by three freeze-pump-

thaw cycles, filled with nitrogen, and then the Schlenk tube was placed in an oil bath for the desired time and temperature. The polymerization was stopped by quenching in ice water. NMR spectroscopy was used to determine conversion of monomer comparing the monomer peak with the ones of the internal standard (anisole). The resultant polymer grafted particles were then precipitated into a large amount of methanol and centrifuged at 8,000 rpm for 5 min and the particles were dispersed back into THF.

Preparation of poly(isoprene-*b*-styrene)-grafted silica NPs

To make block copolymer-grafted particles, the surface polymerization of isoprene on 0.23 g of DoPAT-*g*-silica NPs with graft density of 79 μmol/g was performed similar to that described in the previous section. The resulting PIP-*g*-SiO_2 NPs were dissolved in 5 mL of THF and excess amount of styrene and AIBN (0.94 μmol) were added to a Schlenk tube. The mixture was degassed by three freeze-pump-thaw cycles, filled with nitrogen, and then the Schlenk tube was placed in a 65 °C oil bath for 8 hours. The polymerization was stopped by quenching in ice water. The resultant polymer grafted particles were precipitated into a large amount of isopropanol and centrifuged at 5,000 rpm for 8 min and the particles were dispersed back into 5 mL of THF. The precipitation and centrifugation steps were repeated one more time to obtain the block copolymer anchored particles.

Hydrogenation of polyisprene-g-silica NPs

Hydrogenation of polyisprene-grafted silica NPs was conducted according to the literature.[32] In a typical procedure, PIP-g-SiO_2 NPs (200 mg) were added to 40 ml of xylene at 60 °C in a three-neck flask which was equipped with condenser under nitrogen atmosphere. After dissolution of PIP-*g*-SiO_2 NPs, more than 100% excess amounts of *p*-toluenesulfonyl hydrazide and triethylamine were added to the flask and the temperature

was raised to 115 °C. The hydrophilic impurities were removed by precipitation of the particles in cold methanol (five times) to obtain a white powder product. NMR spectroscopy was used to determine hydrogenation yield by comparing the vinylic hydrogens to those of tetrakis(trimethylsilyl)silane as the internal standard. A bimodal architecture was also synthesized in two steps. The first population was created by reaction of octadecyldimethylmethoxysilane (excess) and amine functionalized particles. The second population was polyisoprene generated by surface initiated RAFT followed by hydrogenation as explained earlier.

General procedures for cleaving grafted polymer from particles

In a typical experiment, 50 mg of polymer-grafted silica particles were dissolved in 4 mL of THF. Aqueous HF (49%, 0.2 mL) was added, and the solution was allowed to stir at room temperature overnight. The solution was poured into a PTFE Petri dish and allowed to stand in a fume hood overnight to evaporate the volatiles. The recovered polymer was then dissolved in THF and analyzed by GPC.

Preparation of polyisoprene nanocomposite filled with PIP-*g*-SiO_2 NPs

A PIP-*g*-SiO_2 NPs sample (M_n = 26 Kg/mol, $Đ$ = 1.5) in THF was mixed with a solution of free polyisoprene (M_n = 77 Kg/mol, $Đ$ = 1.4) in THF in appropriate quantities at room temperature. The solution was stirred for 10 minutes and was cast in a Petri dish and dried in vacuum for 24 h. The final film was used for further characterizations.

Preparation of polypropylene nanocomposite filled with HPIP-*g*-SiO_2 NPs

A sample of HPIP-*g*-SiO_2 (M_n = 12 Kg/mol, 0.5 ch/nm^2) or bimodal C18-HPIP-*g*-SiO_2 NPs (M_n = 23 Kg/mol 0.3 ch/nm^2) in a solvent system of THF/xylene = 4 was added

to a dilute solution of isotactic polypropylene (5 Kg/mol) in toluene at 100 °C. The solution was stirred for 10 minutes and was cast on a hot glass and dried. The final film was used for further characterizations.

4.4 Results and Discussion

Polymerization of isoprene mediated by free DoPAT

Before performing the RAFT polymerization of isoprene on the surface of NPs, detailed studies on the polymerization of isoprene mediated by free RAFT agents were conducted. Previous studies of the polymerization of isoprene by the RAFT technique indicated that selecting a suitable RAFT agent is necessary for successful control. Jitchum et al.[30] compared the use of two types of RAFT agents in the polymerization of isoprene, a dithiobenzoate derivative 4-cyanopentanoic acid dithiobenzoate (CPDB) and a trithiocarbonate derivative 2-ethylsulfanylthiocarbonyl sulfanylpropionic acid ethyl ester (ETSPE) at 60 and 120 °C. At 60 °C both RAFT agents produced low monomer conversions and polymers with broad polydispersities. Upon increasing the temperature to 120 °C, degradation of CPDB was observed leading to an uncontrolled polymerization. However, ETSPE mediated polymerizations showed a continuous growth of polymer chains without any loss of RAFT agent suggesting that a high temperature stable RAFT agent is needed for this reaction. Herein, in this study, we employ 2-(((dodecylthio)carbonothioyl)thio)propanoic acid (DoPAT), a high temperature stable RAFT agent.

Scheme 4.1 shows the synthetic procedure for the RAFT polymerization of isoprene mediated by free DoPAT in solution. The polymerization was performed with the feed ratio of [monomer]/[CTA]/[initiator] = 300:1:0.1 at 115 °C under inert gas conditions.

The kinetic results for the solution RAFT polymerization of isoprene are shown in Figure 4.1 (GPC data shown in Figure 4.2). A linear relationship between monomer consumption and time over the conversion range studied implies a constant radical concentration throughout the polymerization. The controlled nature of the polymerization was demonstrated by the linear increase of M_n with respect to monomer conversion. Molecular weights were in general agreement with theoretical molecular weights, and molecular weight distributions were generally narrow (~1.2) These results were in agreement with previous studies reported by Jitchum[30] and Germack[31] and confirmed that the trithiocarbonate RAFT agent selected for the current studies was suitable for high temperature RAFT polymerizations.

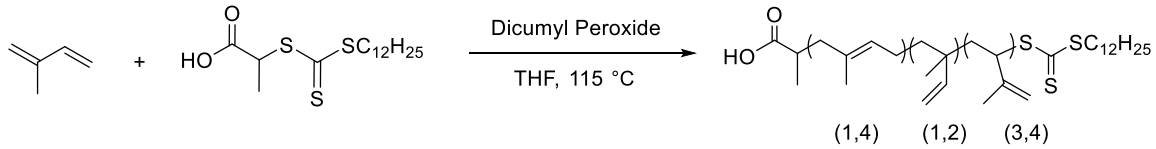

Scheme 4.1. Polymerization of isoprene mediated by free DoPAT RAFT agent.

RAFT polymerization of isoprene from DoPAT-functionalized silica nanoparticles

To perform the polymerization of isoprene onto the surface of particles, modification of the surface was required. Attachment of DoPAT chain transfer agent was carried out in two steps according to the literature. Following the attachment of aminosilane molecules onto the particles' surface, the amino-functionalized silica particles were reacted with activated DoPAT to give DoPAT-grafted SiO_2 NPs (DoPAT-*g*-SiO_2) (Scheme 4.2). The attachment of DoPAT onto silica nanoparticles was confirmed by UV-vis spectrometry. The amount of RAFT agent anchored onto the modified silica nanoparticles was determined quantitatively by comparing the absorption at *ca.* 300 nm for the DoPAT anchored silica nanoparticles to a standard absorption curve made from known amounts of

the free DoPAT. Using this method DoPAT-*g*-SiO_2 NPs with densities of 100 µmol/g (0.42 chains/nm^2) and 32 µmol/gr (0.14 chains/nm^2) were synthesized and used to study the SI-RAFT polymerization of isoprene.

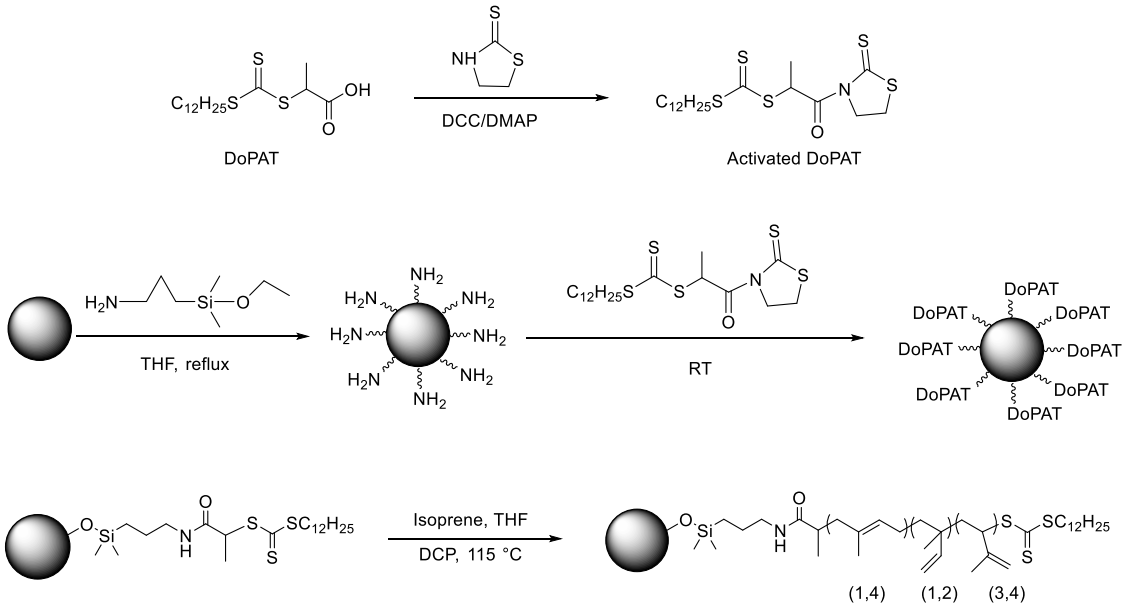

Scheme 4.2. Preparation of PIP-*g*-SiO_2 NPs.

To perform the surface polymerization of isoprene, DoPAT-*g*-SiO_2 particles need to be dispersed in a solvent medium that should be polar enough to disperse silica particles and yet able to dissolve non-polar polyisoprene chains. In this work, tetrahydrofuran (THF) was used as a suitable solvent for the dispersion of silica particles combined with excess monomer as a solvent for the polyisoprene chains. It was found that when the THF to monomer ratio (v/v) was smaller than 1, partial gelation of the polymerization occurred. This gelation could be due to the inter-particle polymeric radical coupling which normally occurs at high concentration of particles.[33] Therefore, a solvent to monomer ratio of 1 was maintained in all polymerizations.

The molar ratio of [initiator]/[CTA] was set to 0.1. This ratio is low enough to minimize termination by surface anchored polymeric radical recombination and also

helped minimize the amount of free polymer derived from the initiator and yet maintains a moderate polymerization rate.[6,7,10] When a reaction was conducted with a higher ratio of initiator ([initiator]/[CTA] = 0.3), partial gelation of the polymerization solution was observed after 4 h and complete gelation was observed after 7 h (Sample 5 in Table 4.1). This experiment showed that a low ratio of [initiator]/[CTA] is essential for controlling the graft polymerization of isoprene.

Table 4.1. Data for the SI-RAFT polymerization of isoprene on DoPAT-g-SiO_2 NPs (0.42 ch/nm^2) using different initiators at various temperatures and conditions.

Sample No.	Initiator	[M]:[CTA]:[I]	Temp. (ºC)	Reaction time (hr)	Conversion (%)	M_n (Kg/mol)	$Đ$
1	AIBN	300:1:0.1	75	7	8	2.7	1.1
2	AIBN	300:1:0.1	75	23	23	4.9	1.09
3	DCP	300:1:0.1	95	7	15	4.6	1.17
4	DCP	300:1:0.1	115	7	38	9.7	1.25
5	DCP	300:1:0.3	115	7		gelation	
6	DCP	10000:1:0.1	115	24	-	44	1.4
7	dTBP	300:1:0.1	135	7	27	8.1	1.17
8	dTBP	2000:1:0.1	135	8	-	27	1.45

The SI-RAFT polymerizations of isoprene were studied at two different RAFT agent densities of 100 µmol/gr (0.42 chains/nm^2) and 32 µmol/gr (0.14 chains/nm^2) to investigate the effect of grafting densities on the polymerization and were compared with the polymerization mediated by free DoPAT. All reactions were conducted under identical conditions using dicumyl peroxide as the initiator at 115 ºC and with the ratio between

species of [monomer]:[CTA]:[initiator] = 300:1:0.1. The polymerizations were conducted at low conversion range to avoid possible gelation or inter-particle radical coupling.[33] The results of the kinetic studies for the SI-RAFT polymerization of isoprene mediated by surface anchored RAFT agents (two graft densities) and free RAFT agent are shown in Figure 4.1. The graphs show a linear relationship between monomer consumption and time for all cases over the range of conversion studied, which indicates a constant free radical concentration during the polymerization. The results in Figure 4.1 also show that the molecular weight increased linearly with monomer conversion for all polymerizations, measured molecular weights were in general agreement with the theoretical molecular weights, and molecular weight distributions were generally narrow. However, the rates of the polymerizations mediated by surface anchored RAFT agents were apparently higher than the polymerization mediated by free RAFT agent under identical conditions. Also, in the case of anchored RAFT agent systems, the polymerization with higher DoPAT density proceeded at a higher rate compared to the system with lower DoPAT density. This trend is opposite that observed in the RAFT polymerization of styrene where the polymerization rate decreased at increasing RAFT agent density. In another comparison between the free and graft RAFT polymerization rates, isoprene behaved similar to styrene where free polymerization rates were lower than grafted polymerization rates but opposite that of methyl methacrylate.[10] From the limited data available in the literature at this time, it is still difficult to discern definitive trends in polymerization rates in these systems. Another difference between the grafted and free RAFT polymerization of isoprene was observed in the GPC results. A collection of GPC traces of polyisoprene prepared by free RAFT (Figure

4.2) and grafted RAFT polymerization (after cleaving from the NPs) (Figure 4.3) are shown.

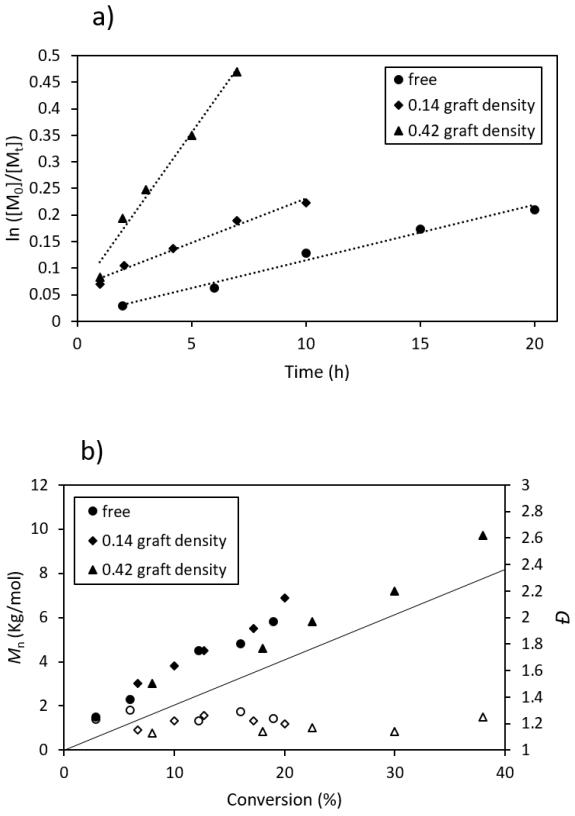

Figure 4.1 (a) First-order kinetic plots and (b) dependence of molecular weight (solid line, $M_{n,\ theory}$) on the conversion for the SI-RAFT polymerization of isoprene on silica nanoparticles; high surface density (triangle, 100 μmol/g, 0.42 ch/nm^2); low surface density (diamond, 32 μmol/g, 0.14 ch/nm^2); free DoPAT, (circle). All polymerizations were conducted under identical conditions with the ratio of [monomer]:[CTA]:[initiator] = 300:1:0.1.

In previous works on the graft polymerization of styrene from nanoparticle surfaces using RAFT, considerable low molecular weight tailing and high molecular weight humps were observed due to the surface radical migration effect and termination by recombination.[6,7] In our work, no apparent high molecular weight hump is observed for the graft polymerization even at monomer conversions up to 38%. However, an apparent low molecular weight shoulder peak was observed at about 1600 s elution time which is

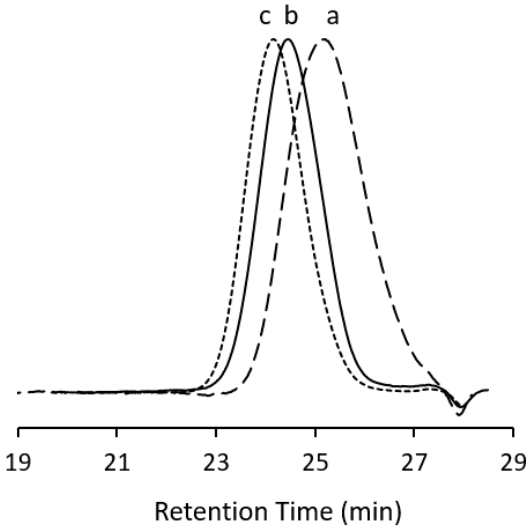

Figure 4.2. GPC traces of polyisoprene prepared from RAFT polymerization mediated by free DoPAT in THF for (a) 6% conversion, M_n = 2500; (b) 12.2% conversion, M_n = 4500; (c) 19% conversion, M_n = 5800; [monomer]:[CTA]:[initiator] = 300:1:0.1.

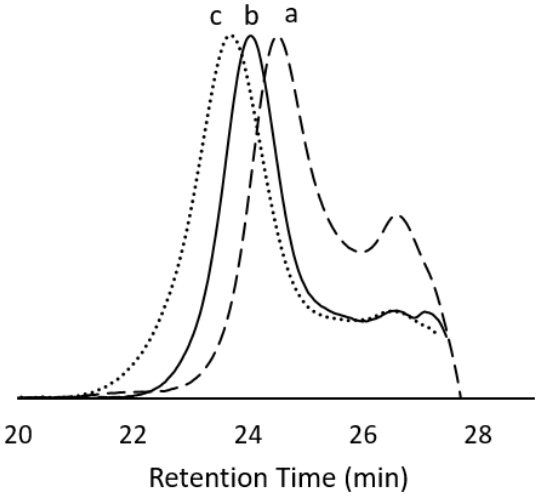

Figure 4.3. GPC traces of polyisoprene prepared from RAFT polymerization mediated by grafted RAFT agents in THF for (a) 18% conversion, M_n = 4600; (b) 30% conversion, M_n = 7200; (c) 38% conversion, M_n = 9700; [monomer]:[CTA]:[initiator] = 300:1:0.1.

equivalent to 900 Da molecular weight. Our first hypothesis was that this low molecular peak could be due to the presence of the surfactants used in the manufacture of silica particles which were cleaved along with the grafted polymer chains from the particles. To

evaluate the origin of this peak, the eluents were collected after passing through the GPC columns, separated, and analyzed by FTIR spectroscopy.

Figure 4.4 shows the FTIR spectra of the polymer and the residual peaks. The strong peaks at 1000-1150 cm^{-1} in the residual sample are ascribed to the Si-O-Si bonds probably from small molecules emanating from the remaining of the etched particles after chain cleavage by HF. The broad peak at 3200-3600 cm^{-1} could also be ascribed to the OH moieties from the silica particles and/or surfactants present on particles. To further evaluate and ensure this hypothesis, a sample of bare silica particles was etched by HF with the same method for polymer chain cleavage explained earlier and analyzed by GPC. The GPC trace of this sample is shown in Figure 4.5 and compared with the cleaved polyisoprene and clearly shows a strong peak that matches the low molecular weight shoulder peak observed in the GPC of the cleaved polyisoprene sample. These results indicate that the shoulder peak could be ascribed mostly to the surfactants and stabilizers used in the manufacture of silica and small molecules produced from the silica particles during the polymer cleavage and not from the SI-RAFT process.

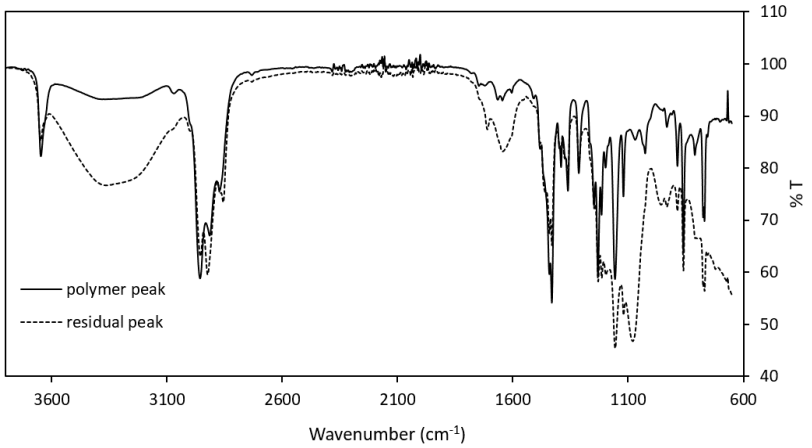

Figure 4.4. FTIR spectra of the collection of two different eluent peaks from the GPC of cleaved polyisoprene.

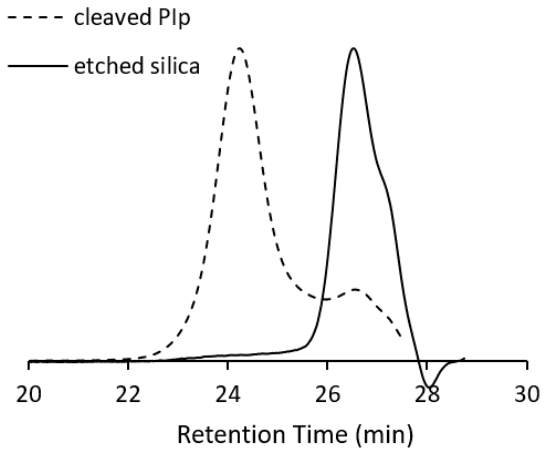

Figure 4.5. GPC traces of cleaved polyisoprene (dashed line) and etched silica (solid line).

The SI-RAFT polymerization of isoprene was conducted at different temperatures using different initiators with ratios between species of [monomer]:[CTA]:[initiator] = 300:1:0.1 under identical conditions. We observed that polymerization at 75 ºC using AIBN as the initiator after 7 h showed low conversion and molecular weight with dispersities as low as 1.10 and at longer times this reaction showed higher conversion and molecular weight (M_n = 4.9 Kg/mol) with low dispersity (Samples 1 and 2 in Table 4.1). When the polymerization was conducted at 95 ºC with dicumyl peroxide as the initiator, the reaction proceeded to higher percent conversion without loss of control (Sample 3 in Table 4.1). These results are interesting when compared to the results of Jitcham et al.[30] and Germack et al.[31] for the bulk RAFT polymerization of isoprene at similar temperatures (76 and 90 ºC) where they observed low conversions and molecular weights (1.5-2 Kg/mol) at these temperatures even after much longer reaction times.

The investigation of the effects of reaction temperature on the graft polymerization was further conducted by choosing two temperatures, 95 and 115 ºC using dicumyl peroxide as the initiator. The kinetic studies of the SI-RAFT polymerization of isoprene at

different temperatures is shown in Figure 4.6. Both polymerizations showed a linear relationship between monomer consumption and time over the conversion range studied. Also a linear increase in molecular weight as a function of conversion was observed. However, at 115 ºC conversion of 38% was reached within 7 h, while polymerization at 95 ºC yielded only 15% conversion within the same time. Relatively low dispersities ($Đ$ < 1.25) were maintained at both temperatures for all conversions investigated in this work. The graft polymerization of isoprene was also performed at 135 ºC using di-tert-butyl peroxide as the initiator and resulted in PIP-*g*-SiO_2 NPs with similar low dispersity (Sample 7, Table 4.1). These results suggest that the SI-RAFT polymerization of isoprene can be performed at a wide range of temperatures with relatively good control over the molecular weight and dispersity. To test if this method is able to produce high molecular weight PIP-*g*-SiO_2, a polymerization reaction with high ratio of [monomer]:[CTA] = 2000:1 was conducted at 135 ºC using di-tert-butyl peroxide as initiator (Sample 8, Table 4.1). PIP-*g*-SiO_2 with polymer molecular weight of 27 Kg/mol and $Đ$ of 1.45 was obtained. In another experiment, a polymerization reaction with [monomer]: [CTA] = 10000:1 using dicumyl peroxide as initiator at 115 ºC was performed for 24 h which resulted in PIP-*g*-SiO_2 with M_n = 44 Kg/mol and $Đ$ = 1.5. Note that the molecular weight distribution for the RAFT polymerization of isoprene is generally higher than that of styrenic and acrylic monomers and this could probably be due to the presence of double bonds in the polymer chains which could increase the chance of chain-chain couplings, particularly at higher temperatures and conversions.[31]

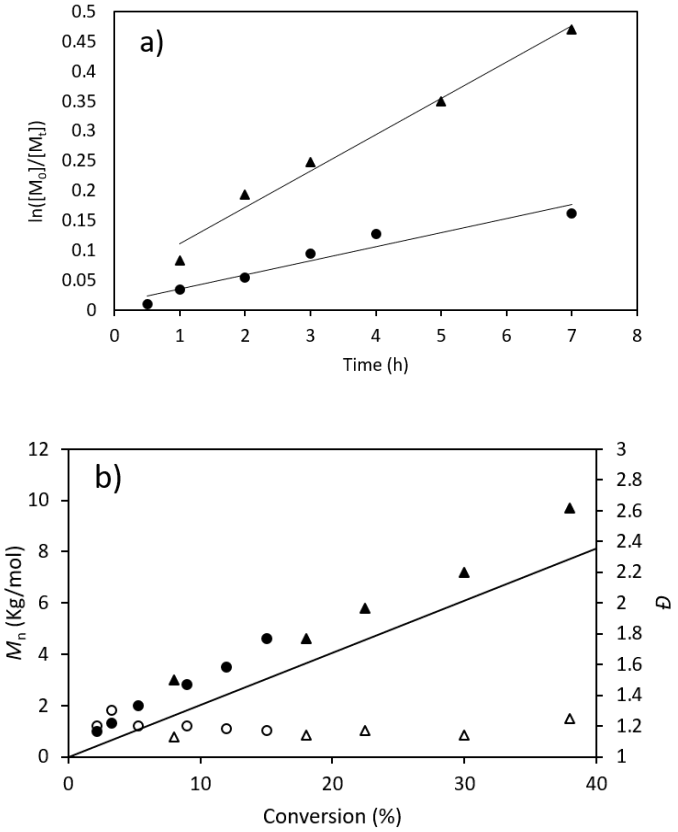

Figure 4.6. (a) First-order kinetic plots and (b) dependence of molecular weight (solid line, $M_{n,\ theory}$) on conversion for the SI-RAFT polymerization of isoprene on DoPAT-*g*-SiO_2 NPs with RAFT agent density of 100 μmol/g, 0.42 ch/nm^2 at 95 ºC (circle) and 115 ºC (triangle) using dicumyl peroxide as initiator. All polymerizations were conducted under identical conditions with the ratio of [monomer]:[CTA]:[initiator] = 300:1:0.1.

To investigate the effects of monomer loading on the SI-RAFT polymerization of isoprene, polymerizations with [monomer]:[CTA] of 100, 300, and 1000 were conducted at 115 ºC. A ratio of [CTA]:[DCP] = 10 was kept for all polymerizations. Polymerizations were performed on the particles with the RAFT agent density of 100 μmol/gr (0.42 chains/nm^2) under identical reaction conditions. Note that the concentration of monomer remained the same since a volume ratio of monomer/solvent = 1 was maintained for all polymerizations.

The results of the kinetic studies are shown in Figure 4.7 including previous data at 115 ºC. All the polymerizations showed a linear relationship between the monomer

consumption and time and relatively the same rate was observed in all polymerizations. All polymerizations were well controlled as the number-average molecular weights increased in a linear fashion with monomer conversion with relatively low molecular weight distributions (<1.25).

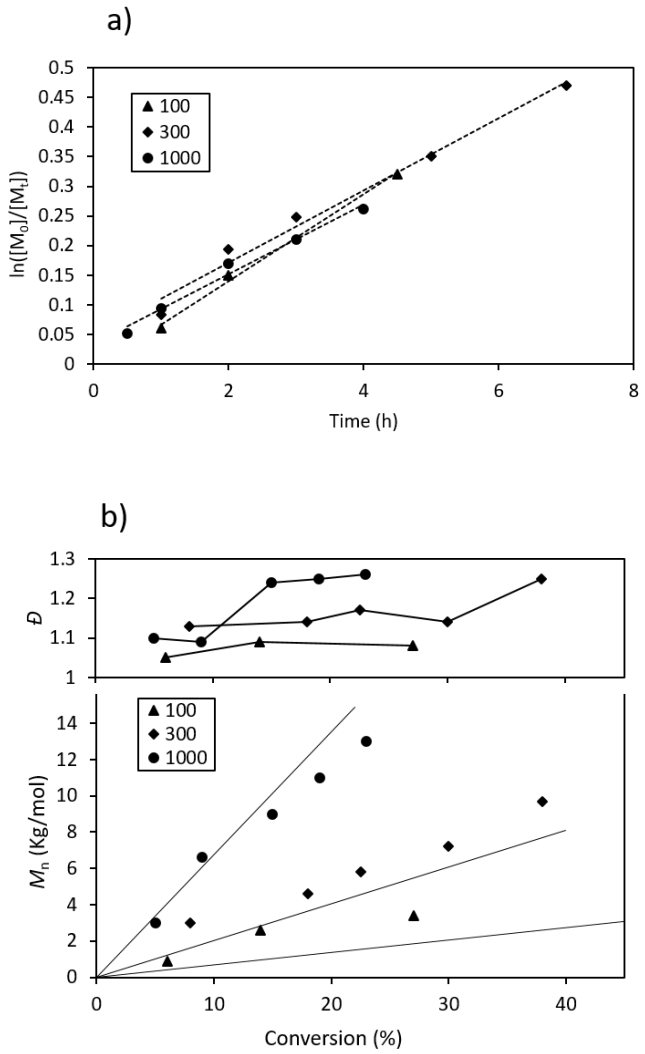

Figure 4.7. (a) First-order kinetic plots and (b) dependence of molecular weight (solid line, $M_{n,\ theory}$) on conversion for the SI-RAFT polymerization of isoprene on DoPAT-*g*-SiO_2 NPs with RAFT agent density of 100 μmol/g, 0.42 ch/nm^2 at 115 ºC with the ratio of [monomer]:[CTA] of 100 (triangle), 300 (diamond), and 1000 (circle). All polymerizations were conducted at identical conditions with the ratio of [CTA]:[initiator] = 10.

^{1}H NMR spectroscopy of PIP-*g*-SiO_2 NPs indicated the presence of products of three types of additions, 1,4-addition, 1,2-addition, and 3,4-additon as shown in Figure 4.8.

The peak at ~5.3 ppm is attributed to 1 H of –C*H*═C$(CH_3)_3$ from the 1,4-addition (both *cis* and *trans*), the broad peak at 5.7-5.9 ppm to 1 H of –C*H*═CH_2 from the 1,2-addition, the one at 4.7-4.9 ppm to 2 H of –C$(CH_3)_3$═C*H*$_2$ from the 3,4-addition, and the peak at 4.9-5.2 ppm to 2 H of –CH═C*H*$_2$ from the 1,2-addition. In a previous report on the bulk RAFT polymerization of isoprene by Jitcham et al.[30], the product isomer ratios were 75% (1,4), 25% (1,2 and 3,4) isomers obtained from the ^{1}H NMR. However, in our study the major product was ~88% 1,4 isomer and the 1,2 and 3,4 isomers were together ~12% of product which was independent of monomer conversion. RAFT polymerization of isoprene mediated by free DoPAT gave the same ratio of isomers (Figure 4.9).

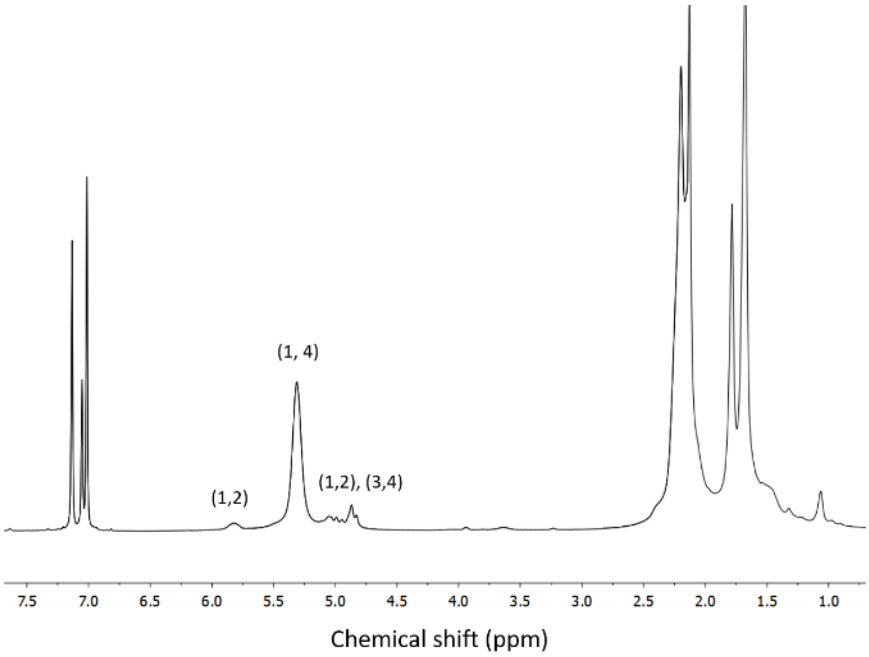

Figure 4.8. ^{1}H NMR spectrum of PIP-*g*-SiO_2 particles in $CDCl_3$ with indication of polyisoprene isomers prepared by SI-RAFT polymerization.

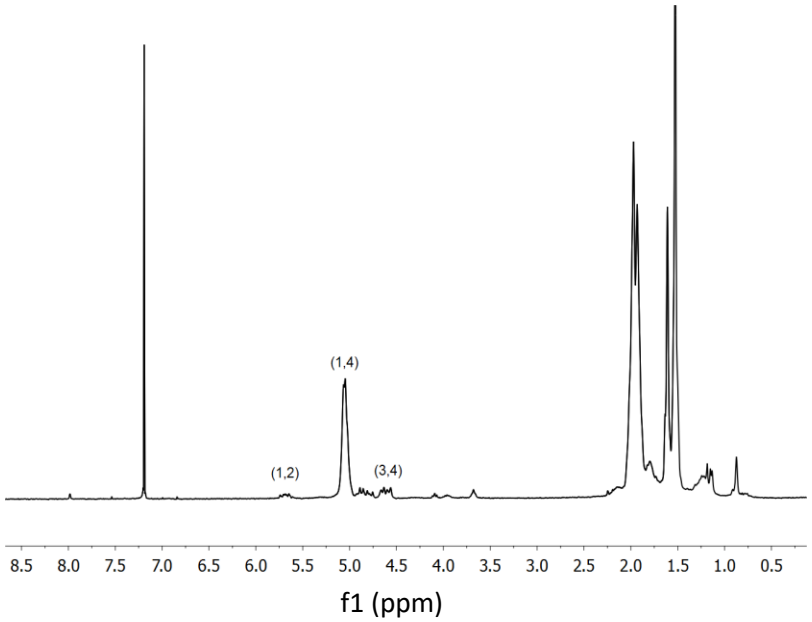

Figure 4.9. ^{1}H NMR spectrum of polyisoprene in $CDCl_3$ with indication of polyisoprene isomers prepared by free RAFT polymerization.

Block copolymerization

A chain extension reaction was carried out on PIP-*g*-SiO_2 NPs. To accomplish this, a recovered sample of PIP-*g*-SiO_2 (79 µmol/gr, M_n = 9.4 Kg/mol, $Đ$ = 1.14) was dissolved in THF and added to a Schlenk tube along with an excess of styrene with AIBN (0.1 equivalent relative to macro-chain transfer agent). Polymerization was conducted at 65 °C to afford a diblock copolymer of (PSt-*b*-PIP)-*g*-SiO_2 NPs (M_n = 23.5 Kg/mol, $Đ$ = 1.16). Figure 4.10 shows the shift of molecular weight distribution in GPC after addition of the second block demonstrating the chain extension polymerization. The formation of the block copolymer could be used as a qualitative indication of the livingness of the polymerization from the particle surface. The complete shift of the GPC trace and low polydispersity of the final block copolymer confirmed the living character and high efficiency of the polyisoprene macro-RAFT agents grafted onto silica nanoparticles. TGA analysis was also used to examine the formation of the homopolymer and block copolymer.

Figure 4.11 shows the TGA analysis of the PIP-*g*-SiO_2 first block and the (PSt-*b*-PIP)-*g*-SiO_2 NPs. A weight gain was observed after addition of each block. Using this method, nanocomposites could be designed so that the outer block would be compatible with the matrix and the inner block could impart specific interphase properties.

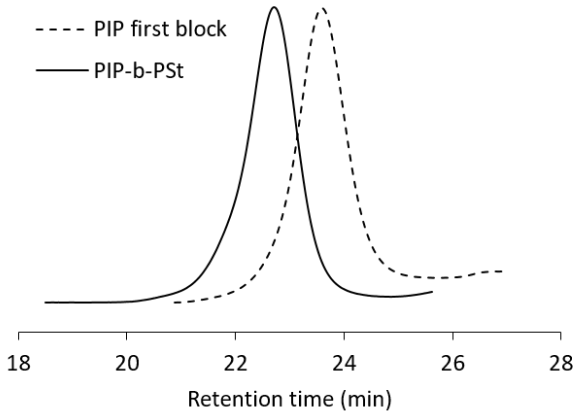

Figure 4.10. GPC traces of the cleaved polyisoprene and polyisoprene-*b*-polystyrene chains.

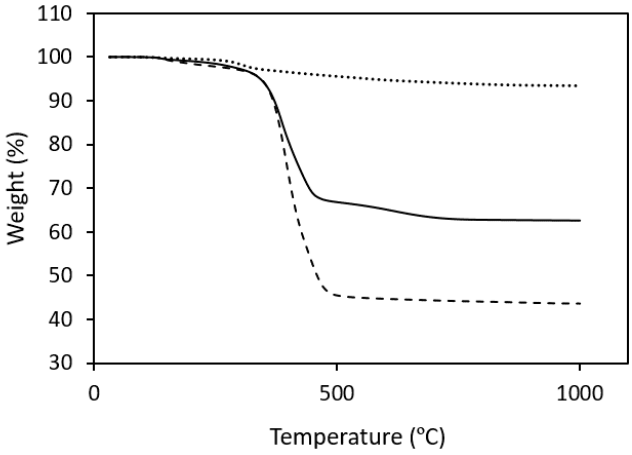

Figure 4.11. TGA of the prepared DoPAT-g-SiO_2 (dotted line), PIP-*g*-SiO_2 (solid line), and (PSt-*b*-PIP)-*g*-SiO_2 NPs (dashed line).

Polyisoprene nanocomposite filled with PIP-*g*-SiO_2 NPs

The morphology of the grafted silica particles and the dispersion of these particles was examined using Transmission Electron Microscopy (TEM). Figure 4.12a shows the

TEM image of a thin layer of PIP-*g*-SiO_2 NPs prepared by casting a drop of dilute suspension of the grafted NPs in THF onto a copper grid and evaporating the solvent. To investigate the compatibility of the grafted particles with polyisoprene matrix, a sample of PIP-*g*-SiO_2 NPs (M_n = 22 Kg/mol, $Đ$ = 1.4) with a chain density of 0.17 ch/nm^2 was synthesized and mixed with polyisoprene matrix (M_n = 62 Kg/mol, $Đ$ = 1.4) through solution mixing and cast in a petri dish. After solvent evaporation, the nanocomposite was sectioned by a cryo-microtome and analyzed by TEM. The chain density of 0.17 ch/nm^2 corresponds to about 110 chains per particle. As shown in the TEM image in Figure 12b this density appears to be sufficient to screen the core-core interactions between silica particles leading to randomly dispersed particles throughout the matrix.

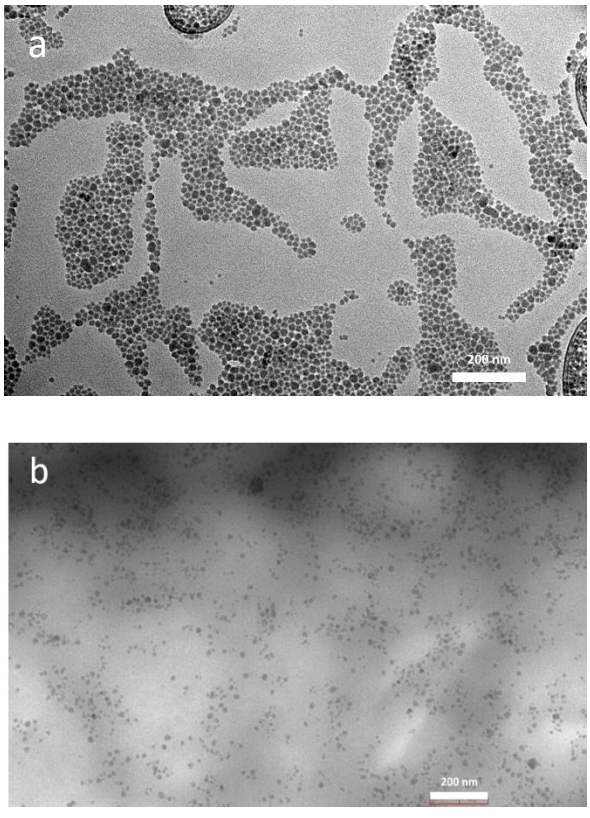

Figure 4.12. TEM micrographs of a) as prepared PIP-*g*-SiO_2 NPs and b) polyisoprene (M_n = 62 Kg/mol) nanocomposite filled with 4% loading of PIP-*g*-SiO_2 NPs (M_n = 22 Kg/mol, $Đ$ = 1.4) with chain density of 0.17 ch/nm^2. (scale bars are 200 nm).

While our initial studies show that the PIP-*g*-SiO_2 NPs were miscible with polyisoprene matrices and have the potential to be used as fillers in the rubber industries, the investigation of the effect of these well-defined particles on different types of rubber nanocomposites is an interesting matter which shall be continued as the focus of our future work.

Hydrogenation of polyisprene-*g*-silica NPs

The hydrogenation reaction of PIP-*g*-SiO_2 NPs is illustrated in Scheme 4.3. *p*-Toluenesulfonyl hydrazide (THS) was used as the source of diimide which carried out the hydrogenation by donating two hydrogen atoms to each double bond of the polyisoprene monomeric units.[32] The hydrogenation yield was determined by ^{1}H NMR spectroscopy by comparing the vinylic hydrogens of polyisoprene at ~5.4 ppm to those of tetrakis(trimethylsilyl)silane as the internal standard at 0.4 ppm (Figure 4.13). The hydrogenation yield was revealed to be 78%. Petzetakis et al.[32] used the same method in the hydrogenation of polybutadiene by THS and obtained a 99% hydrogenation yield. The lower hydrogenation efficiency of THS in our work could be attributed to 1) The difference in the structure of polyisoprene and polybutadiene. The methyl groups in polyisoprene could affect the reactivity of the double bond by steric hindrance. 2) Since the polymer chains are immobilized on the surface of particles, diffusion of the diimide to the double bonds near the surface could be restricted due to the hindrance created by the grafted chains.

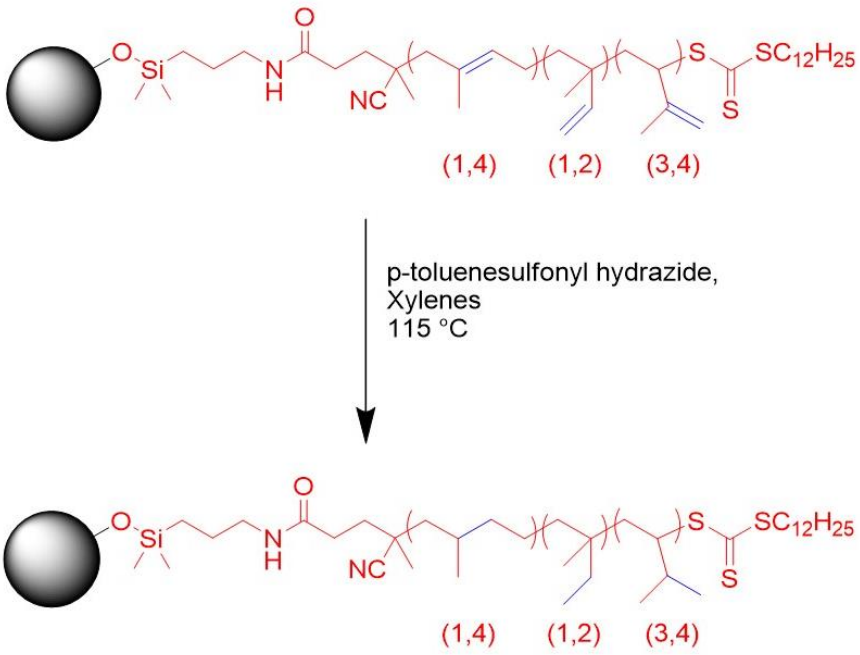

Scheme 4.3. Hydrogenation reaction of PIP-*g*-SiO_2 NPs.

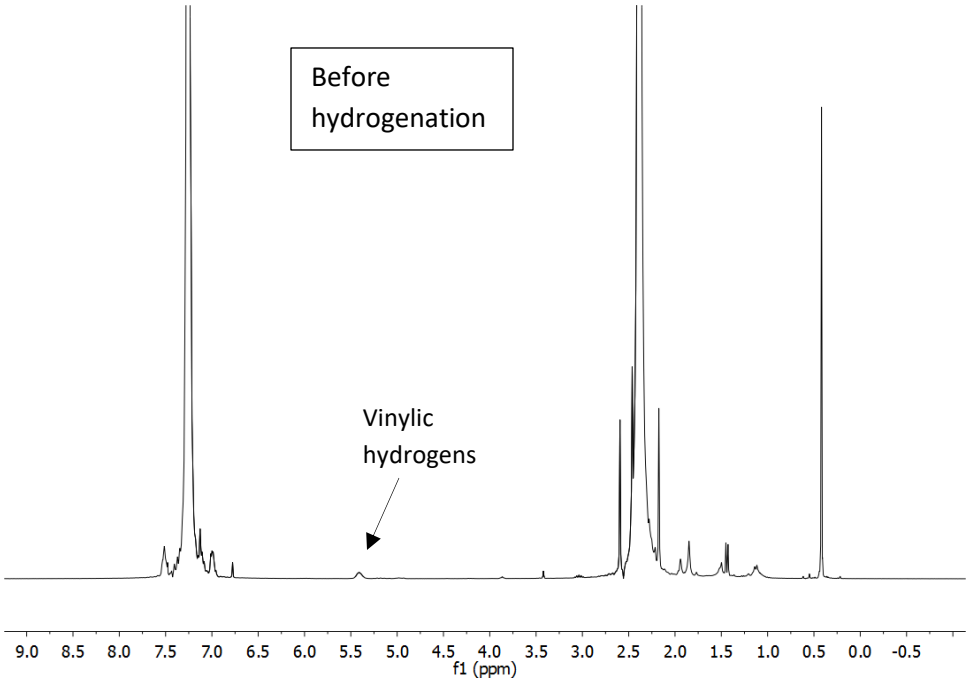

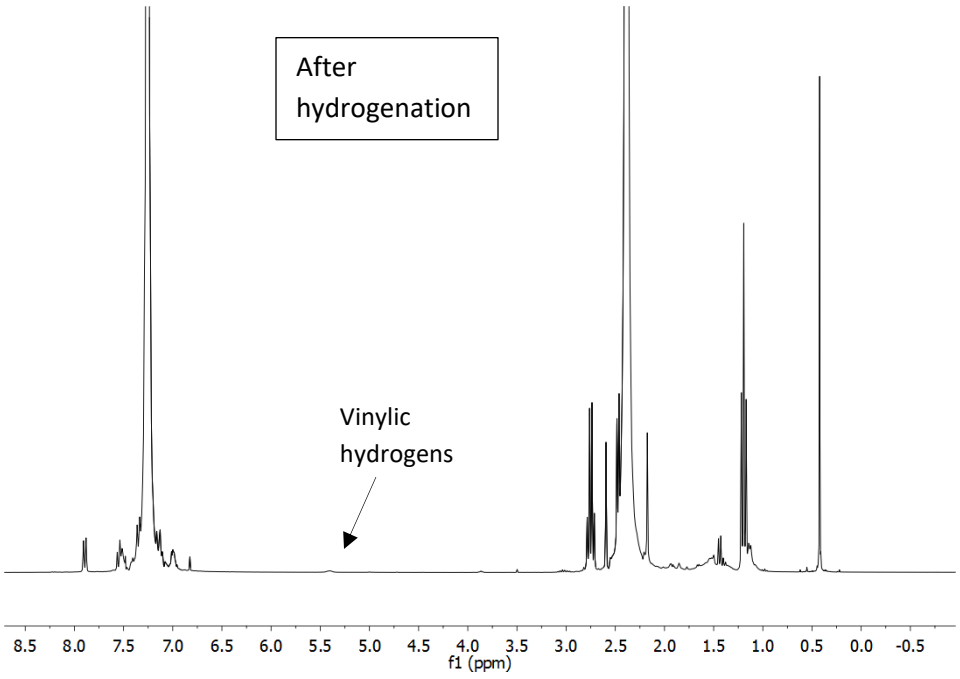

Figure 4.13. ^{1}H NMR spectra of the reaction solution before and after hydrogenation.

Figure 4.14 shows the GPC traces for the cleaved chains before and after the hydrogenation. The GPC curves do not show any significant changes in the polymer peak suggesting that degradation or chain breakage did not occur during the hydrogenation. The peak at 1600 s was attributed to the presence of the surfactants used in the manufacture of silica particles which were cleaved along with the grafted polymer chains from the particles which was discussed earlier in this chapter. Figure 4.15 shows the TGA curves for PIP-*g*-SiO_2 and HPIP-*g*-SiO_2 and reveal only a small difference in the weight loss which could be attributed to the added weight from the hydrogens added to double bond on each repeat unit.

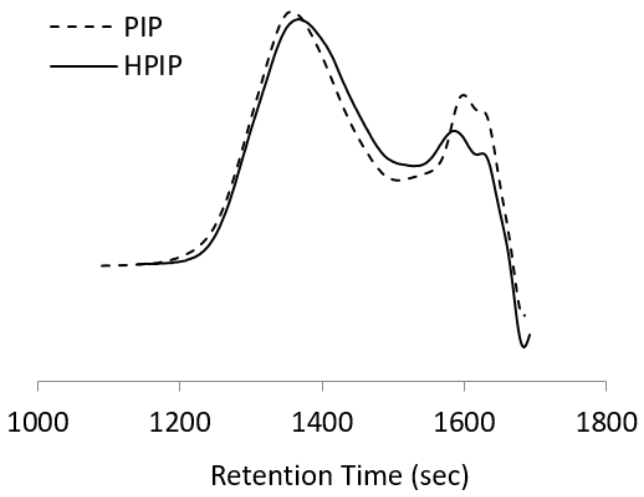

Figure 4.14. GPC traces of the cleaved PIP and HPIP chains.

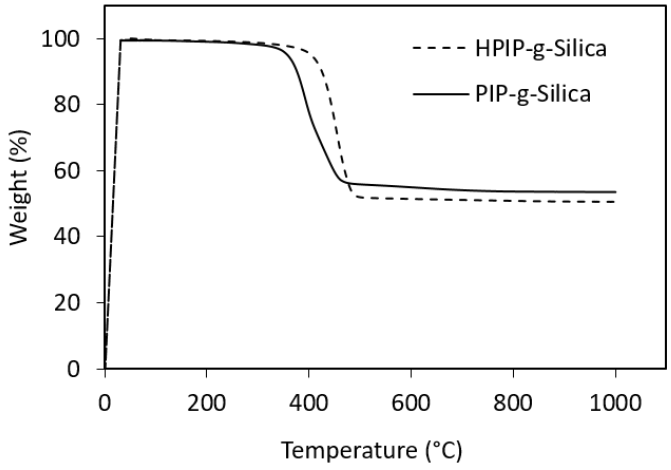

Figure 4.15. TGA curves for the PIP-*g*-SiO_2 and HPIP-*g*-SiO_2samples.

The as prepared HPIP-*g*-SiO_2 NPs were dissolved in a mixture of THF/xylene = 4 and analyzed by TEM and DLS (Figure 4.16 a and b). The solvent mixture was used because THF can dissolve silica and xylene can dissolve the HPIP chains. The drop-cast sample showed an agglomerated dispersion state which was also supported by DLS results. This agglomeration is mostly due to the solvent incompatibility especially evident in the TEM results. When the particle solution was drop-casted on the TEM grid, THF evaporated

quickly and caused aggregation in the remaining xylene (incompatibility of silica and xylene).

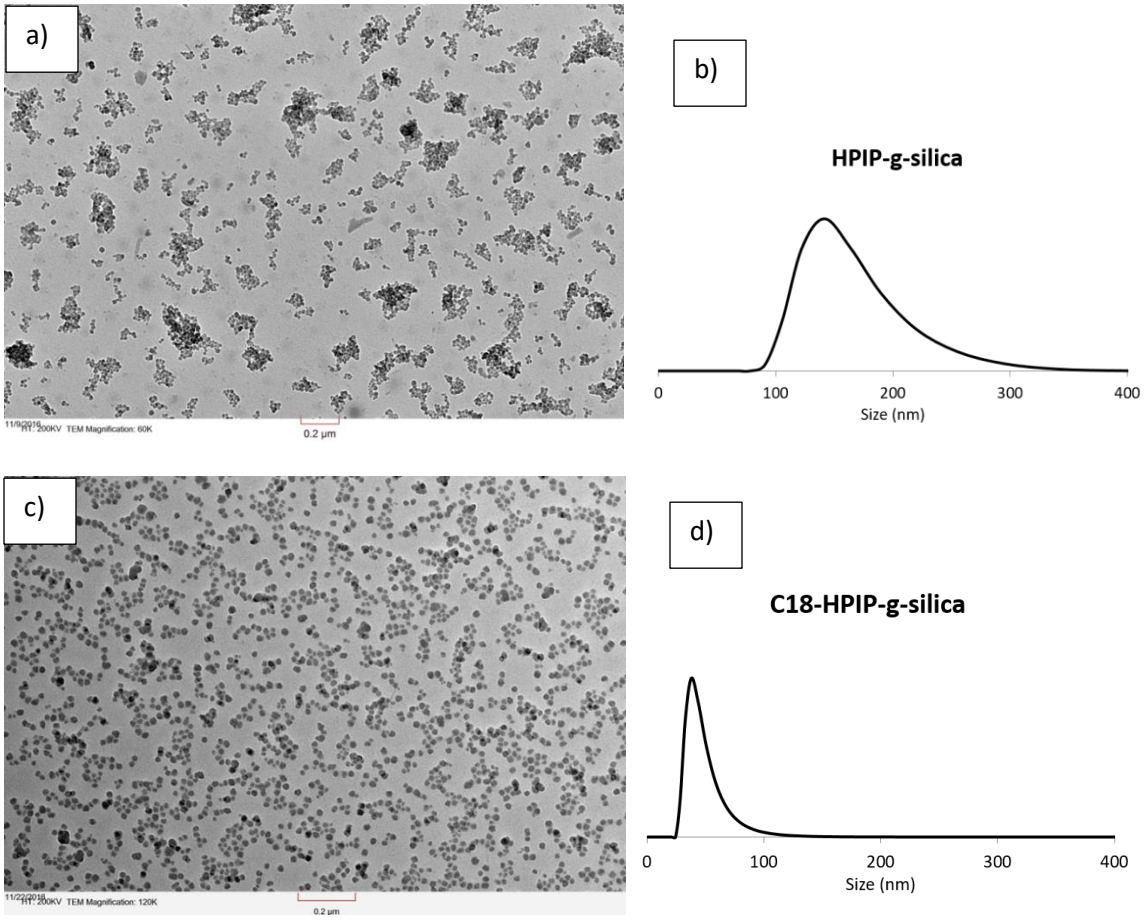

Figure 4.16 TEM and DLS results for the as prepared a), b) HPIP-*g*-SiO_2 (0.5 ch/nm^2, 12 Kg/mol) and c), d) bimodal C18-HPIP-*g*-SiO_2 (0.3 ch/nm^2, 23 Kg/mol) in THF/xylene solution.

To overcome this problem a bimodal architecture was introduced to the particles. A high density of long alkyl chains was attached by reaction of octadecyl silane and amine functionalized particles. The second population was polyisoprene generated by surface initiated RAFT polymerization, followed by hydrogenation. Figure 4.16 c and d show the results for the TEM and DLS of these particles. TEM images of the drop-cast sample showed a significant improvement in the dispersion of particles compared to the

monomodal sample. DLS measurements showed an average diameter of 42 nm which agrees with the expected size for the coated particles.

The bimodal nanoparticles were mixed with an isotactic PP (5 Kg/mol) dilute solution in toluene (10 mg/ml) at 100 ºC and cast directly on a hot TEM grid (100 ºC). After solvent evaporation, the sample was analyzed by TEM (Figure 4.17 a). The TEM image showed a complete dispersion of particles throughout the matrix and proved that these bimodal functionalized particles are compatible with the PP matrix. However, when the same composite was made in 40 mg/ml concentration and was drop-cast on the hot glass and the final film was sectioned by microtome, the particles appeared agglomerated (Figure 4.17 b). The exact reason for this is not clear yet but it could be due to the highly crystalline polypropylene present in the thick film versus the lower crystallinity of very thin films prepared for TEM. Another possible reason could be the difference in the casting substrate which may affect the dispersion of the particles. However, more detailed studies are needed to understand and investigate the effect of different variables on the dispersion of these particles in polyolefin matrices which is currently the focus in our group.

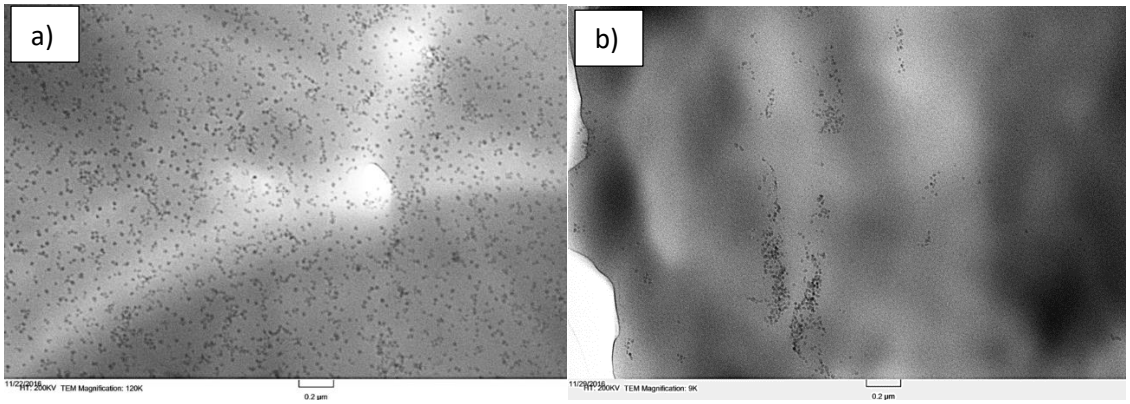

Figure 4.17 TEM images for the 4 wt% bimodal C18-HPIP-*g*-SiO_2 NPs in isotactic PP a) casted on the TEM grid and b) microtomed film.

4.5 Conclusion

A facile method was demonstrated for the synthesis of polyisoprene grafted on silica NPs using a surface-initiated RAFT polymerization technique. A high temperature stable chain transfer agent (DoPAT) was anchored onto the surface of silica particles with controllable graft densities. Controlled radical polymerizations were conducted that produced polymers with low dispersities and predictable molecular weights, and it was found that the surface anchored DoPAT showed excellent control over the surface graft polymerization of isoprene. The kinetics of the isoprene surface polymerizations mediated by the DoPAT-grafted silica nanoparticles at two different surface densities were studied and compared with isoprene polymerization mediated by free DoPAT. Our experiments revealed that the SI-RAFT polymerization of isoprene from particles proceeded with higher rate when compared to polymerization mediated by free RAFT agent and also proceeded at higher rates as the surface density of the RAFT agent increased. The effects of polymerization temperature employing various initiators and also the effects of the [monomer]:[CTA] ratio on the polymerization kinetics were investigated. Chain extension polymerization was performed to produce block copolymer of (PSt-*b*-PIP)-grafted silica nanoparticles. ^{1}H NMR of the product confirmed the presence of ~88% of 1,4-addition isomer along with ~12% of 1,2 and 3,4 isomers. Well-defined PIP-*g*-SiO_2 NPs were mixed with a polyisoprene matrix to prepare a nanocomposite. The final nanocomposite was analyzed by TEM and revealed thorough dispersion and miscibility of silica nanoparticles throughout the polyisoprene matrix. Hydrogenated polyisoprene (HPIP)-grafted NPs were also synthesized by a diimide-based hydrogenation of PIP-*g*-SiO_2 NPs. A bimodal C18-HPIP-*g*-SiO_2 NP sample was synthesized and mixed with isotactic PP matrix and showed

some degree of compatibility with polypropylene. We conclude that this method is an efficient technique for interfacial design of polyisoprene and hydrogenated polyisoprene on nanoparticle surfaces. These particles have potential applications in reinforced rubber and polyolefin nanocomposites where the dispersion and the compatibility of nanoparticles are crucial in achieving enhanced properties.

4.6 References

(1) Khani, M. M.; Abbas, Z. M.; Benicewicz, B. C. *J. Polym. Sci. Part A Polym. Chem.* **2017**, 1–9.

(2) Zou, H.; Wu, S.; Shen, J. *Chem. Rev.* **2008**, *108* (9), 3893–3957.

(3) Moad, G.; Rizzardo, E.; Thang, S. H. *Aust. J. Chem.* **2005**, *58* (6), 379–410.

(4) Gangopadhyay, R.; De, A. *Chem. Mater.* **2000**, *12* (3), 608–622.

(5) Sanchez, C.; Lebeau, B.; Chaput, F.; Boilot, J.-P. *Adv. Mater.* **2003**, *15* (23), 1969–1994.

(6) Tsujii, Y.; Ejaz, M.; Sato, K.; Goto, A.; Fukuda, T. *Macromolecules* **2001**, *34* (26), 8872–8878.

(7) Li, C.; Benicewicz, B. C. *Macromolecules* **2005**, *38* (14), 5929–5936.

(8) Skaff, H.; Emrick, T. *Angew. Chemie - Int. Ed.* **2004**, *43* (40), 5383–5386.

(9) Perrier, S.; Takolpuckdee, P.; Mars, C. A. *Macromolecules* **2005**, *38* (16), 6770–6774.

(10) Li, C.; Han, J.; Ryu, C. Y.; Benicewicz, B. C. *Macromolecules* **2006**, *39* (9), 3175–3183.

(11) Zhao, Y.; Perrier, S. *Macromolecules* **2006**, *39* (25), 8603–8608.

(12) Zhao, D.; Di Nicola, M.; Khani, M. M.; Jestin, J.; Benicewicz, B. C.; Kumar, S. K.

ACS Macro Lett. **2016**, *5* (7), 790–795.

(13) Liu, C. H.; Pan, C. Y. *Polymer (Guildf).* **2007**, *48* (13), 3679–3685.

(14) Zhao, Y.; Perrier, S. *Macromolecules* **2007**, *40* (25), 9116–9124.

(15) Hong, C. Y.; Li, X.; Pan, C. Y. *Eur. Polym. J.* **2007**, *43* (10), 4114–4122.

(16) Khani, M. M.; Woo, D.; Mumpower, E. L.; Benicewicz, B. C. *Polymer (Guildf).* **2017**, *109*, 339–348.

(17) Bhowmick, A. K.; Kuo, C. C.; Manzur, A.; Arthur, A. Mac; Intyre, D. M. *J. Macromol. Sci. Part B* **1986**, *25* (3), 283–306.

(18) Al-Salem, S. M.; Lettieri, P.; Baeyens, J. *J. Hazard. Mater.* **2009**, *172* (2–3), 1690–1694.

(19) Nazhat, S. .; Parker, S.; Riggs, P. .; Braden, M. *Biomaterials* **2001**, *22* (15), 2087–2093.

(20) Nazhat, S. N.; Parker, S.; Patel, M. P.; Braden, M. *Biomaterials* **2001**, *22* (17), 2411–2416.

(21) Hou, S.; Chan, W. K. *Macromolecules* **2002**, *35* (3), 850–856.

(22) Lu, Z. J.; Huang, X. Y.; Huang, J. L.; Pan, G. Q. *Macromol. Rapid Commun.* **1998**, *19* (10), 527–531.

(23) Donderer, M.; Langstein, G.; Schäfer, M.; Nuyken, O. *Polym. Bull.* **2002**, *47* (6), 509–516.

(24) Peng, Y.; Wang, J.; Liu, J.; Dai, H.; Cun, L. *Polym. Int.* **1996**, *39* (1), 63–66.

(25) Kongkaew, A.; Wootthikanokkhan, J. *Polym. Bull.* **1999**, *43* (4–5), 327–332.

(26) Wootthikanokkhan, J.; Tongrubbai, B. *J. Appl. Polym. Sci.* **2003**, *88* (4), 921–927.

(27) Vazaios, A.; Lohse, D. J.; Hadjichristidis, N. *Macromolecules* **2005**, *38* (13),

5468–5474.

(28) Ishizone, T.; Han, S.; Okuyama, S.; Nakahama, S. *Macromolecules* **2003**, *36* (1), 42–49.

(29) Kir, O.; Binder, W. H. *Eur. Polym. J.* **2013**, *49* (10), 3078–3088.

(30) Jitchum, V.; Perrier, S. *Macromolecules* **2007**, *40* (5), 1408–1412.

(31) Germack, D. S.; Wooley, K. L. *J. Polym. Sci. Part A Polym. Chem.* **2007**, *45* (17), 4100–4108.

(32) Petzetakis, N.; Stone, G. M.; Balsara, N. P. *Macromolecules* **2014**, *47* (13), 4151–4159.

(33) Pyun, J.; Jia, S.; Kowalewski, T.; Patterson, G. D.; Matyjaszewski, K. *Macromolecules* **2003**, *36* (14), 5094–5104.

CHAPTER 5

CONCLUSION AND FUTURE WORK

CONCLUSION

The modification of silica surfaces for controlling and designing interfaces was investigated via the development of new synthetic techniques for grafting polymer chains on 15 nm silica surfaces to obtain dispersed NPs in polymer nanocomposites. Reversible addition fragmentation chain transfer (RAFT) polymerization was used for the grafting of polymer chains to the surface of silica nanoparticles in order to allow for the control over the nanoparticle dispersion, grafted brush entanglement, brush graft density, and brush molecular weight, thus controlling the interface between the particles and the polymer matrix.

Controlled radical polymerization of long side-chain alkyl methacrylates such as hexyl, lauryl, and stearyl methacrylate from the surface of 15 nm silica nanoparticles was performed using the RAFT polymerization technique. The kinetics of free RAFT and SI-RAFT polymerizations demonstrated living character of the RAFT process. The prepared PHMA, PLMA, and PSMA-g-SiO_2 NPs were mixed with linear low density polyethylene to obtain nanocomposites. The effect of side chain length on the dispersion of NPs was examined by TEM and revealed that PSMA-g-SiO_2 showed the highest state of dispersion among the three modified particles. It was suggested that the 18 carbon long alkyl side chains make the PSMA more "olefin-like" and are responsible for the compatibility of PSMA-g-SiO_2 with polyethylene due to the molecular similarity. The graft density of PSMA chains was also shown to be crucial in the dispersion of particles throughout the matrix. Particles with lower grafting densities agglomerated whereas the higher densities showed improved dispersions. The agglomeration of lower graft density particles was due to the core-core interaction of the silica particles. The effect of chain molecular weight was

also studied and showed that low molecular weight PSMA grafted particles agglomerated and as the molecular weight increased the state of dispersion improved which was ascribed to the enhanced entanglement of high molecular weight brushes with the LLDPE matrix.

DSC and WAXS revealed that PSMA-g-SiO_2 particles did not greatly affect the thermal and crystalline properties of LLDPE. SAXS studies showed the particle spacing distribution broadened when cooling the samples slowly from the melt to the crystalline state. For the nanocomposites with nanoparticle loadings especially below 20 wt%, it is likely that some of the nanoparticles were pushed out of the way of the growing crystallites, resulting in a broadening of the particle distribution. Storage and loss modulus of the samples were analyzed by DMA and showed improvement by the addition of PSMA-g-SiO_2 NPs. The storage modulus of the polyethylene improved by addition of only 2.5% PSMA-g-SiO_2 and this improvement was found to be more significant at lower temperatures (up to 90%).

Using knowledge gained from the polyethylene compatibility of PSMA-g-SiO_2 NPs, these particles were applied in isotactic polypropylene to investigate the effects of fillers on dielectric properties of polypropylene nanocomposites. Furthermore, anthracene molecules (conjugated ligand) were anchored onto the silica particles as a second brush for dielectric properties enhancement. The dispersion states were shown to occur independent of the presence or absence of anthracene molecules on the nanoparticle surface and were effected by both processing parameters and the inherent thermodynamics of the brush. Dispersed silica nanoparticles with anthracene on their surfaces increased the DBS under both AC and DC test conditions by more than 15%, attributed to the trap states introduced

by these particles interfering with electron avalanches. This same composite also displayed improved AC voltage endurance over the neat control.

The synthesis of polyisoprene grafted on silica NPs using a surface-initiated RAFT polymerization technique was demonstrated. A high temperature stable trithiocarbonate RAFT agent (DoPAT) was anchored onto the surface of silica particles with controllable graft densities. Controlled radical polymerizations were conducted that produced polymers with low dispersities and predictable molecular weights, and it was found that the surface anchored DoPAT showed excellent control over the surface graft polymerization of isoprene. The experiments revealed that the SI-RAFT polymerization of isoprene from particles proceeded with higher rate when compared to polymerization mediated by free RAFT agent and also proceeded at higher rates as the surface density of the RAFT agent increased. The effects of polymerization temperature employing various initiators and also the effects of the [monomer]:[CTA] ratio on the polymerization kinetics were investigated. Well-defined PIP-*g*-SiO_2 NPs were mixed with a polyisoprene matrix and the dispersion of particles was analyzed by TEM and displayed a good state of dispersion for the particles. Hydrogenation of PIP-*g*-SiO_2 NPs was performed using *p*-toluenesulfonyl hydrazide at high temperature to obtain hydrogenated (HPIP)-*g*-SiO_2 NPs. A bimodal C18-HPIP-*g*-SiO_2 NP sample was synthesized and mixed with isotactic PP matrix and showed some degree of compatibility with polypropylene.

FUTURE WORK

More studies could be performed on the effects of PSMA-g-SiO_2 NPs on the mechanical properties of LLDPE nanocomposites. Based on DMA results, the mechanical properties were improved only at low temperatures nevertheless, above 30 °C, where the

PSMA brush melts, the grafted particles were ineffective. A bimodal architecture could be introduced with a high density short brush of a high modulus polymer such as PMMA and low density long brush of PSMA. The short brush could enhance the mechanical properties while the long brush would be polyethylene compatible and would maintain particle dispersion. Another suggestion is to introduce a second monomer within the backbone of the PSMA brush to destroy its crystallinity to change the melting behavior of the PSMA and also to help with better entanglement of PSMA with the polyethylene matrix. SAXS studies showed different interactions between the particles and crystalline polyethylene based on the particles loading. However, the detailed studies of the crystallization of LLDPE was challenging due to the wide crystallization range in this polymer due to high level of branching. An alternative polyolefin such as high density polyethylene or isotactic polypropylene with sharp crystallization could be used as the matrix to study the crystallization behavior of polyolefins in the presence of PSMA-g-SiO_2 NPs.

The results of the dielectric nanocomposite work showed that the grafting of anthracene ligands is an effective way for improving dielectric properties. Investigation into mixed bimodal brush grafted nanoparticles for nanodielectrics is an attractive approach for the synthesis of dielectric nanocomposites. The bimodal brush system could show even further improvements at a well-dispersed state. Multiple monomers can be investigated for the short electroactive brush. Further investigation could be performed to introduce other conjugated ligands such as ferrocene, thiophene, and terthiophene to the bimodal grafted particles to study their effects on nanodielectrics.

The information about the mechanism of surface initiated RAFT polymerization of isoprene is limited. The trend in the rate of polymerizations mediated by free RAFT and

SI-RAFT with different densities was in contrast with RAFT polymerization of styrenic and acrylic monomers. One suggestion for the future work is to investigate the RAFT polymerization of other diene monomers to understand the mechanism of their RAFT polymerization. Moreover, the PIP-*g*-SiO_2 NPs have a lot of potential in reinforced rubber nanocomposites where the dispersion and the compatibility of nanoparticles are crucial in achieving enhanced properties. However, most of the industrial rubber materials are high molecular weight polymers. High molecular weight PIP-g-silica should be synthesized probably by varying the polymerization conditions in order to achieve acceptable compatibility between the grafted PIP and these matrices since based on previous findings brush molecular weight needs to be in the range of the matrix molecular weight. This is a challenge that can be addressed in the future for more practical applications.

APPENDIX A

PERMISSION TO REPRINT

Copyright license for chapter 2 from the manuscript entitled “Poly(alkyl methacrylate)-grafted silica nanoparticles in linear low density polyethylene nanocomposite”

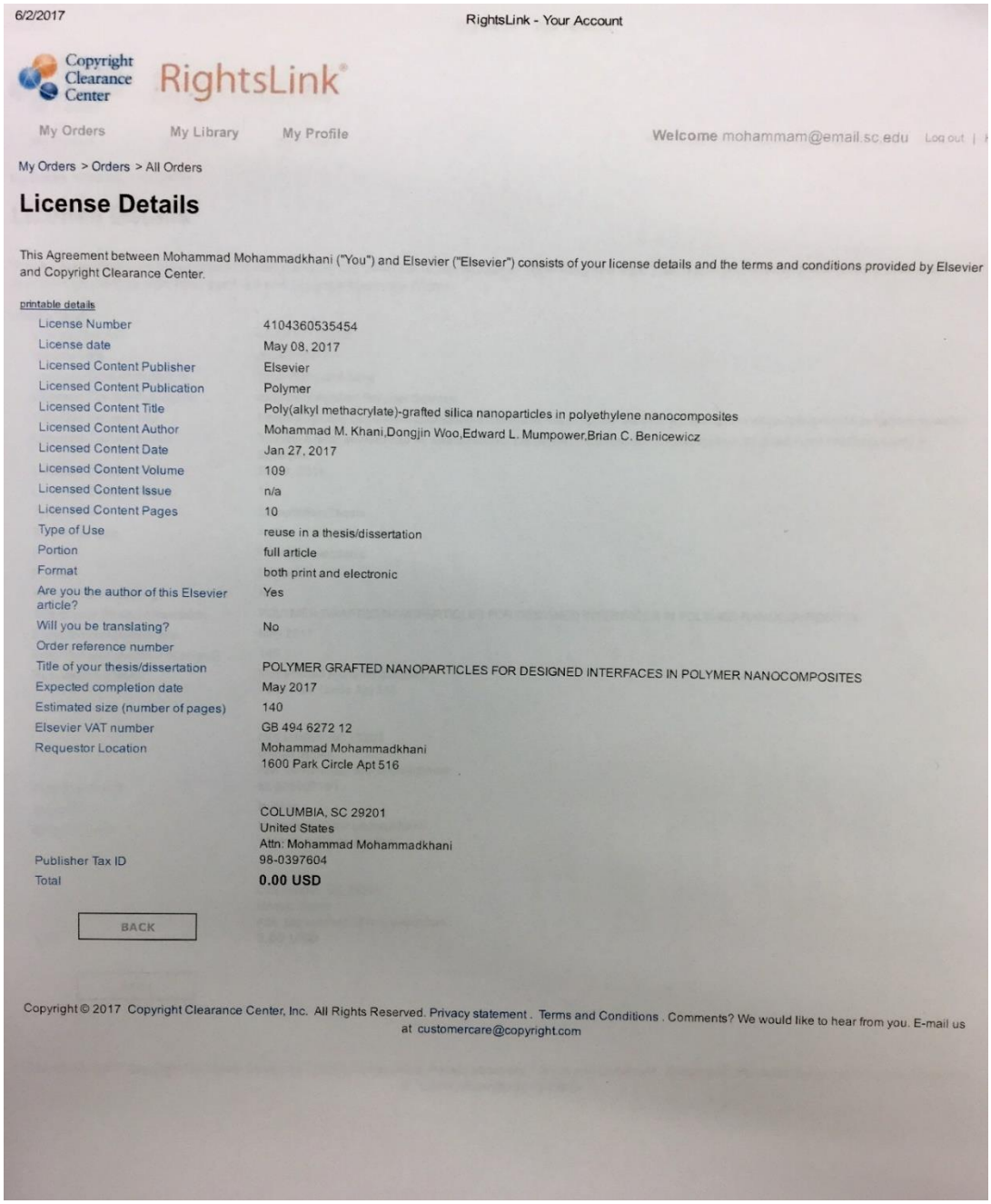

6/2/2017 RightsLink - Your Account

Copyright Clearance Center RightsLink®

My Orders My Library My Profile Welcome mohammam@email.sc.edu Log out

My Orders > Orders > All Orders

License Details

This Agreement between Mohammad Mohammadkhani ("You") and Elsevier ("Elsevier") consists of your license details and the terms and conditions provided by Elsevier and Copyright Clearance Center.

printable details

License Number	4104360535454
License date	May 08, 2017
Licensed Content Publisher	Elsevier
Licensed Content Publication	Polymer
Licensed Content Title	Poly(alkyl methacrylate)-grafted silica nanoparticles in polyethylene nanocomposites
Licensed Content Author	Mohammad M. Khani,Dongjin Woo,Edward L. Mumpower,Brian C. Benicewicz
Licensed Content Date	Jan 27, 2017
Licensed Content Volume	109
Licensed Content Issue	n/a
Licensed Content Pages	10
Type of Use	reuse in a thesis/dissertation
Portion	full article
Format	both print and electronic
Are you the author of this Elsevier article?	Yes
Will you be translating?	No
Order reference number	
Title of your thesis/dissertation	POLYMER GRAFTED NANOPARTICLES FOR DESIGNED INTERFACES IN POLYMER NANOCOMPOSITES
Expected completion date	May 2017
Estimated size (number of pages)	140
Elsevier VAT number	GB 494 6272 12
Requestor Location	Mohammad Mohammadkhani 1600 Park Circle Apt 516 COLUMBIA, SC 29201 United States Attn: Mohammad Mohammadkhani
Publisher Tax ID	98-0397604
Total	**0.00 USD**

BACK

Copyright license for chapter 3 from the manuscript entitled “Morphologically dependent alternating-current and direct-current breakdown strength in silica–polypropylene nanocomposites”

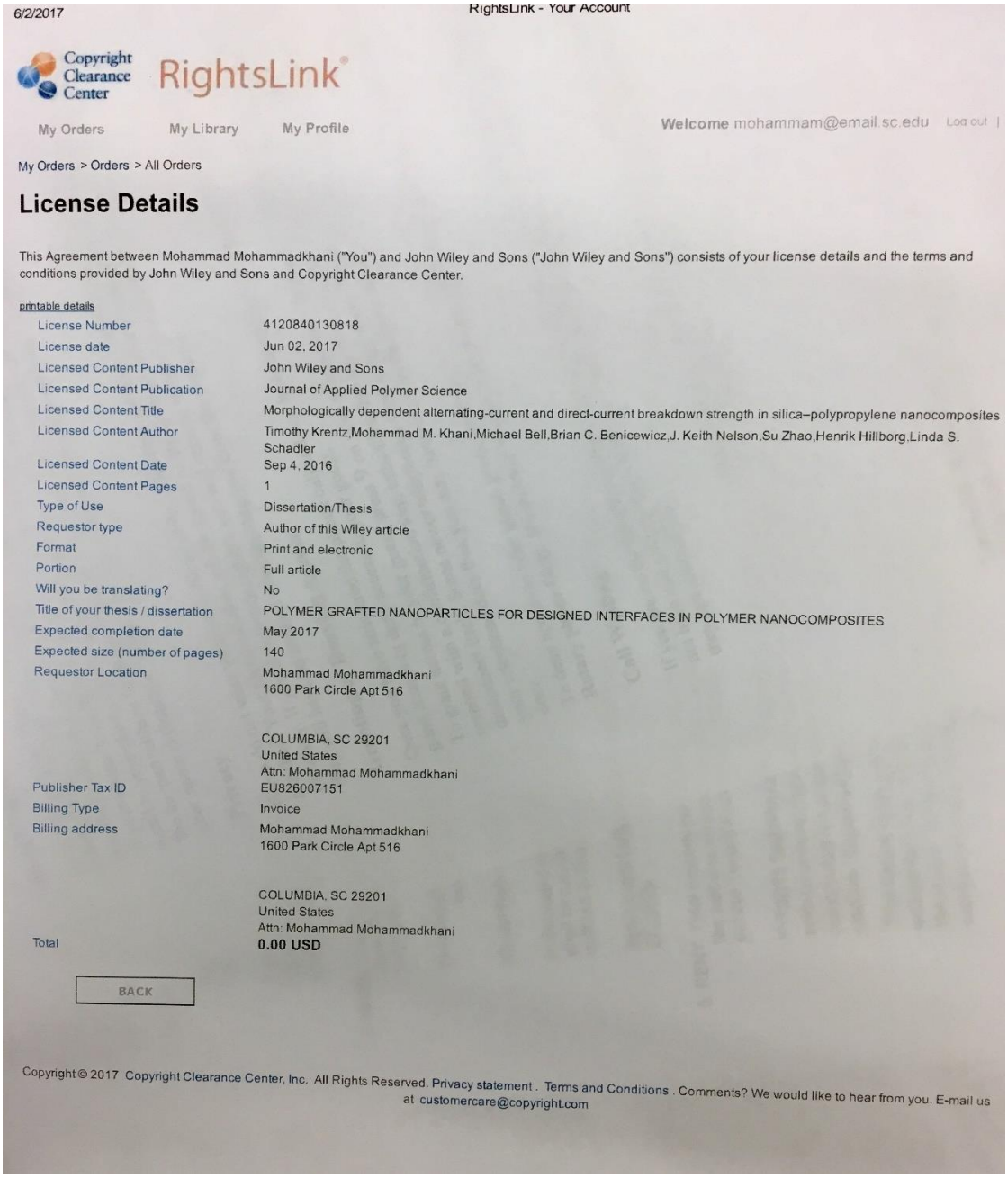

6/2/2017 RightsLink - Your Account

Copyright Clearance Center RightsLink

My Orders My Library My Profile Welcome mohammam@email.sc.edu Log out |

My Orders > Orders > All Orders

License Details

This Agreement between Mohammad Mohammadkhani ("You") and John Wiley and Sons ("John Wiley and Sons") consists of your license details and the terms and conditions provided by John Wiley and Sons and Copyright Clearance Center.

printable details

License Number	4120840130818
License date	Jun 02, 2017
Licensed Content Publisher	John Wiley and Sons
Licensed Content Publication	Journal of Applied Polymer Science
Licensed Content Title	Morphologically dependent alternating-current and direct-current breakdown strength in silica–polypropylene nanocomposites
Licensed Content Author	Timothy Krentz,Mohammad M. Khani,Michael Bell,Brian C. Benicewicz,J. Keith Nelson,Su Zhao,Henrik Hillborg,Linda S. Schadler
Licensed Content Date	Sep 4, 2016
Licensed Content Pages	1
Type of Use	Dissertation/Thesis
Requestor type	Author of this Wiley article
Format	Print and electronic
Portion	Full article
Will you be translating?	No
Title of your thesis / dissertation	POLYMER GRAFTED NANOPARTICLES FOR DESIGNED INTERFACES IN POLYMER NANOCOMPOSITES
Expected completion date	May 2017
Expected size (number of pages)	140
Requestor Location	Mohammad Mohammadkhani 1600 Park Circle Apt 516 COLUMBIA, SC 29201 United States Attn: Mohammad Mohammadkhani
Publisher Tax ID	EU826007151
Billing Type	Invoice
Billing address	Mohammad Mohammadkhani 1600 Park Circle Apt 516 COLUMBIA, SC 29201 United States Attn: Mohammad Mohammadkhani
Total	**0.00 USD**

BACK

Copyright license for chapter 4 from the manuscript entitled “Well-defined polyisoprene-grafted silica nanoparticles via the RAFT process”

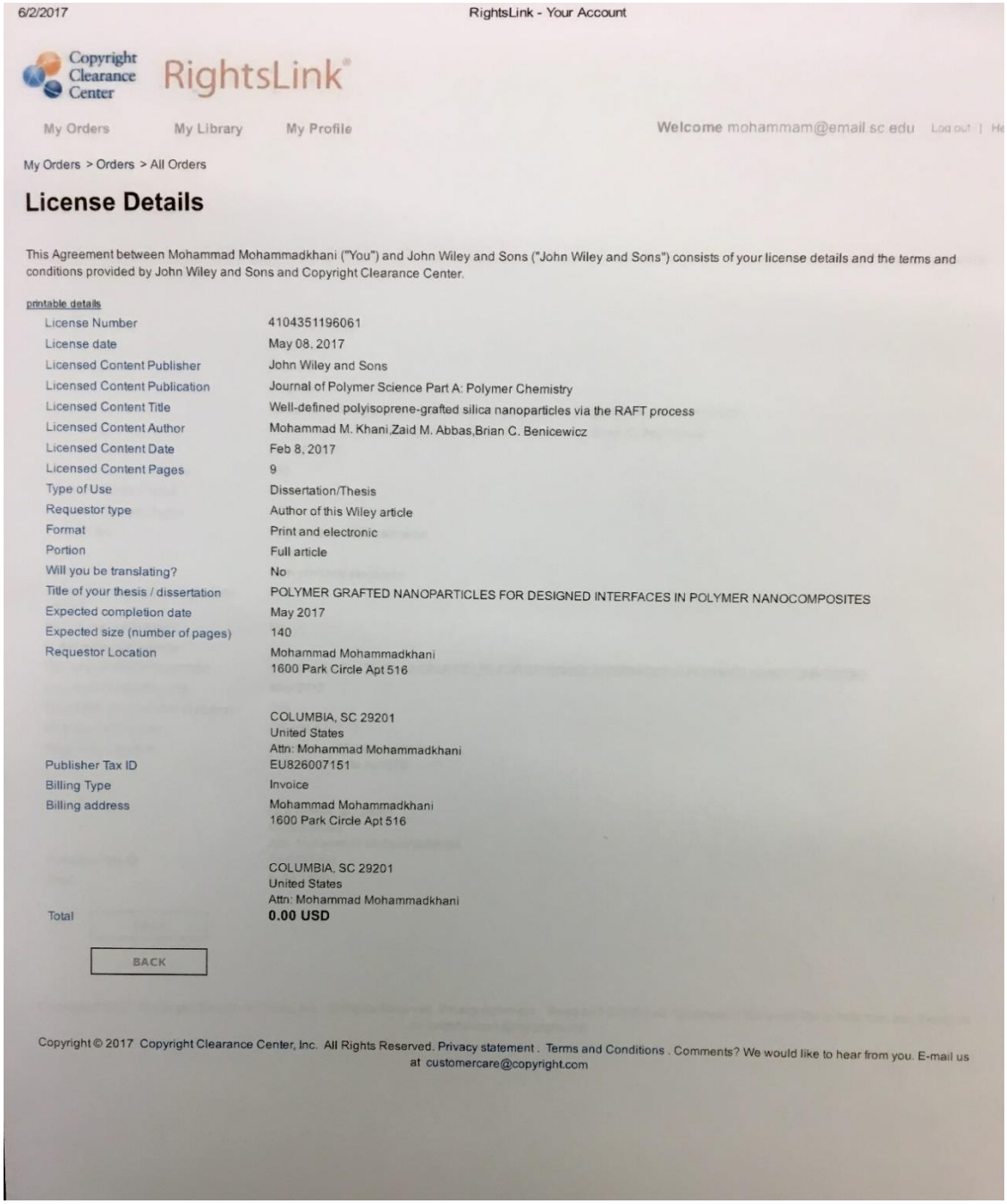

6/2/2017 RightsLink - Your Account

Copyright Clearance Center RightsLink®

My Orders My Library My Profile Welcome mohammam@email.sc.edu Log out | He

My Orders > Orders > All Orders

License Details

This Agreement between Mohammad Mohammadkhani ("You") and John Wiley and Sons ("John Wiley and Sons") consists of your license details and the terms and conditions provided by John Wiley and Sons and Copyright Clearance Center.

printable details

License Number	4104351196061
License date	May 08, 2017
Licensed Content Publisher	John Wiley and Sons
Licensed Content Publication	Journal of Polymer Science Part A: Polymer Chemistry
Licensed Content Title	Well-defined polyisoprene-grafted silica nanoparticles via the RAFT process
Licensed Content Author	Mohammad M. Khani,Zaid M. Abbas,Brian C. Benicewicz
Licensed Content Date	Feb 8, 2017
Licensed Content Pages	9
Type of Use	Dissertation/Thesis
Requestor type	Author of this Wiley article
Format	Print and electronic
Portion	Full article
Will you be translating?	No
Title of your thesis / dissertation	POLYMER GRAFTED NANOPARTICLES FOR DESIGNED INTERFACES IN POLYMER NANOCOMPOSITES
Expected completion date	May 2017
Expected size (number of pages)	140
Requestor Location	Mohammad Mohammadkhani 1600 Park Circle Apt 516 COLUMBIA, SC 29201 United States Attn: Mohammad Mohammadkhani
Publisher Tax ID	EU826007151
Billing Type	Invoice
Billing address	Mohammad Mohammadkhani 1600 Park Circle Apt 516 COLUMBIA, SC 29201 United States Attn: Mohammad Mohammadkhani
Total	**0.00 USD**

BACK